UNIVERSITÀ
DEGLI STUDI
DI PADOVA

Università degli Studi di Padova

Instituto Superior Tecnico - Universidade Tecnica De Lisboa

Centro Interdipartimentale "Centro Ricerche Fusione" Università di Padova

Joint Research Doctorate in Fusion Science and Engineering

EDGE PLASMA CHARACTERIZATION ON THE RFX-MOD DEVICE

Coordinator:
Ch.mo Prof. Piero Martin
Supervisors:
Dr. Emilio Martines
Ch.mo Prof. Maurizio Moresco

Doctoral Student:
Gianluca De Masi

31/01/2011

"Life is like riding a bicycle.
To keep your balance
you must keep moving"
Albert Einstein

Contents

Abstract

The controlled thermonuclear fusion represents one of the most promising future energy source since it would meet the requirements of a clean, renewable and thus, virtually inexhaustible resource. The attempt to reproduce on the Earth the process that powers all the active stars of the universe is, however, made difficult by the present inability to realize in a laboratory an optimal plasma confinement at the conditions of high temperature and density. These conditions are needed to overcome the repelling Coulomb force and to bring the reactant nuclei within the range of their strong interaction. One of the most active research field in nuclear fusion is the study of the plasma (a state of matter consisting in a quasi neutral ensemble of ions and electrons) confinement optimization by exploiting the effect of the magnetic field application.
The work presented in this thesis is to a large extent devoted to the analysis of a particular magnetic configuration: the so called Reversed Field Pinch (RFP). The peculiar shape of the applied magnetic field for plasma confinement gives the name to this toroidal magnetic configuration; in particular, the toroidal component (parallel to the chamber axis) reverses its sign in the outermost region. As explained in the first chapters, this feature leads to several consequences on the confined plasma inside the machine. Historically, the RFP has been characterized from a side, for the ability to achieve high plasma current regimes with an applied magnetic field smaller than in other configuration such as the Tokamak; on the other side, for a poor magnetic confinement due to the presence of a wide spectrum of MHD instabilities (leading to a so called Multiple Helitic state).
The recent results obtained by the RFX-mod RFP experiment (on which this thesis work has been carried out) at plasma current beyond 1.5 MA, demonstrated the possibility to achieve significant improvements in terms of plasma confinement. In particular, the spontaneous transition towards an higher level of self-organization (in the so called Quasi Single Helicity QSH/SHAx states) excited much interest among the fusion community. Unfortunately, at the moment, these improved confinement states (in which the

plasma can reach temperature values of about ten millions degrees) appear almost solely at low density values. At higher density the RFX-mod plasma tends to show the traditional poor confinement features typical of the Multiple Helicity (MH) states. This phenomenology, not totally understood yet, has been related to some processes occurring in the outermost plasma regions particularly exposed to the interaction with the first wall of the chamber.
The thesis research activity aimed to characterize this crucial edge plasma region of RFX-mod, through two particular diagnostic systems: a microwave reflectometer and an insertable electric probe, the so called Gundestrup probe.
The microwave reflectometer is a device that, exploiting the electromagnetic wave reflection by a given plasma layer, is able to evaluate the distance from the antenna (the launcher). According to the launched frequency is possible probing plasma layers with different density values. The high fluctuations level present on a RFP, up to now were hampered any atteimpts to have reliable reflectometric measurements on such a device. The first Ka-band of a new diagnostic scheme (developed in the RFX laboratory), after a preliminary calibration phase, has been continuously operational on the RFX-mod device since the mid of 2009. The experimental validation through the comparisons with different well-established diagnostic systems demonstrated the reliability of the microwave reflectometer also on the RFP configuration. Moreover, the analysis of the large collected data amount allowed characterizing the plasma density dynamics of the edge region. In particular, the reflectometer high time resolution ($\Delta t = 2\mu s$) enabled highlighting the deep relation between the low frequency magnetic plasma fluctuations and the presence of magnetic islands produced by the different MHD instability resonances in the edge. Finally, the study of the averaged behaviour over a large discharges database improved the understanding of the effect of the global parameter changes on the plasma-wall interaction.
The Gundestrup probe is, instead, a special electric probe insertable at different radial position in the plasma. Its peculiar configuration (composed by 10 electrodes) allowed evaluating the different local plasma flow components starting from the ion saturation current data (the current collected by a biased electrode exposed to the plasma). During the research activity has been also developed an innovative method to estimate the parallel and perpendicular (with respect to the edge magnetic field) flow components starting from the floating potential measurements (the potential measured by a floating electrode exposed the plasma). The application of this method, experimental validated on RFX-mod and also on the ISTTOK Tokamak (at the IST Association in Lisbon), allowed to reconstruct the edge radial profiles of the plasma flow. Also in this case the interaction with the strong MHD activity

has been highlighted. In particular, in the low plasma current regimes (in the MH states) the presence of the $m = 0$ mode resonance has been found to produce a significant parallel flow increase. In the high plasma regimes (QSH states) strong flow modulations has been observed according to the edge deformations produced by the MHD dominant mode ($m = 1, n = 7$) and already expected by numerical simulations.
The thesis is organized as follows:

- **Chapter 1**: introduces briefly the basic principles of the plasma magnetic confinement starting from the more general description of a fluid in the presence of a magnetic field, summarized by the MHD equations. Then, the chapter deals with the topic of the plasma equilibrium and stability still in the framework of the ideal and resistive MHD theory. Finally, the main features of two plasma magnetic confinement configurations are analyzed: the Tokamak and, in a more detailed way, the RFP.

- **Chapter 2**: is totally devoted to describe the main features of RFX-mod (the largest RFP in operation). The upgrades of the actual machine with respect to the previous one, the recent results and the open issues to be solved to achieve better results are introduced. Moreover, the chapter treats the complex edge magnetic topology and the tools that will be used in the thesis to investigate it.

- **Chapter 3**: introduces one of the two main diagnostic systems of this work, the microwave reflectometer. In particular, the problem of the reflectometric measurements in the presence of density fluctuations is treated from a numerical point of view. Then, a simplified model for the RFX-mod case is described together with the reflectometer upgrade imposed by the application of this model.

- **Chapter 4**: the Gundestrup electric probe is introduced with an innovative method to evaluate the plasma flow components starting from the floating potential measurements. The experimental validations of this method carried out on RFX-mod and on the ISTTOK Tokamak are reported.

- **Chapter 5**: is devoted to review the reflectometric measurements carried out on RFX-mod. In the first part some benchtests for the reflectometer calibration are reported together with the experimental validation of the measurement through the comparison with the measurements coming from the Edge Thomson Scattering, the interferometer

and the Thermal Helium Beam. Finally an extensive analysis of the main features of the RFX-mod edge density dynamics is presented.

- **Chapter 6**: the main results obtained with the Gundestrup probe and many comparative results coming from several other diagnostic systems are discussed. In particular, the edge flow radial profiles have been reconstructed and the interaction with the edge magnetic topology has been highlighted in the low plasma current regimes; the flow components dynamics has been investigated also in the high current regimes with some interesting results.

- **Chapter 7**: summarizes the results and gives some conclusions, presenting the future developments.

Riassunto

La fusione termonucleare controllata rappresenta una delle piú promettenti future fonti di energia grazie alla sua caratteristica di risorsa pulita, rinnovabile e dunque potenzialmente inesauribile. Il tentativo di riprodurre sulla Terra il processo che da miliardi di anni alimenta tutte le stelle attive dell'universo, é reso, peró, difficoltoso dall'incapacitá attuale di realizzare in laboratorio un confinamento ottimale del plasma in condizioni di alta temperatura e densitá. Queste condizioni sono necessarie per vincere la repulsione Coulombiana e portare i nuclei reagenti al range di distanza della loro interazione forte. Uno dei campi di ricerca piú attivi nell'ambito della fusione nucleare é quello che studia l'ottimizzazione del confinamento del plasma sfruttando l'effetto dell'applicazione di campi magnetici.
Il lavoro presentato in questa tesi é in larga parte dedicato all'analisi di una particolare configurazione magnetica: il Reversed Field Pinch (RFP), la cosiddetta macchina a campo rovesciato. Questa configurazione a geometria toroidale prende il suo nome dalla peculiare forma dei campi magnetici applicati per confinare il plasma; in particolare dalla componente toroidale (parallela all'asse della camera) che nella regione piú esterna inverte il suo segno. Come spiegato nei primi capitoli, questa caratteristica ha diverse conseguenze sulla dinamica del plasma confinato all'interno della macchina. Storicamente, l'RFP si caratterizzava da una parte per la capacitá di raggiungere alti regimi di corrente di plasma con un campo magnetico applicato meno intenso rispetto ad altre configurazioni come il Tokamak; dall'altra per un basso livello di confinamento magnetico del plasma, deteriorato dalla presenza di un ampio spettro di instabilitá MHD (che portano a un cosiddetto stato di Multipla Elicitá).
I recenti risultati ottenuti dall'esperimento RFX-mod RFP (su cui é stato condotto il lavoro presentato nella tesi) a correnti di plasma oltre 1.5 MA, hanno peró dimostrato la possibilitá di raggiungere significativi miglioramenti in termini di confinamento del plasma. In particolare, la spontanea transizione del plasma verso una maggiore auto-organizzazione (nei cosiddetti stati a Quasi Singola Elicitá QSH/SHAx) ha suscitato molto interesse nella

comunitá fusionistica. Attualmente, purtroppo, questi stati di miglior confinamento del plasma (in cui il plasma puó raggiungere temperature dell'ordine dei dieci milioni di gradi) appaiono quasi esclusivamente a bassa densitá. A densitá piú alte il plasma di RFX-mod tende a manifestare le tradizionali caratterisitiche di scarso confinamento degli stati a multipla elicitá (MH). Questa fenomenologia, non ancora del tutto compresa, é stata attribuita a processi che avvengono nelle regioni esterne del plasma, quelle particolarmente coinvolte nell'interazione con la prima parete della camera che lo contiene.
L'attivitá di ricerca della tesi é stato finalizzato a caratterizzare questa cruciale regione esterna del plasma di RFX-mod attraverso due particolari sistemi diagnostici: un riflettometro a microonde e una sonda elettrica inseribile chiamata Gundestrup.
Il riflettometro a microonde é uno strumento che, sfruttando la riflessione di un'onda elettromagnetica di un dato strato di plasma, é in grado di stabilirne la distanza dall'antenna che lancia l'onda. A seconda della frequenza lanciata é possibile sondare strati di plasma con densitá differenti. L'alto livello di fluttuazioni presenti sulle configurazioni RFP, fino ad ora, aveva sempre impedito di ottenere misure riflettometriche attendibili in questo tipo di macchina. La prima banda Ka di un nuovo schema diagnostico (sviluppato nel laboratorio RFX), dopo una fase di calibrazione, ha operato su RFX-mod in maniera continua dalla seconda metá del 2009. La validazione sperimentale attraverso il confronto con diversi e consolidati sistemi diagnostici ha dimostrato l'affidabilitá del riflettometro a microonde anche sulla configurazione RFP. Inoltre, l'analisi della grande quantitá di dati raccolti ha permesso di caratterizzare la dinamica di densitá della regione di bordo. In particolare, l'alta risoluzione temporale ($\Delta t = 2\mu s$) dello strumento ha permesso di mettere in rilievo la stretta connessione tra le fluttuazioni a bassa frequenza del plasma e la presenza delle isole magnetiche prodotte dalla risonanza delle differenti instabilitá MHD al bordo. Infine lo studio dell'andamento medio del plasma esterno su un grande database di scariche ha reso possibile una migliore comprensione dell'effetto della variazione dei parametri globali della scarica sull'interazione plasma-parete.
La sonda Gundestrup é invece una particolare sonda elettrica inseribile nel plasma a differenti posizioni radiali. La sua speciale configurazione (composta da 10 elettrodi) le permette di valutare le differenti componenti locali del flow di plasma a partire dai dati di corrente di saturazione ionica (la corrente raccolta da un elettrodo carico esposto al plasma). Durante l'attivitá di ricerca é stato anche sviluppato un metodo innovativo per ricavare il flow parallelo e perpendicolare rispetto al campo magnetico al bordo a partire dai dati di potenziale flottante (il potenziale a cui si porta un elettrodo flottante

inserito nel plasma). L'applicazione di questo metodo, validato sperimentalmente su RFX-mod e anche sul Tokamak ISTTOK (presso l'Associazione IST di Lisbona), ha permesso di ricostruire i profili radiali al bordo del flow di plasma. Anche in questo caso é stato possibile evidenziarne l'interazione con la presenza delle instabilitá MHD. In particolare nei regimi a bassa corrente (in stati MH) l'effetto delle isole magnetiche create dalla risonanza dei modi $m = 0$ produce un significativo aumento del flow parallelo al campo magnetico. Nelle scariche ad alta corrente (in stati QSH), invece, si sono osservate forti modulazioni nelle diverse componenti di flow in accordo con le deformazioni prodotte dal modo MHD dominante ($m = 1, n = 7$) e previste da precedenti simulazioni numeriche.
La tesi é organizzata nel seguente modo:

- **Capitolo 1**: introduce brevemente i principi di base del confinamento magnetico del plasma partendo dalla descrizione piú generale della dinamica di un fluido in presenza di un campo magnetico sintetizzata dalle equazioni MHD. Successivamente vengono affrontati gli argomenti dell'equilibrio e delle instabilitá di plasma sempre nel quadro della teoria MHD (ideale e resistiva). Infine si analizzano le principali caratteristiche di due configurazioni per il confinamento magnetico del plasma: il Tokamak e, in maniera piú approfondita, l'RFP.

- **Capitolo 2**: é totalmente finalizzato alla descrizione delle principali caratteristiche di RFX-mod (il piú grande RFP del mondo tra quelli operativi). Vengono presentati le modifiche apportate alla macchina rispetto a quella precedente, gli ultimi risultati raggiunti e i problemi da risolvere per raggiungere performance migliori. Inoltre viene introdotta la complessa topologia magnetica di bordo e gli strumenti che verranno utilizzati nel resto della tesi per analizzarla.

- **Capitolo 3**: presenta una delle due diagnostiche principali di questo lavoro, il riflettometro a microonde. In particolare viene affrontato il problema delle misure riflettometriche in presence di fluttuazioni di densitá da un punto di vista numerico. Viene, quindi, introdotto un modello semplificato per il caso di RFX-mod e le modifiche che l'applicazione di questo modello ha imposto rispetto all'originale configurazione del riflettometro.

- **Capitolo 4**: viene presentata la sonda elettrica Gundestrup e anche un innovativo metodo per calcolare le componenti di flow di plasma a partire dalle misure di potenziale flottante. Sono anche riportate le

validazioni sperimentali di questo metodo su RFX-mod e sul Tokamak ISTTOK.

- **Capitolo 5**: é dedicato alle misure del riflettometro a microonde. Nella prima parte sono riportati i test a banco per la calibrazione dello strumento e la validazione sperimentale della misura attraverso il confronto con le misure di diagnostiche come il Thomson Scattering di bordo, l'interferometro e il Thermal Helium beam diagnostico. Infine un'estesa analisi delle principali caratteristiche della dinamica di densitá della regione esterna di RFX-mod e una prima discussione dei risultati.

- **Capitolo 6**: vengono descritti i principali risultati ottenuti con la sonda Gundestrup e sono presentati molti risultati comparativi provenienti da diverse diagnostiche. In particolare, sono stati ricostruiti i profili medi di flow e l'interazione con la topologia magnetica esterna nei regimi a bassa corrente; la dinamica delle componenti di flow é investigata anche nei regimi ad alta corrente con alcuni interessanti risultati.

- **Capitolo 7**: riassume i risultati traendone le principali conclusioni e presentando gli sviluppi futuri.

Chapter 1

Magnetic confinement

1.1 Introduction

> There's an old African proverb that says "If you want to go quickly, go alone. If you want to go far, go together." We have to go far quickly. And that means we have to quickly find a way to change the world's consciousness about exactly what we're facing, and why we have to work to solve it [1].

With these words, after winning the Nobel Peace Prize in 2007, Al Gore exhorted world to get a sense about the Earth climate change caused by the global warming. The fact that he was awarded with such a wide-spreading acknowledgement for his efforts on the enviromental issues, puts emphasis on two great challenges of the present-age: the need for a worldwide diffusion of a more sustainable education and the haste for finding clean and renewable energy sources. The research on nuclear fusion, that is also the main subject of this Doctorate, aims exactly to satisfy this latter request.
The energy production through nuclear fusion reactions is, actually, the process that powers all active stars. Synthetically, it consists in the union of two light nuclei producing an heavier one. In the sun for example the following reaction occurs:

$$\begin{aligned} p + p &\rightarrow D + e^+ + \nu_e \\ D + p &\rightarrow {}^3_2\mathrm{He} + \gamma \\ {}^3_2\mathrm{He} + {}^3_2\mathrm{He} &\rightarrow {}^4_2\mathrm{He} + 2p \end{aligned}$$

where p is a proton, D a deuterium atom, γ an high energy photon, e^+ a positron and ν_e an electron neutrino. The energy release (according to the Einstein equation $E = mc^2$) is due to the difference in mass between

reactants and products. In order to bring within the range of their strong interaction the two nuclei, the repelling Coulomb force has to be overcome over a relatively long distance. The conditions to achieve this scope require the reactants be confined at sufficient high values of density and temperature.
At these values of temperature, matter is in a state of ionized gas. In particular we define the plasma as an ionized gas of neutral and charged particles in globally neutral condition which exhibits collective properties [2, 3].
On the stars gravity provides the force balancing the enormous pressure gradients leading to the particle confinement. On the Earth there are two schemes of plasma confinement explored and studied:

- *inertial confinement*
- *magnetic confinement*

In the first confinement approach, small high density plasmas are created for times in the order of nanoseconds compressing a small pellets of D-T fuel using laser-driven implosion.
In the magnetic confinement (on which we will polarize our attention) ions and electrons, at a density of about $10^{20}\ m^{-3}$, are constrained to follow magnetic field lines (see fig. 1.1).
For both of them the main difficult is maintaining the plasma temperature

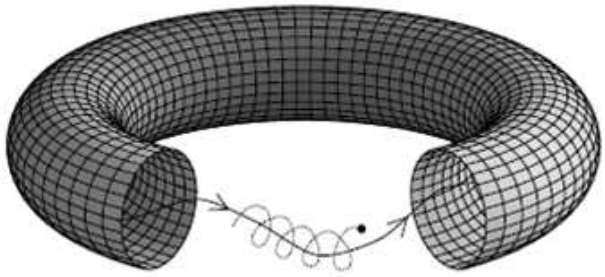

Figure 1.1: A picture showing the principle of toroidal confinement. A charged particle gyrates (dotted line) around a magnetic field lines (continuous line) and it is confined within the vacuum vessel

and density values needed for fusion reactions against the losses mechanisms (due to Coulomb collisions, turbulence and escaped particles). This balance is well described by the so called Lawson's criterion in which, usually, the losses mechanisms are referred to a typical energy confinement time τ_E. A detailed formulation of this criterion can be found in [4].

Hystorically, the magnetic confinement developed starting from the first experiments about the pinch effect in which a current channel contracts through the self-magnetic field of the current, investigated by Bennet in 1934 [5]. We briefly recall that, due to Lorentz force, a particle of mass m and charge q that enters a uniform magnetic field $\mathbf{B}$ with velocity $\mathbf{v}$ moves along a helical trajectory (with anti-clockwise rotation for positive charge). The helical radius (*Larmor radius*) is given by:

$$r = \frac{mv_\perp}{|q|B} \tag{1.1}$$

where $v_\perp$ is the component of the velocity perpendicular to the magnetic field. Moreover the rotation frequency (*cyclotron frequency*) does not depends by the velocity, and is given by:

$$\omega_c = \frac{|q|B}{m}. \tag{1.2}$$

The parallel component of the velocity $v_{||}$ is unaffected by the magnetic field. The early pinch experiments was the basis of the first attempt, in 1951, to confine plasma in a magnetic field by Cousins and Ware [6, 7].
Nowadays, the most advanced research field for the magnetic confinement is based on the optimization of different toroidal device configurations. Among these, the main features of Tokamaks and Reversed Field Pinches will be treated in this chapter. First, a basic introduction on the MHD theory describing the behaviour of a plasma in the presence of a magnetic field will be given.

1.2 The resistive MHD equations

The *MagnetoHydroDynamics* (MHD) theory is at the bottom of the magnetical confinement principle. In particular, the resistive MHD equations are able to describe a large variety of macroscopic phenomena occuring in a plasma under the effect of different magnetic field configurations. A rigorous treatment of this topic can be found in [2, 3, 8], here we just present the main concepts that we recalled later on.
The characterization of the plasma, thought as an electrically conducting fluid, in the presence of a magnetic field $\mathbf{B}$ can be obtained by combining the classical hydrodynamics equations and the Ohm's law under some assumptions. In particular we consider the macroscopic charge quasi-neutrality $n_i \approx n_e$ and small ion Larmor radius compared with the scale-length of the

fluid motion. By further simplifying the model we treate the behaviour of the 2 species (ions and electrons) in terms of the single-fluid variables ρ, $\mathbf{v}$ and $\mathbf{j}$ (respectively the mass density, the fluid velocity and the current density). This produces an equation system as follows:

$$\frac{\partial \rho}{\partial t} + \nabla \cdot (\rho \mathbf{v}) = 0 \tag{1.3}$$

$$\nabla \cdot \mathbf{j} = 0 \tag{1.4}$$

$$\rho \left[\frac{\mathbf{v}}{\partial t} + (\mathbf{v} \cdot \nabla)\mathbf{v} \right] = -\nabla p + \mathbf{j} \times \mathbf{B} + \nu \nabla^2 \mathbf{v} \tag{1.5}$$

$$\mathbf{E} + \mathbf{v} \times \mathbf{B} = \eta \mathbf{j} \tag{1.6}$$

where ν is the kinematic viscosity and η the plasma resistivity. In deriving eqs. (1.3-1.6) the stress tensor has been decomposed in a diagonal term (the pressure) and an off-diagonal term (the viscosity), and a noncompressibility ($\nabla \cdot \mathbf{v} = 0$) hypothesis has been used [9, 10]. This equation system defines the so called *visco-resistive Magnetohydrodynamics*, while the ideal MHD equations can be derived from the system 1.3-1.6, by simply considering a null resistivity. As we will see in the next section, however, η plays a fundamental role in the description of many phenomena taking place in the fusion devices, such as reconnection events, instabilties growth and dynamo effect.
By combining Faraday's law written as:

$$\nabla \times \mathbf{E} = -\frac{\partial \mathbf{B}}{\partial t} \tag{1.7}$$

with Ohm's law, it is simple to derive the following equation, which describes the coupled dynamics of the magnetic and fluid velocity fields in the resistive MHD framework:

$$\frac{\partial \mathbf{B}}{\partial t} = \nabla \times (\mathbf{u} \times \mathbf{B}) + \frac{\eta}{\mu_0} \nabla^2 \mathbf{B} \tag{1.8}$$

In particular, this equation reproduces the time evolution of the magnetic field $\mathbf{B}$ and in the right hand side relates it with two well known concept in magnetic confinement fusion, the dynamo(first term) and the resistive diffusion (second term). This two processes act in different time scale. More in details, for a magnetic structure of size l, the resistive diffusion time defined as:

$$\tau_R = \frac{\mu_0 l^2}{\eta} \tag{1.9}$$

is the longest time scale described by the resistive MHD equations; on the contrary, at the dynamo term corresponds the velocity propagation of the so

called Alfvén waves [8, 11, 12]:

$$v_A = \frac{B}{\sqrt{\rho\mu_0}} \tag{1.10}$$

traveling the aforementioned distance l in the time scale of the so called Alfvén time:

$$\tau_A = \frac{l}{B}\sqrt{\rho\mu_0} \tag{1.11}$$

that represents the fastest time scale in resistive MHD dynamics. This quantities can be also used in the eq.1.8 to describe the dynamics of the magnetic field in terms of τ_A, τ_R and l. The diffusion time is, thus, proportional to S^{-1}, being S the so called Lundquist number [13], defined as:

$$S = \frac{\tau_R}{\tau_A} \propto \frac{I_p T^{3/2}}{Z_{eff} log\Lambda (m_i n_e)^{1/2}} \tag{1.12}$$

where I_p is the current flowing in the plasma, T is the temperature, Z_{eff} is the effective charge due to various ion species, m_i is the ion mass and $log\Lambda$ is the Coulomb alghoritm [14]. The Lundquist number characterizes thermodynamic and turbulence properties of a fluid. Usually, being $\eta \ll 1$, S has very high values. Typically in the laboratory plasmas of thermonuclear interest $S \sim 10^6$ while in the astrophysical plasma $S \sim 10^{12}$ (solar corona).

1.2.1 MHD equilibrium and stability

Whilst the presence of a small resistivity is able to describe particular plasma behaviours, the ideal MHD allows simplifying some other important concepts of the plasma physics. Let us consider the equilibrium condition, with $\partial/\partial t = 0$ and $\mathbf{v} = 0$ in the MHD equation. We obtain:

$$\mathbf{j} \times \mathbf{B} = \nabla p \tag{1.13}$$

that describes the balance between the magnetic force and the thermal expansion force in a plasma. For the magnetic surfaces verifying this condition it is worth noting that the pressure is costant all along the magnetic field, since $\mathbf{B} \cdot \nabla p = 0$, defining a kind of costant pressure surfaces, and the current density lines lie on these surfaces, since $\mathbf{j} \cdot \nabla p = 0$.
The presence of well defined magnetic surfaces is at the bottom of the plasma magnetic equilibrium. In toroidal geometry the magnetic surfaces are nested whose cross-section in a poloidal plane forms a set of smooth closed curves.

Between these surfaces we can identify some special magnetic surfaces, the so called rational surfaces, which are characterized by the fact that their field line close upon themselves after one or several transit around the machine.
If we introduce an expression for $\mathbf{j}$ in the balance equation (eq.1.13) by using the Ampere's law, we obtain the so called pressure balance condition:

$$\nabla\left(p+\frac{B^2}{2\mu_0}\right)=\frac{1}{\mu_0}(\mathbf{B}\cdot\nabla)\mathbf{B} \tag{1.14}$$

where the equilibrium condition is realized by the balance between the gradient of magnetic and kinetic pressure against the action of bending and parallel compression of the magnetic field. The ratio between the averaged p over the plasma volume and the magnetic pressure, defines an important parameter for the MHD equilibrium $\beta =< p > /(B^2/2\mu_0)$. The toroidal or the poloidal magnetic field separately can be used in the above definition, and in this case the β parameter is called poloidal β_θ or toroidal β_ϕ respectively.
In order to study the equilibrium stability is, however, convenient studying the resistive MHD. The aforementioned equation system (eqs.1.3,1.4,1.5,1.6) predict that under certain conditions a small perturbation in a fluid quantity, like for example the density, the fluid velocity, or the magnetic field, can grow unstable in time. These phenomena are called MHD instabilities [2, 3, 15]. They are present in all the toroidal fusion devices, where they influence in many ways the global plasma properties, and can deteriorate the plasma confinement performances.
It is useful defining the toroidal coordinates (r; θ; ϕ): r is called radial coordinate, θ and ϕ are the poloidal and toroidal angles, respectively. With R and a we indicate the major and minor radius of the torus. A perturbation $\tilde{\mathbf{A}}$ of a quantity $\mathbf{A}$ in a toroidal plasma can be analyzed in terms of Fourier formalism as follows:

$$\tilde{\mathbf{A}}(r,t)=\sum_k \tilde{A}_k(r)e^{i(\mathbf{k}\cdot\mathbf{r}-\omega t)}=\sum_k \tilde{k}(r)e^{i(m\theta+n\phi-\omega t)} \tag{1.15}$$

where $\mathbf{k}=(k_r,k_\theta,k_\phi)=(k_r,m/n,n/R)$ is the wavevector in toroidal coordinates, and m and n are the poloidal and toroidal mode number, respectively. Each couple (m,n) represents a helical perturbation, or mode. A helical magnetic perturbation with wavevector $\mathbf{k}$ can become unstable if it fulfills the resonance condition $\mathbf{k}\cdot\mathbf{B}=0$, where $\mathbf{B}=(0;B_\theta;B_\phi)$ is the equilibrium magnetic field.
We, now, introduce a crucial parameter for the toroidal device stability, the

so called safety factor q, which is defined as a function of radius as:

$$q(r) = rB_\phi/RB_\theta \tag{1.16}$$

This quantity is related to the fact that in the toroidal devices both a poloidal component B_θ, which is mainly generated by an externally driven toroidal plasma current j_ϕ, and a toroidal component B_ϕ, which in some configurations is only in part produced by currents owing in external conductors, are present. The inverse of this quantity represents the number of poloidal turns done by a helical field line per one toroidal turn.
In terms of safety factor q the aforementioned resonance condition leads to a conclusion that the helical MHD instabilities can grow only at radial positions where q assumes rational values (that is $q = -m/n$). These crucial positions are called rational or resonant surfaces.

1.3 Magnetic confinement in toroidal devices

Several magnetic field geometries have been investigated for many years in fusion research to seek the best conditions for plasma confinement. Up to now, the toroidal geometry has given the best confinement performances. This section will be dedicated to a brief introduction to the principles of magnetic plasma confinement in toroidal devices, lying at the bottom of the so called Tokamak (the most widespread magnetic configuration) and Reversed Field Pinch (on which we more carefully focused).

1.3.1 Tokamak

The main concept of Tokamak was proposed in 1952 by two russian physicists, Tamm and Sacharov, and was realized for the first time by another russian scientist, L. A. Artsimovich [16]. We will treat here the basic features of this configuration.
The tokamak is a toroidal device in which the poloidal magnetic field is created by the toroidal current I_p flowing through the plasma. A strong toroidal magnetic field is generated by a toroidal field coil system. The toroidal current is induced by means of a transformer and the plasma itself form the secondary winding of the transformer, the primary being wound on an iron core. The toroidal geometry of the plasma leads to two hoop forces which are both in the direction to expand the plasma ring. The first of these forces results from the natural tendency of a current loop to expand in an effort to lower its magnetic energy. The second force is the resultant of the sum of

centrifugal and $\nabla \cdot \mathbf{B}$ forces experienced by the individual particles during their motion along the field lines. Both these forces can be compensated by providing a vertical magnetic field that interacts with the toroidal current to give an inward force.
If the applied vertical field is spatial non-uniform and increases with the major radius, the plasma turns is found to be vertically unstable. Such a vertical field shaped is e.g. mandatory when, in attempt to increase the plasma pressure, the plasma is pushed as much as possible to the high field side, thus creating a D-shaped plasma, i.e. having elongation and triangularity. An externally applied horizontal magnetic field can then be used to maintain the plasma well centered.
Stability criterion for tokamak configuration gives restrictive condition on the value of q on axis and at the edge of the plasma. It can be shown that the conditions are [14]:

$$q(r) > 1, ; \quad q(0) \geq 1, \quad \frac{q(a)}{q(0)} \geq 3 \tag{1.17}$$

The criterium $q(r) > 1$ is also known as Kruskal-Shafranov limit and is very important for stability reasons, since the presence of a $q = 1$ surface would destabilize a strong $m = 1, n = 1$ kink instability which would cause severe confinement losses, and in some cases violent current disruptions.
This condition requires also $B_\phi \gg B_\theta$ and with a typical values $R/a \approx 3$ it turns out to be $B_\phi \geq 10 B_\theta$. Thus imposes a limitation on the maximum achievable plasma current through Ohmic heating. For this reason additional complex heating methods, like for example neutral beam or radiofrequency heating, are needed to reach thermonuclear conditions.

1.3.2 RFP

The Reversed Field Pinch (RFP) [17, 18] is an axisymmetric toroidal system in which the plasma is confined by a combination of a toroidal field B_ϕ, produced largely by poloidal currents in the plasma, and a poloidal field, B_θ, produced by the plasma current flowing round the torus.
The RFP aims to confine the plasma exploiting the same pinch effect also lying at the bottom of the Tokamak theory. The main difference is, instead, represented by the magnetic field components amplitude (being $B_\theta \approx B_\phi$ in the RFPs and $B_\theta \ll B_\phi$ in the Tokamaks) and behaviour (B_ϕ reverses its sign at the edge in the so called reversal region), as shown in fig.1.2. In terms of safety factor $q = rB_\phi / RB_\theta$ (where a and R are respectively the minor and the major radius) this means that for the RFP $q < 1$ all along the minor

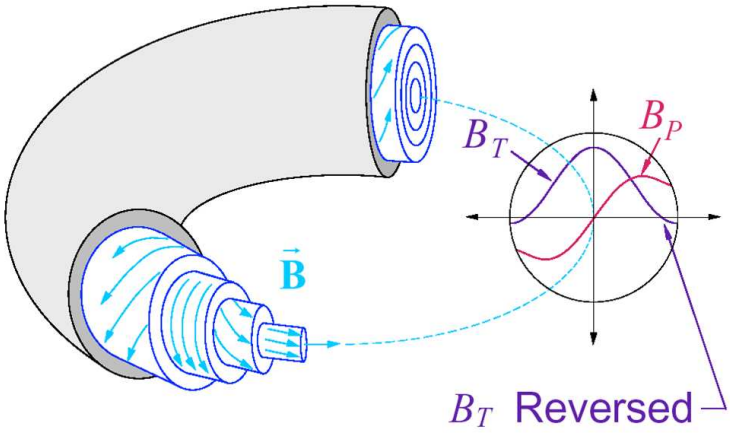

Figure 1.2: Sketch of the main RFP magnetic field configuration. On the right the radial profiles of B_ϕ (blue) and B_θ (red).

radius a (see fig. 1.3).
In general, the RFP concept covers an important role in the plasma physics and in the fusion science for two reasons.
First, it represents an alternative configuration to the Tokamak one, and can explore the same plasma current range despite a magnetic field demand one order of magnitude lower. For this reason, although severe limitations in terms of confinement properties (discussed further on), a possible RFP fusion reactor could be in principle technologically less challenging.
The second point of remark is that the RFP equilibrium and many its peculiar properties can be explained on the basis of relaxation theory [19], dynamo effect and other important objects of the study of plasma physics and astrophysics also beyond the energy production by the nuclear fusion.
Hystorically, a spontaneous self-generated reversed toroidal field at the wall was observed for the first time in the ZETA experiment (a pinch device) [20, 21] at Harwell in the mid 1960s. Some discharges revealed a so called "queiscient period" of long stability and improved confinement in a system that otherwise appeared to prove itself unstable. Edge field reversal was also observed in several early toroidal devices ([17] and references therein). However, the appearance of reversed field was both unexpected and incosistent with the predictions of theory [22] prevailing at that time, so that this configuration experienced only a modest expansion until the early 1970s.
The theoretical foundations of the Reversed Field Pinch configuration was layd only later thanks to the Taylor's model [19] published in 1974 and based on variational principle. He explained the RFP equilibrium demonstrating

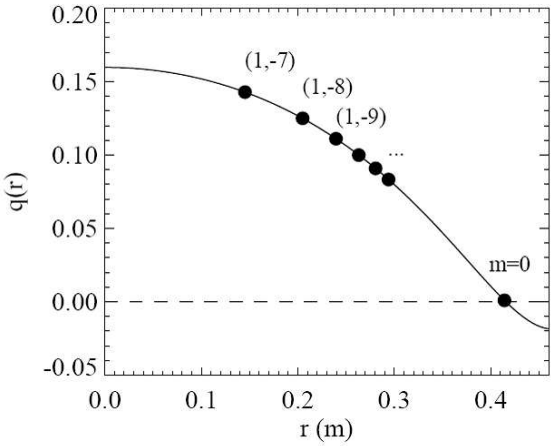

Figure 1.3: Typical RFP radial profile of the safety factor $q = aB_\phi/RB_\theta$. Many resonance surfaces for the MHD instabilities (marked with the poloidal and toroidal Fourier components m, n) are present in the internal plasma layers. The $q = 0$ region is a resonance surface for all the MHD instabilities with $m = 0$ toroidal periodicity.

that it represents (under some assumptions) a near minimum energy state to which the plasma spontaneously relaxes. More in details, it is obtained by minimizing the magnetic energy W, written as:

$$W = \int \frac{B^2}{2\mu_0} \tag{1.18}$$

with respect to the single constraint that the total magnetic helicity K:

$$K = \int_V \mathbf{A} \cdot \mathbf{B} dx \tag{1.19}$$

is invariant (being V the plasma volume). $\mathbf{A}$ is the vector potential given by $\mathbf{B} = \nabla \times \mathbf{A}$. This implies to impose slow variations of K with respect to W (condition experimentally verified [23]). A system like that, which conserves the toroidal flux, has a energy minimum state ($\delta [W - \lambda K]$) at the equilibrium in a so called *force-free* configuration ($\nabla p = 0$), described by the equation:

$$\nabla \times \mathbf{B} = \mu \mathbf{B} \tag{1.20}$$

where the magnetic permeability μ is constant in space and the current is everywhere parallel to the magnetic field.
In a cylindrical geometry the solution for the eq.1.20 is given by the zero-

order J_0 and the first order J_1 Bessel functions:

$$B_r = 0, \quad B_\theta = B_0 J_1(\mu r), \quad B_\phi = B_0 J_0(\mu r). \quad .$$

The derived model is called the Bessel function model (BFM) and the magnetic field components behaviour approximatively reproduces the experimental one shown in fig.1.2. For a complete description of BFM solutions it is useful introducing two parameters, the *reversal parameter* F and the *pinch parameter* Θ defined as:

$$\Theta = \frac{B_\theta(a)}{< B_\phi >} \quad F = \frac{B_\phi(a)}{< B_\phi >} \tag{1.21}$$

where $< B_\phi >$ is the average of B_ϕ over the poloidal section. In general,

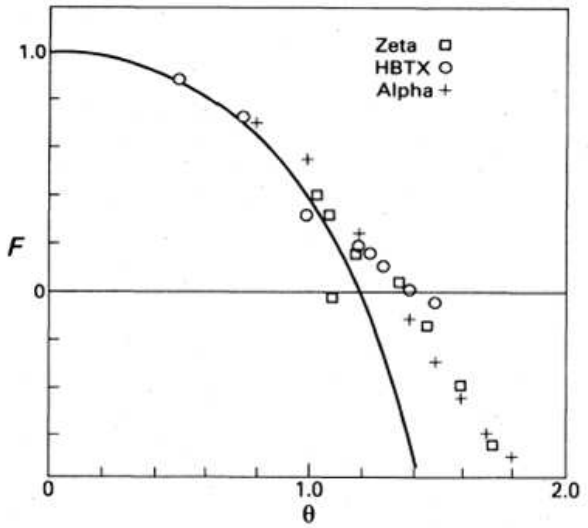

Figure 1.4: Schematic $F - \Theta$ diagram as predicted by the BFM model (continuous line) and experimental values found in different devices.

since the toroidal field reverses for $r \leq a$, in the RFP the reversal parameter F is always negative and the value Θ is usually high. On the contrary, the Tokamaks could be characterized with low Θ values and F positive everywhere.
The most common way to display the BFM model predictions is the $F - \Theta$ diagram (fig.1.7), in which the RFP states (the configurations with a edge reversed toroidal field) are supposed to exist for $\Theta > 1.2$. The experimental points overplotted in the same figure show a qualitatively reasonable agreement. Anyway there are some discrepancies likely due to a radial profile of

$\mu(r)$ not uniform and to the impossibility to experimentally realize a purely force-free configuration because of the presence of a non-zero pressure gradient.
For a more quantitative analysis of equilibria in RFP plasma, two main models were proposed later, the Modified Polynomial Function Model (MPFM) [24] and the so called $\mu\&P$ model [25]. Both of them had to introduce a perpendicular current density, related to the presence of pressure gradient, and allow the parameter μ to have a radial dependence.

Configuration sustainment and dynamo effect

According to the linear MHD theory, in a resistive plasma, the currents would decay with a characteristic resistive time, τ, which would tend to flatten the toroidal field profile and thus to loss the magnetic reversal. In fact the RFP, as a static conductor subjected to resistive diffusion, is described by the following equation:

$$\frac{\partial \mathbf{B}}{\partial t} = \frac{\eta}{\mu_0}\nabla^2\mathbf{B} \tag{1.22}$$

The toroidal component of the magnetic field is expected to decade exponentially with the time constant τ. Generally, the experimental evidence demonstrated as the RFP configuration lasts as long as the plasma current is sustained, thus also longer than the predicted resistive diffusion time (fig. 1.5). This suggests that some mechanism is necessary to regenerate the mag-

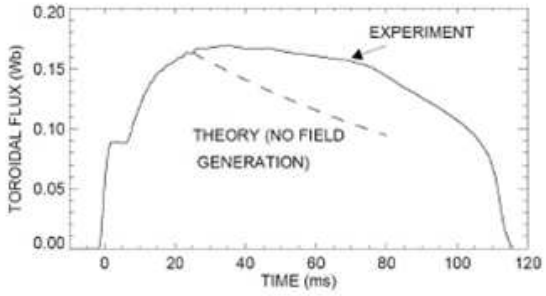

Figure 1.5: Example of experimental evolution of the toroidal flux and expected behaviour from the linear MHD

netic field continuously lost through resistive diffusion.
A way to formally display the presence of this peculiar RFP mechanism is

writing the Ohm's law for the component parallel to the mean field:

$$E_{\|} = \frac{(\mathbf{E} + \mathbf{u} \times \mathbf{B}) \cdot \mathbf{B}}{B} = \eta j_{\|} \tag{1.23}$$

$E_{\|}$ has the same form of B_{ϕ}, reversing its sign at the edge. On the contrary from the eq.1.23 $E_{\|}$ should follow the $j_{\|}$ profile that experimentally is found to flow always in the same direction (see fig. 1.6).

This discrepancy is usually related to the so called dynamo effect [12, 26]. In

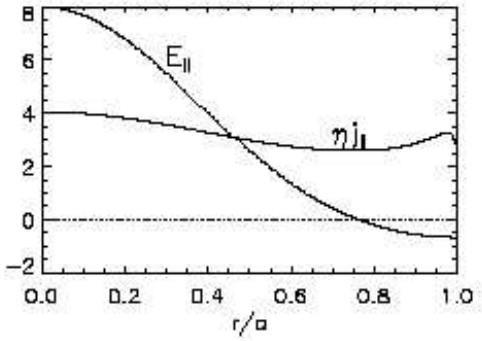

Figure 1.6: Typical radial profile of $E_{\|}$ and $\eta j_{\|}$ in a RFP configuration. The discrepancy is accounted for the dynamo term E_d.

fact, by separating each quantities (magnetic and velocity fields) in a mean-field plus a fluctuation term, a new electric field term arises in the parallel Ohm's law, which is called dynamo electric field E_d, and is given by the coherent interaction of the velocity and magnetic field fluctuations :

$$E_{\|} + E_d = E_{\|} + < \tilde{\mathbf{v}} \times \tilde{\mathbf{b}} >= \eta j_{\|} \tag{1.24}$$

The sustainment of the RFP configuration is, thus, strongly related to the presence of a self-organized velocity field in the plasma (dynamo). More in details, this process implies the existence of a finite plasma resistivity on which can arise the MHD *tearing* instabilities responsible for the dynamo term and for another quite peculiar RFP feature that will be treated in the next section.

Multiple Helicity

In its standard operation, the RFP is actually characterized by a broad spectrum of resonant MHD instabilities (see fig.**??**), supposed, until the recent

RFP results (see next chapter), necessary for the sustainment of the reversed configuration through the dynamo mechanism.

In particular, these instabilities are driven unstable by a gradient in the

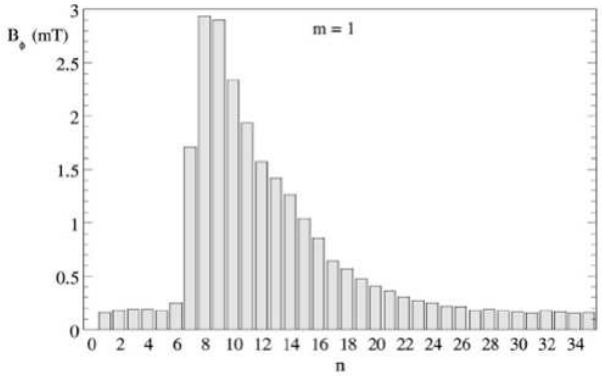

Figure 1.7: Typical RFP spectrum of the MHD tearing instabilities.

current density parallel to the magnetic field and are known with the name of *tearing* modes [27]. This name comes from the fact that the magnetic field lines tear and reconnect during the mode evolution: it is possible to show that, when this gradient is sufficiently high, a tearing instability is triggered, which causes the magnetic field lines to bend and reconnect. The resultant magnetic configuration is characterized by the formation of a so called magnetic island.

The q profile shown in fig.1.3 highlights the presence of several resonant surfaces in the region internal to reversal surface. In particular, all the tearing modes with periodicity $m = 1$ and $n \leq 2/(Ra)$ can be simultaneously destabilized (Multiple Helicity). The superposition of the islands due to these resonant magnetic perturbations tends to destroys the magnetic surfaces in the innermost plasma with a detrimental effect on the global confinement and usually leads to a complete stochastization of field lines. As already mentioned, the continuous excitation of these modes and their non-linear interaction is also at the bottom of the RFP configuration sustainment, through the dynamo effect.

Moreover, at the edge, where well conserved magnetic surfaces could be exist unperturbed, the presence of reversal surface ($q = 0$) destabilizes all the modes with $m = 0$,$n \geq 1$ periodicity, being itself a resonant surface for these instabilities. Thus, the edge field lines appears strongly modified by the presence of the magnetic islands related to this mechanism (see section 2.2).

Finally, a complex non-linear interacting mechanism between $m = 1$ and $m = 0$ modes leads to the growth of a localized plasma deformation (see

fig.2.8). This is due to a coupled $m = 0, n = 1$ instability, also known as Slinky or Locked Mode [28, 29] causing a strong stationary plasma wall interaction. This represented a severe limitation in the RFP performance but was always thought as an unavoidable ingredient for the dynamo mechanism. In the following chapter, on the opposite, the recent results obtained on the RFX-mod device (the largest RFP in operation) will show how a reversed configuration sustainment is possible also with the presence of a single dominant tearing mode in the so called QSH state.

Chapter 2

The RFX-mod experiment

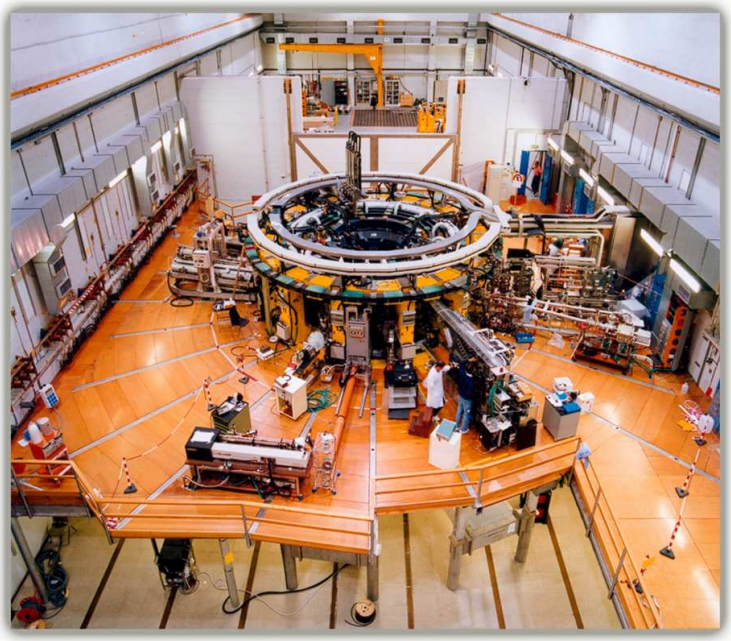

Figure 2.1: Top view of the RFX-mod experiment.

2.1 Main features and latest results

The **R**eversed **F**ield E**X**periment *modified* (RFX-mod) [30], the upgraded version of the previous RFX [31], is a toroidal device for the study of the magnetically confined plasma in the RFP configuration. Located at the Ionised Gas Institute (IGI) [32] of the National Research Council (CNR) [33]

of Padova, it is operational since 2004 under the management of the Consorzio RFX, a research organization promoted by CNR, ENEA (the Italian National agency for new technologies, Energy and sustainable economic development) [34], University of Padova [35], Acciaierie Venete S.p.A. (a private partner) [36] and INFN (the Italian National Institute of Nuclear Physics) [37], within the framework of the Euratom - ENEA Association.
The mission-oriented RFX fusion science program is shaped to provide a focused contribution to ITER and its accompanying fusion program [38].
The main parameters of the RFX-mod device (the largest RFP in operation) are shown in the tab.2.1. As in all RFPs, plasma heating is purely ohmic. Although a toroidal magnetic field ten times smaller (the whole magnetic system is shown in fig.2.2), this device allows exploring current regimes (up to 2 MA) comparable to those of the large tokamaks.

With respect to the original RFX design, the present machine underwent

Table 2.1: Main RFX-mod parameters.

Major radius	2 m
Minor radius	0.459 m
Toroidal magnetic field	≤ 0.7 T
Plasma current	≤ 2 MA
Discharge duration	≤ 0.5 s
Plasma density range	$\approx 1 \div 10 \times 10^{19} m^{-3}$
Plasma volume	$\sim 10\ m^3$

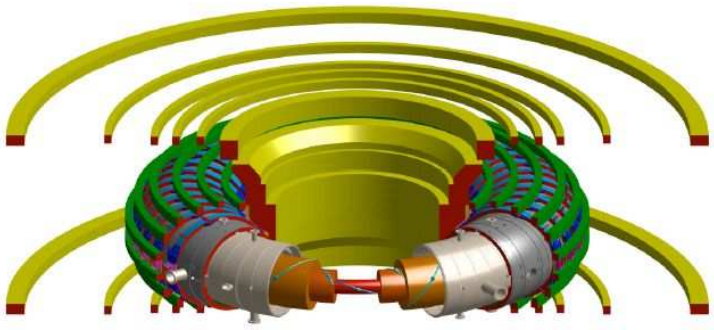

Figure 2.2: Magnetic system of RFX-mod: the magnetizing winding (yellow), the field shaping coils (green), the toroidal ciricuit (blue).

some crucial modifications that allowed significant performance improvements.
The original RFX thick stabilizing shell (which had a magnetic field penetration time constant shell = 500 ms) was replaced with a thinner one, whose

time constant for penetration of vertical magnetic field ($\approx$ 50 ms) is $\approx$ 10 times shorter than pulse duration. Moreover, RFX-mod has been equipped with the one of the most advanced system for feedback control of MHD stability with active coils among the fusion devices. The system is based on 192 active saddle coils, which cover the whole plasma boundary (fig. 2.3). The coils are arranged in 48 toroidal locations; in each toroidal location there are 4 poloidal coils, according to the low m/high n structure of MHD modes in the RFP (where m and n are the poloidal and toroidal mode numbers, respectively). Each coil is independently driven by individual power supplies and can produce a radial magnetic field up to 50 mT dc and 3.5 mT at 100 Hz [30, 39, 40, 41]. Different algorithms for real-time tearing modes control has been developed to exploit the full capability of the feedback system, the most important being the Virtual Shell (VS) scheme [40] and the Clean Mode Control (CMC) [42]. The latter, in particular, has drastically changed the performance of the device, reducing the amplitude of the dynamo modes at the plasma boundary, mitigating their phase and wall locking and finally removing the aliasing of the sidebands limiting the VS control scheme [43].

Another important modifications concerned the first wall, composed by

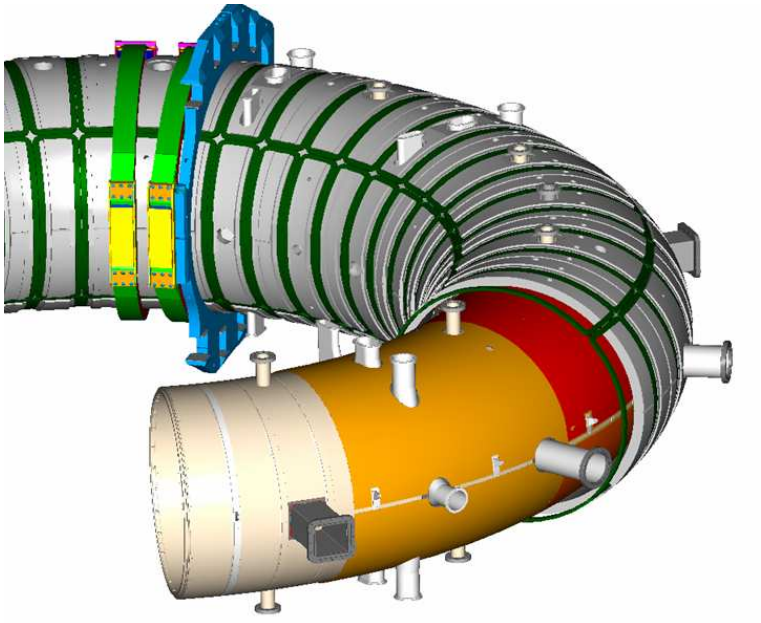

Figure 2.3: Set of 192 saddle coils (4 poloidal positions $\times$ 48 toroidal positions) surrounding the RFX-mod shell

2016 graphite tiles, covering completely the inner part of the vacuum vessel. In the new machine the tiles have been redesigned to achieve a more uniform

power deposition on the plasma facing surface, to minimize the emissivity due to plasma wall-interaction and finally to give housing to a large number of in-vessel probes. These design requirements led to a substantial reduction of the tile thickness with respect to the original design [44].
By way of example of the effect of these hardware and software modifications, in fig.2.4 the progressive improvements in the maximum plasma current as well as in the duration of the RFX-mod discharges are shown [38].

The plasma current increase (the 2 MA have been achieved in 2010) is

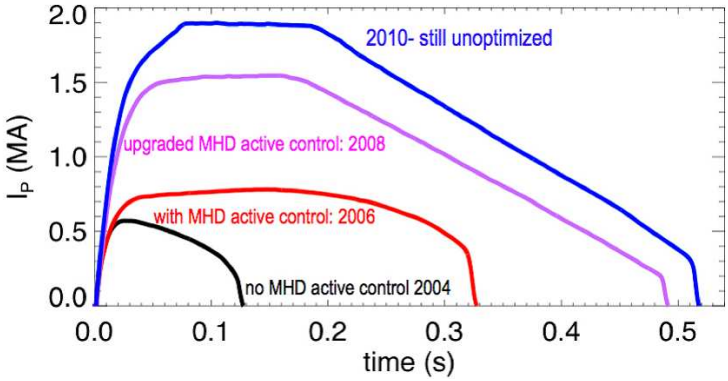

Figure 2.4: Plasma current waveforms obtained in RFX-mod since its restart in December 2004

only the most evident one among a turn of outstanding achievements that considerably enhanced the interest about the RFX-mod developments and enriched the RFP physics.
In fact, the traditional picture of a poor confinement characterising the RFP plasmas was overcome by the discovery of a spontaneous transition towards even more attractive self-organized equilibria, namely the *Q*uasi *S*ingle *H*elicity (QSH) and the *S*ingle *H*elical *Ax*is (SHAx) states. In the past, the aforementioned dynamo process (see previous chapter) [12, 23, 26], linked to the RFP self-organization, led to a quite chaotic configuration. The destabilization of a wide spectrum (in terms of Fourier components with m and n respectively the poloidal and the toroidal periodicity) of $m = 1$ modes (*M*ultiple *H*elicity states) and the subsequent superposition of the associated resonating plasma layers caused the magnetic surfaces destruction giving rise to a stochastic plasma core [45].
Whilst the previous regime was expected by several theoretical predictions [46, 47] to be improved by the existence of a RFP state featuring a single dominant mode (*S*ingle *H*elicity state), the first experimental observations of a regime intermediate between MH and SH are more recent [48, 49, 50].

Since the amplitude of the secondary modes is still finite, they have been dubbed as Quasi Single Helicity states. These states are characterized by a different whole tridimensional magnetic topology according, in RFX-mod, to the innermost resonant $m = 1$, $n = 7$ mode helicity (see fig. 2.5).

A further plasma current increase ($I_p > 1.5$ MA) has been accompanied

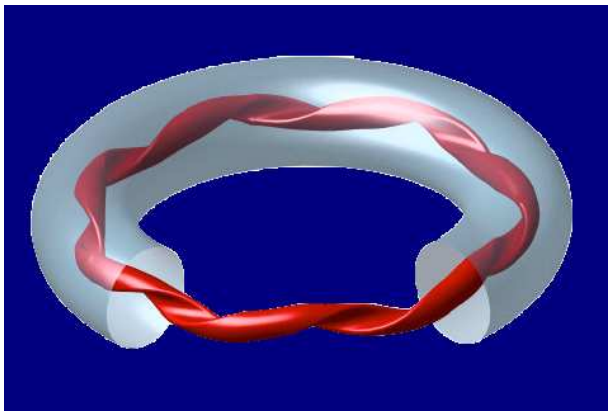

Figure 2.5: Internal flux surface of the helical plasma during SHAx states

by the observation of a new class of QSH states named single helical axis (SHAx) [51, 52], previously numerically predicted [53]. These states are characterized by a purer single helical spectrum with a further reduction in secondary modes and an amplitude of the dominant mode which exceeds a threshold of approximately 4% of the total magnetic field at the edge (see fig.2.6). This transition is accompanied by a further deep modification of the magnetic topology with respect to standard QSH states: indeed in the SHAx the O-point corresponding to the magnetic axis and the island X-point collapse one onto the other, the island separatrix is expelled from the plasma and the island O-point survives as the main magnetic axis of a spontaneously occurring helical plasma.

In both QSH and SHAx cases, periodical back-transitions towards the MH state occur. However, the QSH properties (magnetic order and duration) are experimentally found to favourable scale with the Lundquist number S and with the plasma current increase [52].

At the same time, also the thermal and transport properties appear strongly modified by the magnetic topology changes.

Thanks to the presence of well conserved magnetic flux surfaces in the core, a hotter region ($T_e \geq 1$ keV) occupying a good fraction of the total plasma volume is created (see fig.2.7). Electron internal transport barriers (eITB) develop at high plasma current [54, 55] and strong temperature gradients are observed. At the extreme edge the preliminary observations of external

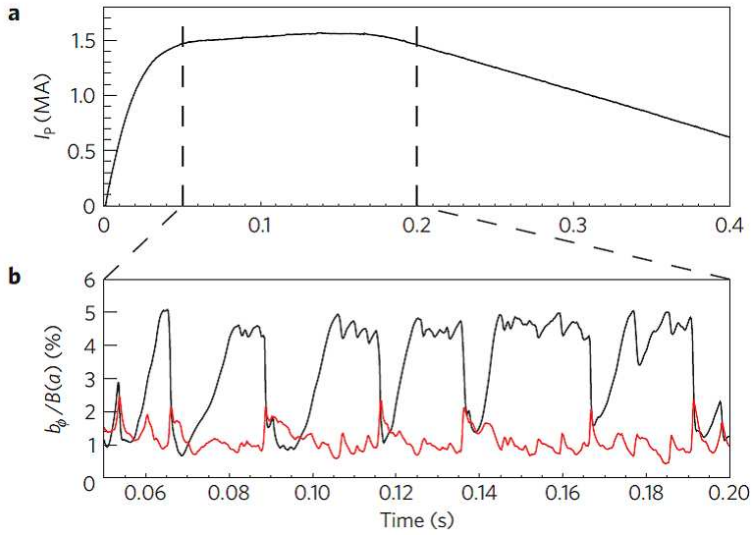

Figure 2.6: **a**.Plasma current as a function of time. The vertical dashed lines delimit the so-called flat-top phase of the discharge. **b**.The black curve shows the amplitude of the m=1,n=7 dominant mode during the flat-top phase of the discharge, and the red curve shows the amplitude of the secondary modes, defined as the square root of the sum of their squared amplitudes. The periodical back-transitions to the MH state are marked by the strongly decrease of the dominant mode amplitude.

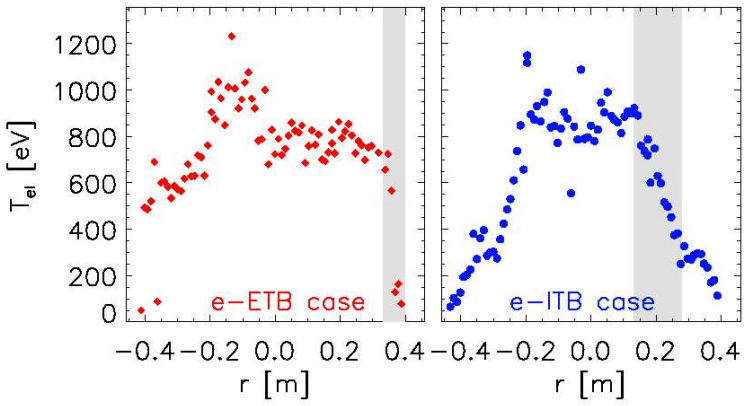

Figure 2.7: Electron temperature profiles in high plasma current RFX-mod discharge featuring electron edge (left) and internal (right) transport barriers.

transport barriers [55] deserve further deepenings (fig.2.7).

2.2 The RFX-mod edge

The RFX-mod edge is a quite complex region characterized by a very fast dynamics and a turn of outstanding phenomena. Definitely, most of them are linked to the inversion of the toroidal component B_ϕ of the magnetic field in the so called reversal region (see fig.**??**).
The magnetic topology, for instance, is the mirror of this condition. In fact, all the m=0 MHD modes resonate, due to the presence of a q=0 surface, creating a chain of poloidally symmetric islands in the outer plasma. The radial position of these islands can be externally imposed by setting the value of the so called reversal parameter F defined as $F = B_\phi(edge)/ < B_\phi >$ (see previous chapter).
Globally, at more markedly negative F values ($F < -0.15$) the m=0 islands close entirely into the chamber (see fig.2.8), while for F values close to 0 or shallow ($F > -0.05$), the island field lines intercept the first wall before closing again [56].
In the MH regimes, the $m = 0$ modes tend to phase lock to each other and,

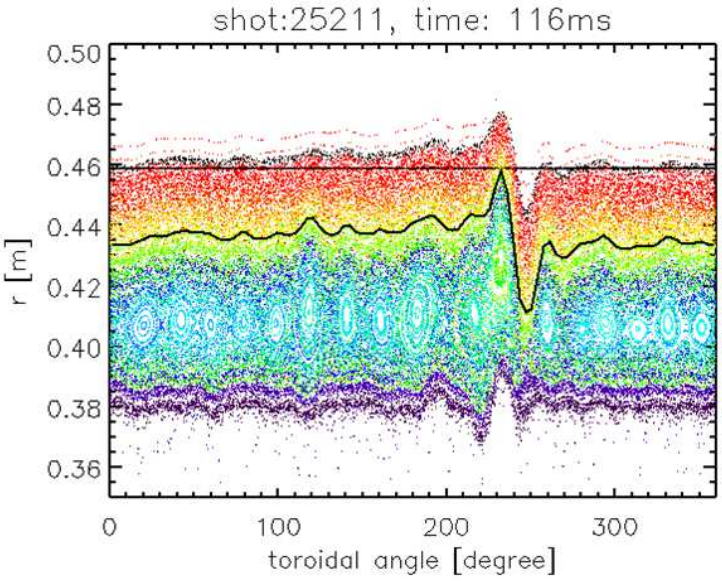

Figure 2.8: Poincaré plot in the (r, ϕ) plane of the outer region of the RFX-mod device for a MH state and a deep F value. The $m = 0$ island chain is evident at around $r = 0.4$ m.

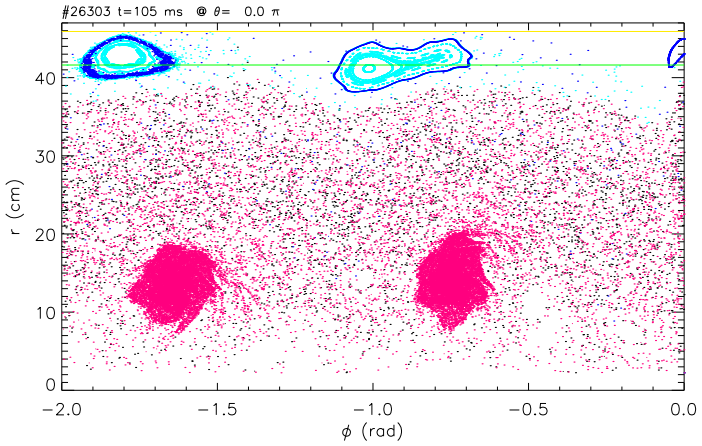

Figure 2.9: Zoom of a Poincaré plot in the (r, ϕ) plane for the equatorial region made by the ORBIT code. The $m = 0$ island chain (blue) and the more internal $m = 1$ deformation (red) are shown.

according to their phase relation, toroidally close to the $m = 1$ phase locking position [57, 58]. Thus, the topological characteristics of the external region in these regimes is quite complicated, with the large helical deformation due to phase and wall locking of the m = 1 modes and the funnel-like shape of the plasma column due to the aforementioned phase locking of the m = 0 modes. Interpretation of data coming from this region of the plasma requires, consequently, a detailed comparison with the local magnetic topology. Fig.2.8 shows an accurate reconstruction of the outer region of the RFX-mod experiment referred to a MH state, obtained with a Field Line Tracing (FLiT) code [59].
In the customary high plasma current RFX-mod operations, the transition to the Quasi Single Helicity states drastically changes this picture. In fact, the inner (m=1, n=7) helical structure toroidally rotating during the QSH states imposes a similar toroidal n=7 periodicity to the aforementioned $m = 0$ pattern. The phase relation between the $m = 0$ islands and the main helical $m = 1$ deformation is defined by the tridimensional geometry. In the equatorial region ($\theta = 0$, where the main diagnostic systems are located) a reconstruction made by the another field line tracing code (ORBIT [60], [61]) reveals a phase $\Phi = \pi/4$ between the two maximum $m = 0$ and $m = 1$ deformations (see fig. 2.9). As result of this mode coupling the external region presents a more regular behaviour in which the islands field lines can eventually act as a kind of divertor for the inner confined plasma [56] operating at shallow F values (see fig.2.10). This topological change has a direct

beneficial effect on the global confinement since the $m = 0$ islands intercepting the wall in different toroidal positions mitigate the strong plasma-wall interaction occurring in the phase locking position during the MH states.

Nevertheless, locally the m=0 deformation can slightly differ, because of the presence of secondary modes of the dominant (m=0,n=7) mode, so that the local edge picture sometimes can not be simply described by a single global parameter (the F value, for instance) even in the QSH regimes.

Furthermore, all of the RFP scenarios are characterized by a significant sawtooth activity related to dynamo relaxation events that periodically determine a temporary 'back transition' (see previous section) from the QSH towards a more chaotic MH state and usually destroy the precast magnetic order [62] also at the edge. The time evolution of the F signal clearly shows rapid changes linked to these phenomena analogously to the behaviour of the dominant mode amplitude (see fig.2.6).

To analyze this extremely lively region the reconstructions made with the field line tracing codes, such as FLiT, are very useful. Unfortunately such a code needs a non negligible time to produce a single snapshot at a fixed time instant. Studying the edge evolution solely with this tool appear a hard task. For this reason, in order to compare the time evolution of the magnetic topology with the diagnostic data for instance, could be easier considering the local displacements ($\delta_{m=0}$, $\delta_{m=1}$) respectively due to the m=0 and the

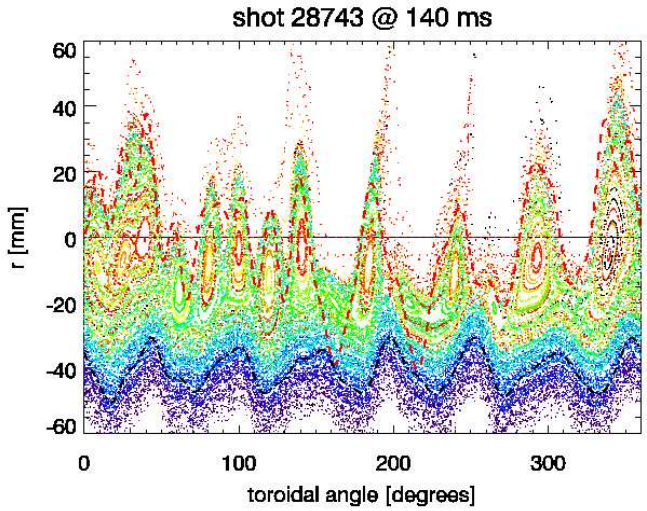

Figure 2.10: Poincaré plot in the (r, ϕ) plane of the outer region of the RFX-mod device for a QSH state. The local displacement $\delta_{m=1}$ (dashed blue line) and the more external $\delta_{m=0}$ (dashed red line) are overplotted.

m=1 MHD modes [63]. These two signals are reffered to the average shift of the plasma column and, superimposed on the Poincaré plot in fig.2.10, even if in a less accurate way, allow to figure the periodic deformations at the edge. In the next chapter, this two signals will be often recalled as most immediate tool to investigate the edge topology dynamics.

2.3 Open issues and aim of the work

The previously depicted improved regimes have found to appear solely at low values of collisionality, with $n_e/n_G \leq 0.25$, being n_G the Greenwald parameter [64]. QSH and SHAx states can not usually be obtained at high n_e values. This represents a kind of empirical limit at the moment for the RFX-mod operations, likely due to edge phenomena and in particular to localized plasma wall interaction (PWI) [65] which leads to a density accumulation and plasma cooling. Even the aforementioned back-transitions to the MH states are attributed to reconnection events [38, 62] linked with a non uniform PWI.
The localized PWI is also considered responsible for the poor density control in the RFX-mod discharges [66] together with the high fuel (hydrogen) recycling caused by the first wall graphite tiles. Moreover, the neutral particles coming from the wall in this process would favour the formation of hollow density profiles and, thus, the disappearance of the transport barriers characterizing the improved SHAx regimes.
Since the optimization of the high density regimes is, however, crucial to make the confinement improvements fusion relevant, the RFX-mod research activity is moving in two interconnected directions.
From the operative point of view, different wall conditioning techiniques have been already tested to mitigate the graphite wall response to the plasma interaction. The preliminary lithization by means of Li pellet injection [67] showed some beneficial effects on the edge density and temperature profile, but the Lithium quantity injected was too low to have very significant improvements. An alternative technique is represented by the glow discharges [68] that can empty the wall by the hydrogen absorbed during the operations. Also this techinque showed effective results on the density control although limited to the subsequent discharges.
On the other side, a great diagnostic and theoretical effort is devoted to understand the complex edge dynamics in order to achieve a better control of the PWI.
The work presented in this thesis follow to a large extent this latter branch of research. In particular, the RFX-mod edge is characterized by means of a mi-

crowave reflectometer and an insertable Gundestrup probe able to reveal the local density and flow properties in several operative conditions. The theoretical and operational development of the experimental equipments are also described. The different regimes and the different associated edge density features have been monitored with the Reflectometer, aiming to possibly individuate the main phenomena leading to a local enhanced PWI. The plasma flow components, now recognized to have an important role in the formation of the QSH states [69] in the RFPs, are evaluated and studied with the Gundestrup probe. In both cases, the relation with the edge magnetic topology is investigated and discussed as an unseparable ingredient to understand the RFP edge mechanisms.

2.4 Diagnostic tools

Even if the reconstruction of the edge magnetic topology represents a crucial support to investigate the edge properties, the presence of a superposition of different phenomena, often makes the data interpretation very difficult. The estimation of whatever quantity at the edge made by any kind of diagnostic has to take into account several effects that can affect the measurement: the periodical sawtooth activity, the global density fluctuations (due to the poor control), the global magnetic regime, the local modulation imposed by the QSH tridimensional geometry, the first wall response to the conditioning (lithium injection, glow, boronization) etc... However, while the analysis of the data coming from a single diagnostics could be inadequate for a deep investigation, the cross-checks between the large diagnostic set operating on the edge of RFX-mod turned out to be very useful.
In particular, in this thesis work many comparative analyses are presented in order, for instance, to confirm the reliability of an experimental result or the applicability of an interpretation model. The main features of the microwave reflectometer and the Gundestrup probe are extensively presented in the chapters 3 and 4 respectively. A brief description of the other diagnostic system installed in RFX-mod and used in this analysis follows:

- a **multichord interferometer** (located at the toroidal angle $\phi = 22.3°$ and the poloidal angle $\theta = 0°$) [70, 71], which measures the electronic density averaged along 14 lines of sight. The density is evaluated measuring the phase variation induced in a CO_2 laser beam ($\lambda = 10 : 6\mu m$) that passes through the plasma;

- a **Thomson scattering** diagnostic ($\phi = 82.3°$, $\theta = 0°$) [72], which provides a 84-point radial profile of electron temperature by analyzing the scattering properties of the plasma when a high power laser beam is injected; the repetition rate is of about 25 ms, for a maximum number of 10 pulses in a discharge;

- a **Edge Thomson Scattering** ($\phi = 52.3°$, $\theta = 0°$) [73], which provides a 6-point radial profile of the edge (r/a = [0.8÷1]) electron temperature analgously to the main Thomson scattering system. A single profile per discharge is provided;

- a **Gas Puffing Imaging** diagnostic ($\phi = 322.3°$, $\theta = 0°$) [74, 75], consists of a gas-puffing nozzle, an optical system for the GPI function and three triaxial magnetic pick-up coils. The optical system measures the line radiation (668 nm) emitted from locally puffed He in hydrogen discharges. The fan of 16 lines of sight (LoS) of GPI lies on the plane (r, ϕ), perpendicular to the main magnetic field at the edge. The LoS are 5 mm toroidally spaced and have an effective field-of view of 4 mm (both toroidally and poloidally). The bandwidth is 2 MHz. The magnetic system measures the time evolution of the three edge magnetic field components $\dot{B}_\theta$, $\dot{B}_r$ and $\dot{B}_\phi$. One of the radial array of LoS is used for the measurements of the edge electron temperature and density. The experimental method consists on the observation of the intensity of three emission lines of the HeI ;

- a **bolometric tomography** ($\phi = 202.3°$, $\theta = 0°$) [76, 61], which allows the imaging of the plasma radiation emissivity pattern. A four-camera imaging system (housing a total of 48 detectors) is devoted to the bolometric measurements. The detectors are low-noise metal resistor bolometers, with an active area of $3.8 \times 1.3 mm^2$. Starting by these measurements an inversion scheme allows to evaluate the complete imaging reconstruction;

- the **U-probe** ($\phi = 217.3°$, $\theta = 0°$) [77, 78] consists of two fingers, 88 mm apart each other along the toroidal direction (perpendicular to the edge magnetic field). Each finger is equipped with a 2D array of electrostatic pins and a radial array of 3-axial magnetic probes with a radial and toroidal resolution of 6 mm. This diagnostic system

(mounted on an insertable manipulator) provides local measurements of plasma density, electron temperature and floating potential as well as their respective radial gradients.

- a **triple fixed probe** ($\phi = 82.3°$, $\theta = 312°$) [79, 80], which evaluates the time evolution of the edge electron temperature T_e at a radial position $r/a = 1$ with a high time resolution (5 MHz). This device is composed by three graphite pins (measuring respectively the floating potential V_f, a reference positive potential V_{pp} and the ion saturation current I_s) located in a Macor case.

Chapter 3

Ultrafast Microwave Reflectometer

3.1 Introduction

Measuring plasma density is crucial for any fusion oriented machine. Usually, in magnetically confined plasmas several diagnostic systems, based on different basic principles, work simultaneously in order to get this kind of measurement.
Definitely, the multichannel interferometry is the most common and well established non-perturbative technique to obtain a reliable density profile, starting from the single *line averaged* measurement of each chord [81]. Unfortunately, the features of non-local and low space resolved measurement do not make it suitable for density fluctuations studies or for monitoring the localized events taking place at the edge of Tokamaks and Reversed Field Pinches.
On the other hand, an alternative technique as the use of the insertable Langmuir probes (discussed in the next chapter), even if characterized by a sufficiently high time resolution and able to reveal the local plasma properties, is nowadays limited to the extreme edge, because of the huge power loads delivered in the large fusion devices. Moreover, all of the information gathered from the insertable probes has to take into account the perturbation induced into the plasma by the probe itself.
In different ways, finally, other systems for density measurements as the Thomson scattering or the Spectroscopy, lack an adequate time resolution [81].
In this context, the more recent (with the respect to the aforementioned diagnostics) microwave reflectometry, featuring a very local and non perturbative

measurement, found in the past years an ever growing number of applications on Tokamaks: to get the edge density profile, to monitor the plasma radial position, to study the edge turbulence, the plasma rotation, etc... This diagnostic system turned out to be a very flexible and simple tool with respect to the considerable amount of information that can produce with a high temporal and spatial resolution. On the contrary, on Reversed Field Pinches reflectometric measurements were always hampered by the intrinsic properties of the edge region of this magnetic configuration characterized by a high level of density fluctuations (see section 3.3).
A significant part of this thesis is devoted to presenting a new-concept ultrafast microwave reflectometer, thought and developed to overcome these limitations on the RFX-mod RFP experiment. In particular, this chapter will deal first with a general view of the basic principles of reflectometry and then will treat in a more detailed way the simulation work and the design of the first Ka-band of the RFX-mod ultrafast microwave reflectometer.

3.2 Theoretical basis of reflectometry

The basic idea underlying any reflectometric measurement, relies in the reflection of an electromagnetic wave launched into the plasma, once it met the so called cut-off layer.
The wave theory analysis [81, 82] reveals that two characteristic modes can propagate in an uniform plasma in the presence of a constant magnetic field B_0: the O (ordinary) and the X (extraordinary) modes. These two modes are the solutions of the Appleton-Hartree formula obtained in the approximation of a 'cold' plasma (i.e. the effects of a finite temperature are not considered) for the propagation perpendicular to the mean magnetic field.
In the O-mode the electric field of the wave is parallel to the magnetic one of the plasma and the relative refraction index can be written as:

$$\eta_O^2 = 1 - \frac{f_p^2}{f^2} \tag{3.1}$$

where f is the frequency of the traveling wave and $f_p = \left[n_e e^2/(2\pi)^2 \epsilon_0 m_e\right]^{1/2}$ is the plasma frequency. The condition so that a wave can no longer propagate into a medium and is back reflected (cut-off condition), is:

$$\eta^2 \leq 0$$

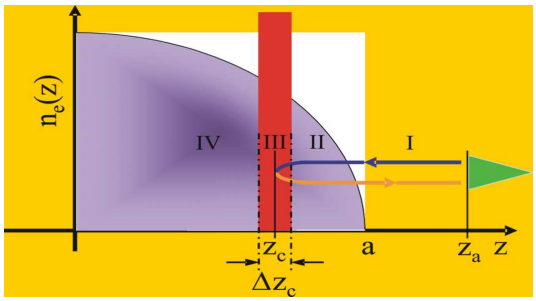

Figure 3.1: Schematic representation of the reflectometry theoretical principle

where η is its refractive index. In the case of the O-mode this condition will be written as:

$$\eta_O^2 \leq 0 \quad \Leftrightarrow \quad f \leq f_p$$

In other words, since the plasma frequency f_p is in practice only a function of the electron density n_e, an ordinary wave, launched into the plasma, will be reflected from the layer (the *cut-off* layer) with density equals to a critical density n_c:

$$n_c = \frac{m_e \epsilon_0 (2\pi f)^2}{e^2} \tag{3.2}$$

defined by the wave frequency f. Fig.3.1 simplifies the aforementioned concept.

In the X-mode propagation the electric field is polarized perpendicular to the plasma magnetic field and the refractive index η_X assumes a more complex form, since the interaction with the local magnetic field:

$$\eta_X^2 = 1 - \frac{f_p^2}{f^2} \frac{f^2 - f_p^2}{f^2 - f_p^2 - f_{ce}} \tag{3.3}$$

through the dependence on the electron cyclotron frequency $f_{ce} = eB/(2\pi m_e)$. In this case the total reflection of the wave occurs when:

$$\eta_X^2 \leq 0 \quad \Leftrightarrow \quad f \leq f_{U,L} \tag{3.4}$$

where $f_{U,L}$ are the so called *upper* and *lower* cut-off frequencies of the X-mode, both satisfying the condition 3.4. The corresponding cut-off layer will have a critical value of n_e for a given B.

In both cases the basic information required to deduce the position x_c of the cut-off layer is the *phase delay* $\Phi(f)$ introduced in the launched wave by the plasma.

Differently from the FM radar technique, from which reflectometry has come, this phase delay is not only due to the back reflection by the target (the cut-off layer for reflectometry or an aircraft for a militar radar, for instance), but suffers from the presence of a turn of layers with density $n_e < n_c$ (see fig. 3.1). Thus, in the reflectometric applications to fusion plasmas, the phase delay of the reflected wave is the result of the modications introduced by all the crossed layers, and can be expressed as [83]:

$$\Phi(f) = \frac{4\pi f}{c} \int_{x_0}^{x_c(f)} \eta(x, f) dx + \Phi_v(f) \tag{3.5}$$

where: x_0 is the radial position of the plasma boundary, $x_c(f)$ is the radial position of the cut-off layer (that, obviously, depends on the frequency f of the probing wave) and $\Phi_v(f)$ is the phase delay outside the plasma (when considering the launching antenna at a finite distance x_v from the plasma). On the other hand, analogously to the FM radars, by considering eq. 3.5, it is evident that the quantity, linked to the position of the cut-off layer x_c, is the so called *group delay*, $d\Phi(f)/df$ rather than $\Phi(f)$. This quantity is equivalent to the time of flight after which the wave reflected from the cut-off layer would come back. For this reason it is also known as *time delay* and is defined as:

$$\tau_g = \frac{1}{2\pi} \frac{d\Phi(f)}{df} \tag{3.6}$$

In practical implementations, this quantity is deduced by the comparison of the reflected signal with a *reference* signal, sent to a waveguide with known optical path.
We can perform the explicit calculation for the ordinary mode (since it is mathematically easier and is the one used in the RFX-mod reflectometer) and its refraction index η_O as defined in the eq. 3.1. By inverting eq. 3.5 and by supposing to have measured or computed and subtracted the contribution $\Phi_v(f)$ due to the wave propagation in the vacuum, we find:

$$x_c(f_p) = \frac{c}{\pi} \int_0^{f_p} \frac{\tau_g(f)}{\sqrt{f_p^2 - f^2}} df \tag{3.7}$$

This is a fundemental concept of the traditional reflectometry and involves that a sweep in the frequency of the probing wave is needed to have a measurement of x_c because it is related to the $\tau_g(f)$ knowledge (eq. 3.6). Since, in the most common applications (Tokamaks), the microwave reflectometers are used to get a broad density profile and not only the radial position of a single cut-off layers, two kinds of technological approaches have been devel-

oped to face this requirement.
In one, the frequency is swept over a broad range and the measurement of τ_g as a function of f in the range of interest allows a complete reconstruction of the relative density profile. In the other, the density profile is evaluated by the interpolation of each value of τ_g, measured by sweeping different indipendent sources over a narrow range of frequencies. This latter was also the original solution thought for RFX (see next sections).
Nevertheless, in both the configurations a further complication arises from the fact that the position of the cut-off layer is not fixed during a measurement and, usually, is affected by the presence of variable levels of density fluctuations. This latter effect, in particular, can seriously hinder a correct analysis of the reflected signal, since the τ_g detection is based on a supposed constructive interference with the plasma. Also in this case, several methods concerning improvements in either the hardware components [84] or the data processing [85] have been successfully developed in Tokamaks and Stellarators, while in Reversed Field Pinches this problem turned out to be harder to solve.

3.3 Reflectometry and density fluctuations

As already mentioned the key quantity to infer for any reflectometric scheme is the so called *time delay* $\tau_g = \frac{1}{2\pi}\frac{d\Phi(f)}{df}$, conveying the information about the position x_c of the cut-off layer inside the plasma. As long as the probed regions can be likened to a plane reflector, the analysis of the received signal in the light of the previous model is quite simple. Unfortunately, in the most part of fusion plasmas this is not the case because of the presence of the density fluctuations. It means that during a measurement (a frequency sweep) the probing wave, launched into the plasma, can experience spatial displacements of the cut-off layer and/or can be reflected by different small sub-reflectors modifying the ideal plane reflector in a rough surface. The effect of these density fluctuations can produce on the received signal large variations (with amplitude depending on the fluctuations level), up to the point of making the data interpretation physically meaningless.
This problem has from the beginning accompanied the diagnostic developments of the reflectometry on Tokamaks. Nevertheless, once optimized for this kind of analysis, some special configurations of the microwave reflectometers have represented very reliable tools to study the edge plasma turbulence properties (see for instance [84, 86, 87, 88]) being able to reveal the local plasma fluctuations with a sufficiently high temporal and spatial resolution.

Specifically, in the literature, the effect of the density fluctuations on the reflectometric measurement was split in two parts: when the refractive index, $\eta = \eta(x) + \tilde{\eta}(x)$, varies only along the direction, x, of the wave propagation (and, thus, of the density gradient) and when, instead, the spatial turbulence is spread over two dimensions, i.e., $\eta = \eta(x) + \tilde{\eta}(x, y)$. In the first case, under the condition of fluctuations located close to the cut-off layer (or, similarly, one can imagine an oscillating cut-off layer position, $x_c \equiv x_c(t)$) and characterized by sufficiently long wavelenghts, the effect on the probing wave can be still studied within the geometric optics and a correct reconstruction of τ_g requires only to adjust the frequency modulation rate to the typical time scale of the density fluctuations in order to *freeze* them during a measurement.
The problem becomes signicantly heavier to solve in the presence of $2D$ random fluctuations even with long wavelengths, since the received phase features many different random contributions. An accurate analytical and numerical analysis [83, 84], revealed how, where the fluctuations level is sufficiently high, the phase signal is completely uncorrelated with the plasma dynamics, hidden in the random noise.
In the same papers different solutions, concerning hardware improvements (such as two frequencies reflectometer, 2D array of detectors) to mitigate this deleterious effect has been proposed. More in general, new reflectometric techniques (pulse technique [89], ultrafast sweep method [90, 91, 92]) and software improvements (as the use of *a priori* information on the plasma and of the neural networks [85]) allow nowadays on Tokamaks to counteract the effect of density fluctuations and even to recognize these diagnostic systems (correlation reflectometry [88] and Doppler reflectometry [87], for instance) as fundamental tools for plasma turbulence study.
On the contrary, on Reversed Field Pinches, the edge turbulence thwarted a similar development of the diagnostic reflectometry, mainly because of the greater complexity of the problem (see next section), to be solved by a smaller research community (the RFP's one with respect to the Tokamak's one). As a matter of fact, the RFX-mod microwave reflectometer data represent the first successfully application on a RFP of such a diagnostic system.

3.3.1 A simplified model for the RFX-mod case

A first theoretical approach to this topic can be found in [93]: the presence of strong density fluctuations in the outer plasma of RFX was treated as a 1D problem. In particular, it was highlighted the effect on the beat signal of a totally reflecting layer placed at an average position x_0 oscillating with a

displacement $\delta_x(t)$. This simplification to take into account for the changes in the edge density profile during a measurement turned out successively to be unsatisfactory. However, the main conclusion of this preliminary analysis was the formulation of a criterion under which a correct recovery of the τ_g is possible, namely, as long as the typical frequency of the beat signal f_b is greater than the bandwidth B_w of the phase variation caused by fluctuations measured at a fixed frequency:

$$f_b > B_w/2 \tag{3.8}$$

In order to achieve a f_b value satisfying such condition, in the same paper an increase in the frequency sweep rate, v_{sw} was proposed and preliminarly tested in particular operational ranges of RFX.
In the wake of the numerical studies carried out by Mazzucato [83] for the Tokamak case, and in the light of the inability to overcome the limitations imposed by the edge fluctuations, a 2D model of the reflectometric measurement has been proposed also for RFX-mod [94]. This model mimicks the

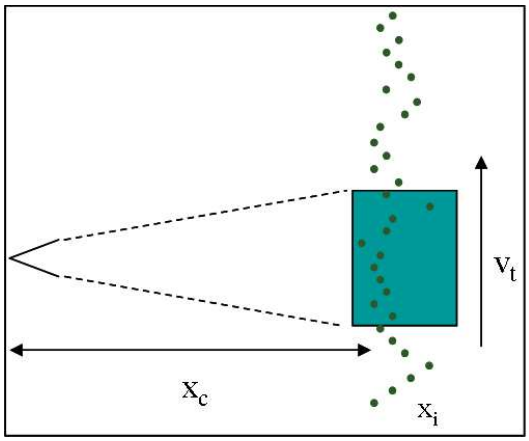

Figure 3.2: Sketch of the model used to mimick the reflectometric measurement in the presence of density fluctuations and toroidal flow

interference pattern of the reflected wave as produced by a distorting surface. More in detail, such a pattern is thought as a sum of the contributions of each scattering element composing the reflecting surface. In this way, it is possible to tailor the dynamics of the reflectometric measurement on the real characteristic of the edge density behaviour of RFX. In fact, the data coming out by gas puffing imaging [95] and Langmuir probes [96] are used to define a function $S(k)$ describing the k spectrum of the fluctuations, and the strong egde toroidal flow (up to ten times larger than in a Tokamak) is

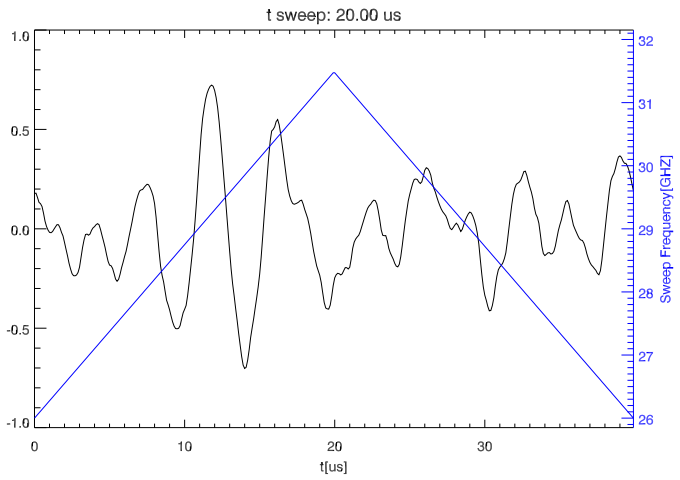

Figure 3.3: Beat signal computed from a numerical simulation in presence of a high level of density fluctuations for a slow (4 GHz in 20 μs) triangular modulation (in blue)

taken into account by computing at each time step the distance of the single scattering points according to $S(k)$ (see sketch in fig. 3.2).
This model highlighted the deleterious effect of the coupling between short wavelenght density fluctuations and toroidal flow that can seriously jeopardize a correct extrapolation of τ_g from the received signal for measurements made both at a single frequency or with an unoptimized frequency sweep. The same paper proposed a further increase of the frequency sweep (with respect to the previous 1D analysis) to cope with the cases with a high level of edge turbulence and to satisfy the aforementioned condition (eq. 3.8).
In the figs. 3.3 and 3.4 the received signal, as computed from the numerical simulations, is shown for 2 cases with the same level of fluctuations but with different frequency sweep rates. It is evident how a so called *ultrafast* sweep rate (4 GHz in 1 μs) is needed to get a physically useful signal.

Moreover this model investigated also the effect of the long wavelenghts density fluctuations, eventually producing a significant Doppler shift in the τ_g. For a laboratory plasma (radially moving with a velocity $v \ll c$), this contribution can be estimated and cancelled using a triangular modulation in the frequency sweep (see figs. 3.3 and 3.4), since it affects in a opposite way the ascending and the descending modulation.
In fact, for an ideal reflecting surface (for the sake of simplicity in this calculation we do not consider any density gradient) placed at a distance $x = x_c(t)$ from the antenna, the phase delay $\Phi(t)$, during a monotonic frequency sweep,

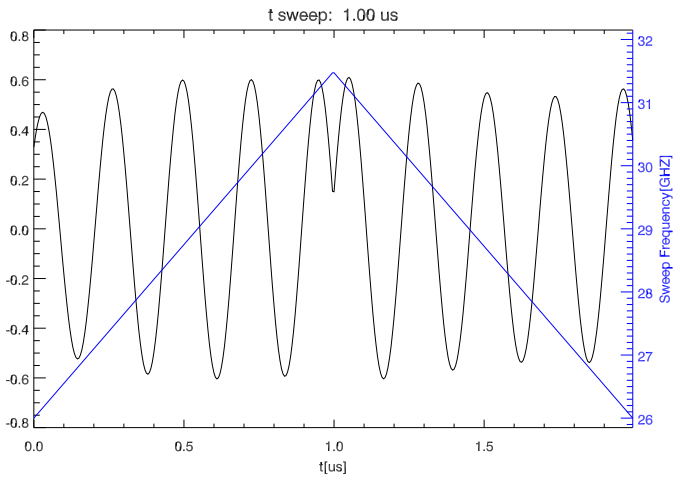

Figure 3.4: Beat signal computed from a numerical simulation in presence of a high level of density fluctuations for a ultrafast ($4\,GHz$ in $1\,\mu s$) triangular modulation (in blue)

can be expressed as:

$$\Phi(t) = 2\frac{2\pi}{c} f(t) x_c(t) \tag{3.9}$$

and the time delay τ_g:

$$\tau_g = \frac{1}{2\pi}\frac{d\Phi(t)}{dt} = \frac{2}{c}\left[\alpha x_c(t) + f(t)v\right] \tag{3.10}$$

where $\alpha = \Delta f/\Delta t$ is the sweep rate and v is the radial velocity of the reflecting layer (producing the Doppler shift). When applied to the practical implementations, between two different frequencies $f_1(t_1)$ and $f_2(t_2)$, this formula gives the beat frequency f_b of the received signal:

$$f_b = \frac{2}{c}\left[\alpha\langle x_c(t)\rangle_{t_1}^{t_2} + F_0 v\right] \tag{3.11}$$

where F_0 is the central frequency of the sweep. By using a triangular modulation, we will obtain two separate beat signals, differing in the direction of the frequency sweep:

$$f_b^{\pm} = \frac{2}{c}\left[\pm\alpha\langle x_c(t)\rangle^{\pm} + F_0 v\right] \tag{3.12}$$

Their difference and their sum will give respectively the mean position $\langle x(t)\rangle$ (averaged over the duration of the triangular sweep) of the reflecting layer

and its radial velocity v [94].
Unfortunately to estimate the radial velocity from the receveid signal, the condition of constant plasma velocity is needed. This can be achieved only by raising the frequency sweep at least to 20 GHz per μs. Actually, the possible correlated Doppler shift, induced in the group delay by the long wavelenght density fluctuations, can be still subtracted by simply averaging the result over the two bidirectional frequency sweeps (representing a new concept in such a measurement).

3.4 Design of the RFX-mod ultrafast reflectometer

The RFX-mod microwave reflectometer [97] was originally designed with 5 bands, covering a frequency range between 26.5 GHz and 110 GHz to operate in the plasma density range (9×10^{18} to $1.5 \times 10^{20} m^{-3}$) foreseen for RFX. Each circuit (fig. 3.5) was an O-mode homodyne system in which a sweep control (the driver) steered the microwave source (a high speed IMPATT oscillator for each band) with a frequency sweep modulation rate up to 0.1 $GHz/\mu s$. The highest sweep rate technologically available at that time was used, since the whole diagnostic system was already thought to face the problem of the density fluctuations.
In this scheme, a part of the produced microwave was sent to a so called *delay line* (a waveguide with known optical path), while the other part was sent to the plasma by the antenna, eventually passing through a polarization rotor (to avoid mode mixing). The wave reflected by the plasma was again collected by the antenna and sent to the mixer together with the part of the original wave previously sent to the delay line. From the output of the detector (see for instance fig. 3.8), namely the so called *beat signal* between reflected and reference wave, it is possible to extract the τ_g value.
The whole system (all the five bands) could cover a complete sweep in 1.25 ms.
This diagnostics, similar to the FM radar technique, turned out to be unable to probe, except in some special cases [98], the density layers of the outer regions of the RFX experiment. The reasons of the failure of this preliminary scheme have been successfully highlighted in the aforementioned theoretical analysis [93, 94] that drove the upgrade of part of the orginal system [99] to meet the requirements imposed by the operational conditions of the RFX-mod.
To test the reliability of such a model, the first upgraded Ka-band (26.5-40

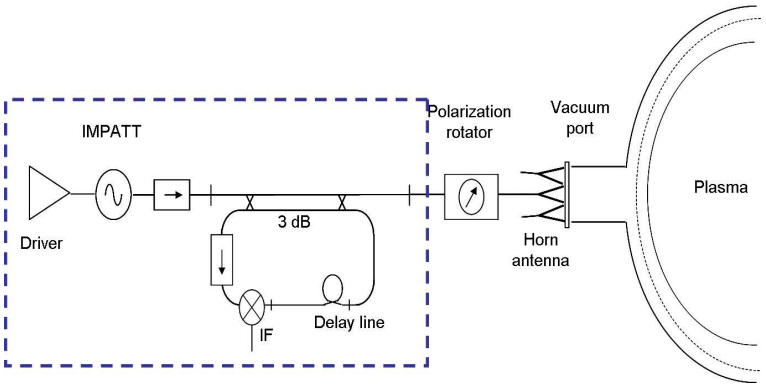

Figure 3.5: Basic representation of one the five subbands of the RFX reflectometer circuit

GHz) has been installed on the RFX-mod device in 2009.

After a calibration phase needed to obtain the time-frequency characteristic curve of the different sources (see chapter 5), the actual configuration of the system enables us to measure the distance of the density cut-off layer corresponding to the sweep central frequency (for the microwave source in the range $26.5 - 30.5\ GHz$ this corresponds to 1-1.1 $\times 10^{19} m^{-3}$) with a time resolution $\Delta t = 2\mu s$ ($\alpha = 4\ GHz/\mu s$), but does not allow to estimate the plasma radial velocity and the relative Doppler shift, for which a higher sweeping rate would be needed.

The analysis of the measured time delay τ_g is linked to the cut-off layer radial position x_c through a straightforward calculation. The phase delay $\Phi(f)$ for the ordinary mode is given by:

$$\Phi(f) = \frac{4\pi f}{c} \int_0^{x_c(f)} \eta_O(x, f) dx \tag{3.13}$$

where the refraction index is:

$$\eta_O(x, f) = \sqrt{1 - \frac{f_p^2(x)}{f^2}}$$

being $f_p(x) = \sqrt{\frac{e^2}{4\pi^2 \epsilon_0 m_e} n_e(x)}$ the plasma frequency and $x_c(f)$ the radial position of the density cut-off layer corresponding to the probing frequency f. In the approximation of linear density profile ($f_p^2(x) = \beta x$) the eq.3.13 becomes:

$$\Phi(f) = \frac{4\pi f}{c} \int_0^{x_c(f)} \sqrt{1 - \frac{x}{x_c(f)}} dx \tag{3.14}$$

where the distance of the cut-off layer has been expressed as $x_c(f) = f^2/\beta$. Finally, after some simple maths, the phase delay $\Phi(f)$ becomes:

$$\Phi(f) = \frac{4\pi f^3}{\beta c}\frac{2}{3}. \tag{3.15}$$

Thus group delay τ_g can be expressed as a function of x_c:

$$\tau_g = \frac{1}{2\pi}\frac{d\Phi(t)}{dt} = \frac{4}{c}\alpha x_c \tag{3.16}$$

where, analogously to the eq. 3.10, we introduced the sweep rate α. Looking at the calculations made in the absence of density gradient (previous section, eqq. 3.9-3.12), we can conclude that the effect of the layers with density $n_e < n_c$, in the case of linear profile, is simply to figure the cut-off position at a doubled distance with the respect to the real one. All the analyses presented in the next chapters will take into account this consideration. Where necessary, this model can be easily modified in order to take into account different density profiles. Up to now, looking at the data from the available edge diagnostics of the RFX-mod (Edge Thomson Scattering and Thermal Helium Beam), there is no indications for non-linear density profiles.

Chapter 4

Gundestrup Probe

4.1 Introduction

"Perhaps the most natural approach to diagnosing the particle distribution functions within the plasma is to propose insertion of some kind of probe that directly senses the particle fluxes" [81].
Actually, the idea of a direct measurement of the main plasma parameters (density, temperature, plasma potential) through one or more (organized in special arrays) electrodes was among the earliest diagnostic methods in the plasma physics, thanks also to the studies of Irwing Langmuir (awarded with the Nobel Prize in Chemistry in 1932), whose name is now used to name generally the electrostatic probes.
The hardware simplicity of these systems, that promoted in the past a wide diffusion in the plasma physics and a quick development, has been always accompanied by the limitations linked to the perturbation that the probes insertion induces into the plasma and by a more complicated theoretical interpretation of the results (especially in presence of a magnetized plasma) [81].
In fusion plasmas, furthermore, the application of the Langmuir probes has become, nowadays, limited, according to the considerable power increase in the largest devices, at the outermost regions (the only ones in which a solid object can survive). However, since the plasma edge is recognized to be crucial for the global performance of whatever magnetic configuration, the interest about this topic is still intact.
Among the huge amount of information that can be obtained from the different kind of probes, in this thesis we focused our attention on the plasma flow properties of the edge region of RFX-mod, analyzed through a special probe array, the so called Gundestrup probe [100], an advanced Mach probe concept

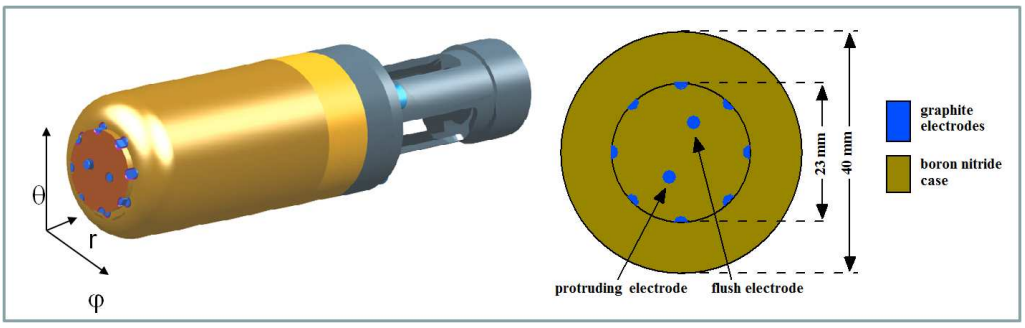

Figure 4.1: Sketch of the Gundestrup probe mounted on an equatorial port of RFX-mod (left); frontal view of the probe (right). At the RFX-mod edge the magnetic field is almost totally along the θ direction.

operational also in several other fusion devices (see for instance [101, 102] and references therein).
The Gundestrup system used in RFX-mod is equipped with 8 directional pins located on a 23 mm diameter circle perpendicular to the radial direction (see tab.4.1). Two additional cylindrical pins, namely the protruding and the flush electrode, are located in two equispaced points on the diameter (see fig.4.1). All of the pins are electrically insulated by a boron nitride case, as shown in fig.4.1.
The probe is mounted on an insertable support, whose radial position can be changed remotely after each discharge, and exploits an equatorial port of the RFX-mod vessel located at $\phi = 247.30°$. Each pin can collect indipendently ion saturation current, I_s (roughly, the current collected by a biased electrode exposed to the plasma) or floating potential, V_f (the potential measured by a floating electrode inserted into the plasma) measurements. We will not describe for the sake of semplicity in a detailed way the concepts of ion and electron saturation currents (I_s and I_{es} respectively) and floating and plasma potentials (V_f and V_p) that will be used in the following; however they are related to the more general Langmuir probe theory whose an accurate description can be found for instance in [103].
In the next section it is theoretically described how this probe can provide information on the edge flow components with a high time resolution, while the second part of the chapter will deal with the experimental validation of the theoretical model. Finally, in chapter 6 the experimental results will be presented and discussed.

Pin number	θ
1	22.5°
2	62.5°
3	112.5°
4	157.5°
5	202.5°
6	247.5°
7	292.5°
8	337.5°

Table 4.1: Angular position of the Gundestrup pins with respect to the equatorial direction. The edge magnetic field direction lies in the range $\theta = [-82° \div -89°]$

(see fig.6.6).

4.2 Analysis models for Gundestrup data

In this section we present a brief review of the models widely used in the fusion community to deduce the different components of the edge flow starting from the ion saturation current (I_s) measurements for different kind of electrostatic probes (from a simple directional Langmuir probe to a Mach probe). Furthermore, we introduce a new method developed to evaluate parallel and perpendicular edge flow components with respect to the local magnetic field based on the floating potential (V_f) measurements for a Gundestrup probe array [100].
This new method turned out to be very useful to reconstruct the radial profiles (up to 10% of the minor radius of the RFX-mod) of parallel and perpendicular edge flow and to investigate the flow pattern associated to different local magnetic topologies [104, 105], enabling to overcome many problems related to the use of the ion saturation current configuration.
A validation of this method through different experimental cross-checks has been necessary and is presented at the end of this chapter.

4.2.1 Review of models for I_s configuration

Several theoretical models have been proposed in the past years for probe data interpretation in presence of plasma flow. The basic common idea has been to relate the ratio $R = I_{s,u}/I_{s,d}$ of the ion saturation currents collected from the pin(s) facing the flux tube of the magnetic field (upstream direction, $I_{s,u}$) and the opposite ones (downstream direction, $I_{s,d}$), to the Mach number

M of the unperturbed flow in the plasma. M is defined as the drift velocity of the ions, v_d, normalized to the ion sound velocity, $c_s = [k_B (T_e + T_i) m_i]^{1/2}$, where T_i and T_e are the ion and electron temperature and m_i is the ion mass. Following the classification given in Peterson et al.[106], all of these models can be approximated by the formulation:

$$R = e^{KM} \tag{4.1}$$

with K a model-dependent factor for $M < 1$, and they can be classified as either *magnetized* or *unmagnetized* describing respectively the dependence or independence of the collected ion saturation current on the orientation of the probe surface with respect to the magnetic field.
Roughly, the magnetized or unmagnetized classification depends on the comparison between the probe dimension r_p, and the ion and electron Larmor radii r_{Li} and r_{Le}; a discussion about the choice of the suitable interpretation model based on the assumptions of each model is proposed further on.

Magnetized Model

The magnetized model is based on the 1D fluid description of the SOL in presence of only parallel drift developed by Hutchinson [107], taking into account particle diffusivity and viscosity. In a highly elongated presheath along the field, the ions are accelerated toward the sheath, reaching it at or near the sound speed c_s. Transport equations present in fact singularities at $M_{par} = \pm 1$, that is the equivalent to Bohm criterion for sheath formation. Ions move into presheath region by diffusing across the magnetic field surface surrounding the presheath flux tube. The density difference of the ions reaching the pins' probe from the upstream or downstream direction is taken into account by introducing two coefficients α and β as a function of the parallel Mach number M_{par} in the unperturbed plasma. The value of this parallel drift velocity can be inferred from the ratio R of the two currents upstream and downstream adjusted by a factor $K = 2.27$ [106, 107].
Several authors [100, 106, 108] proposed an 'intuitive' extension of the Hutchinson model in presence of a perpendicular drift based on the experimental evidences. In particular in MacLatchy et al.[100] an *ad hoc* geometrical model for the Gundestrup probe array to estimate both parallel and perpendicular Mach number, taking into account particle diffusivity, can be found. Afterwards Van Goubergen [109] provided an extension of the Hutchinson's 1D theory in a more rigorous way to include a finite perpendicular drift. In analogy with [107], the transport equations are affected by a singularity that determines the maximum parallel speed in the presheath, but are 'corrected'

by the presence of the perpendicular drift:

$$M_{par,MPSE} = \frac{M_{perp}}{tan(\theta)} \pm 1 \tag{4.2}$$

where θ is the angle between the normal direction to the pin's probe surface and the magnetic field. This boundary condition at the magnetic presehath edge (MPSE) implies that, in presence of perpendicular flow, the parallel flow has to adapt itself such that eq.4.2 is fulfilled. To relate the upstream and downstream asymmetry to the unperturbed Mach numbers, the ratio between the respective ion saturation currents can be written as:

$$R = exp\left[c\left(M_{par} - \frac{M_{perp}}{tan\,(\theta)}\right)\right] \tag{4.3}$$

The parameter c is a fitting parameter, but it is easily identifiable with the constant K in Peterson's formalism. Its value lies between 2.3 and 2.5 and weakly depends on M_{par} . In Gunn et al.[102] this model has been used to perform some edge flow measurements on the CASTOR tokamak using Gundestrup probes and an experimental relation has been proposed to describe the dependence of the parameter c on the value of M_{par}, according to Van Goubergen model predictions.

Unmagnetized Model

The case of a probe in an unmagnetized collisionless plasma has been treated thoeretically by Hudis and Lidsky [103] with a fluid approach. They supposed, in a 1D free fall frame, that the ion drift velocity, v_d, can be directly deduced by imposing at the sheath, the usual Bohm criterion (the ion velocity $v_i = c_s$) and a simple energy conservation relationship accounting for potential drop towards the probe and streaming velocity either into or away from the probe. Once again using Peterson's notation the ratio R between the upstream and downstream ion saturation currents can be written as:

$$R = exp\left[2M\frac{\sqrt{2\,(T_eT_i + T_i^2)}}{T_e}\right] \tag{4.4}$$

where the model-dependent factor K is a function of the ion and electron temperature T_i and T_e. In [108] an analysis of the relationship between the ratio of the upstream and downstream probe current densities R and the Mach number M shows as the Hudis and Lidsky model gives a Mach

number which is about 25% higher than the Hutchison's magnetized one. Such a simple model has been more recently criticized [110]; nevertheless it has been used in several papers [106, 108] to compare different predictions for the Mach numbers from different models. In the same papers [106, 108] the unmagnetized theory of Hudis and Lidsky has been extended for multiple pin probe arrays in order to generalize the model in presence of a perpendicular drift. To account for arbitrary angles between the magnetic field and the probe surface the cosine of this quantity has been introduced in the expression of the ion saturation current collected by each pin:

$$I_{is} = I_{is,0} \exp\left\{ \frac{\left[v_{th,i} - v_d \cos\left(\theta - \theta_d\right)\right]^2}{c_s^2} \right\} \tag{4.5}$$

where θ_d marks the direction that the flow is coming from, the parallel and perpendicular components being determined by the respective projections of v_d; $I_{is,0}$ is a constant taking into account the probe area, the electric charge, the plasma density and the ion sound speed; $v_{th,i} = (k_B T_i / m_i)^{1/2}$ is the ion thermal velocity.

4.2.2 Gundestrup probe in V_f configuration

In Jachmich et al.[111] the effect of a streaming plasma on the floating potential of a Langmuir probe has been studied. The voltage difference arising between probe tip exposed to the plasma and a ground probe, normally the enclosing wall of the device, is defined as the floating potential V_f. The floating potential is related to the ion and electron saturation currents, I_s and I_{es}, through the plasma potential V_p and the electron temperature T_e by the formula [112]:

$$V_f = V_p - T_e ln \frac{I_{es}}{I_{is}} \tag{4.6}$$

In [111], the difference δV_f of the measured floating potentials of two opposite plates of a split probe has been linked to the parallel Mach number of the measured floating potentials of two opposite plates of a split probe has been linked to the parallel Mach number of the unperturbed plasma flow. Starting from the magnetized Van Goubergen model, for the case in which the magnetic field is parallel to the normal direction of the probe surface, the relation can be written as:

$$M_{par} = \frac{\delta V_f}{2T_e} = \frac{V_{fl,u} - V_{fl,d}}{2T_e} \tag{4.7}$$

where, in analogy to the ion saturation current models, the plate facing the magnetic field has been considered in upstream direction with respect to the opposite one (downstream direction). Our aim in the next section is to derive a practical method based on the floating potential measurements for a Gundestrup probe array in presence of both parallel and perpendicular drift velocity.

Magnetized and Unmagnetized model

Let us first consider equation 4.6. With respect to the magnetic field direction the upstream/downstream ion saturation current collected by a probe's pin can be written as a function of the floating potential V_f [111]:

$$I_{is_d^u} = I_{es,0} exp\left[\frac{e\left(V_{fl_u^d} - V_p\right)}{T_e}\right] \tag{4.8}$$

The ratio R between the upstream and downstream collected ion saturation currents becomes:

$$R = \frac{I_{is_u}}{I_{is_d}} = \frac{I_{es,0} exp\left[\left(V_{fl_u} - V_p\right)/T_e\right]}{I_{es,0} exp\left[\left(V_{fl_d} - V_p\right)/T_e\right]} \tag{4.9}$$

Thus, a very straightforward calculation yields:

$$R = exp\left(\frac{\Delta V_f}{T_e}\right) \tag{4.10}$$

Now, let us point our attention to the Van Goubergen magnetized model. Including an arbitrary angle θ between the normal to the probe surface and the magnetic field, he found a relation between the quantity R and the parallel and perpendicular flow of the unperturbed plasma. By substituting in 4.3, the value of R deduced in 4.10, we find, after some maths:

$$\frac{\Delta V_f}{T_e} = K\left(M_{par} - M_{perp} cot(\theta)\right) \tag{4.11}$$

being K a model-dependent factor as described above. This relation links directly the parallel and perpendicular flow components to the measured difference between the upstream and downstream floating potential in a magnetized frame.
For the unmagnetized model the calculation is less immediate but it gives a result as easy to interpret as the magnetized case. Starting from eq.4.5,

given in [108], we try to deduce a relation linking the change in the streaming velocity v_d, to the difference between the floating potential V_f, in analogy to what just made for the magnetized case. By substituting the value I_s from eq.4.8 into eq.4.5, we find a relation linking the floating potential V_f to the streaming velocity v_d:

$$V_f = T_e ln\left(\frac{I_{is,0}}{I_{es,0}}\right) + V_p + T_e\left[\frac{v_{th,i} - v_d cos(\theta - \theta_d)}{c_s}\right] \tag{4.12}$$

in which the same parameters mentioned for I_s configuration appear. It is convenient to consider again the difference between the upstream and downstream measured floating potentials. What we get, after some maths, is:

$$\frac{\Delta V_f}{T_e} = -4\frac{v_{th,i}}{c_s^2} v_d cos(\theta - \theta_d) \tag{4.13}$$

where, introducing a streaming Mach number M_d as the streaming velocity normalized to the ion sound speed, all of the constant parameters on the right side are only function of the ion and electron temperature. As in [108], the parallel and perpendicular flow components are determined by the projections of M_d with respect to the direction of maximum flow θ_d. It is interesting to note that in all of the calculations made to derive eq.4.11 and eq.4.13 no further assumptions have been introduced with respect to those considered in [108] and [109].

4.2.3 Different methods for different conditions

For all the models based on the ion saturation current measurements a key parameter is represented by the comparison between the ion Larmor radius r_{Li} and the probe dimension r_p. In fact, in order to apply a magnetized or an unmagnetized theory, understanding the mechanism by which the ions are collected by the probe is particularly important. In this sense, a first classification has been proposed by Stangeby and McCracken [113], between the strong magnetic field (SF) regime, when $r_{Le} < r_p < r_{Li}$, and the very strong magnetic field (VSF) regime, when $r_p > r_{Le}, r_{Li}$. In the latter case the magnetized models can be applied, whereas the application to the SF regime is questionable.
More in detail, the magnetized model was developed by Hutchinson [107] for the case in which $r_p \gg r_{Li}$,λ_D (being λ_D the Debye lenght defined as $\lambda_D = \sqrt{\frac{\epsilon_0 k_B T_e}{n_e e^2}}$) , but it was applied in [100, 108, 102] also in the case for $r_p \approx 2r_{Li}$. In particular in Gunn et al.[102], a numerical simulation showed a

good agreement between the Hutchinson's assumption and the approximation of finite ion Larmor radius except the angles between the probe surface and magnetic field around 90° and 270°. Elsewhere the same angular positions have not been considered for the analysis because rendering the collection area of the pins indeterminate [100] or the additional diffusive terms (not considered in this model) non negligible [108]. Also for these reasons, none of the 8 pins of the Gundestrup probes operating on the outer region of the RFX-mod device lies in the mentioned angular positions (see fig.4.1).
For the unmagnetized model, Hudis and Lidsky developed their theory for a collisionless plasma, with $T_i < T_e$ and $\lambda_D \ll r_p < r_{Li}$ but later, in [108], it has been extended to the condition $T_i = T_e$, as suggested by different spectroscopic measurements in the outer region of RFX and the upgraded RFX-mod.
In particular, some recent analysis [104, 105] performed during several low current discharges, showed as the electron temperature T_e varies, as a function of the radial position, from a few eVs in the tile shadow, to around 40 eV at the maximum probe insertion explored ($r_p/a \sim 0.9$). Hence, in that region the ion Larmor radius r_{Li} experiences significantly changes, from around $2mm$ to $6-7mm$, while the electron Larmor radius reaches values of around $0.1mm$. Being the probe radius 1 mm, it means that a priori choice between the unmagnetized and magnetized models could be inappropriate.
In the previous section we found two equations relating the floating potential measurements to both parallel and perpendicular components of the plasma flow. These equations have been deduced from a magnetized model [109] and an unmagnetized one [108]. In order to verify which one is suitable for the RFX-mod case and, also, to compare the results coming from the I_s and V_f measurements, in the next sections different cross checks have been considered.
These comparisons provided an experimental validation of this new method showing as the assumptions considered for the models based on the ion saturation current measurements can be rightly extended to an extensive analysis of the flow properties in the edge region of the RFX-mod based on the floating potential measurements.

4.3 Experimental validation

The relation between ion saturation current and plasma flow has been studied and continuously refined for several years, as shown by the huge available literature (see previous section). On the contrary, except for the preliminary attempts presented in [111], the reliability of a floating potential based model

to deduce the edge flow components has never been tested.
For this reason in these following two sections we will describe the great effort devoted in validating the results coming from the floating potential configuration measurements with respect to the well established ion saturation current method. The experimental validation was obtained through the comparison of the two different configurations in several operative conditions and on two different experiments: RFX-mod and ISTTOK. A further check of the method validity have come from flow data obtained with indipendent measurements performed by different diagnostics.

4.3.1 Gundestrup probe on RFX-mod

The insertion of the Gundestrup probe inside the RFX-mod chamber is strongly limited to the extreme edge when the pins are set to collect ion saturation current. The interaction between biased electrodes and streaming plasma, especially in low density discharges, can produces severe current arcs, potentially dangerous for the experimental equipment and strongly limiting the collected useful data. The Gundestrup V_f configuration has the main advantage of eliminating this problem, so that the number of available discharges.
Nevertheless, the significant power loads delivered during the discharges do not allow probe insertions deeper than the 10% of the minor radius a of the machine with plasma current I_p kept below $400kA$ even in the V_f configuration.

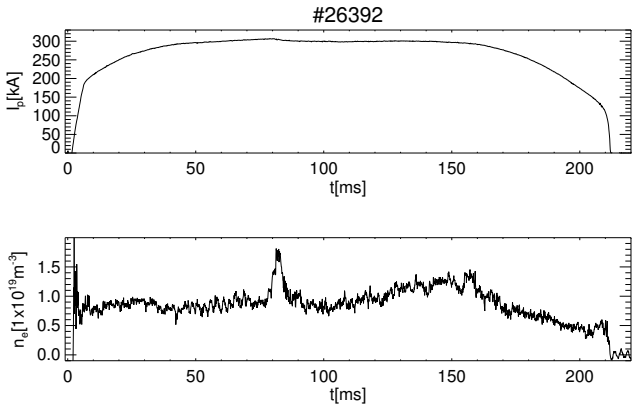

Figure 4.2: #26392: Typical time evolution of plasma current (top) and electron density (bottom) during the low plasma current RFX-mod experimental campaign with the Gundestrup insertion.

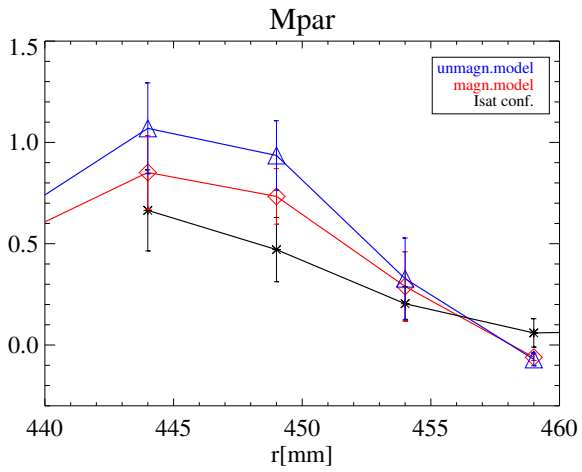

Figure 4.3: Radial profile of the parallel Mach number for the three different methods: V_f configuration (blue for the unmagnetized model and red for the magnetized one) and I_s configuration (black). Each symbol is obtained averaging the data over the flat top phase of the different considered discharges.

In the explored region, however, different cross-checks have been performed, collecting separately I_s and V_f measurements in similar discharges and simultaneously by using different configurations for each pin in the same shot. A first comparison concerned the reconstruction of the parallel Mach number M_{par} radial profile as estimated by the traditional I_s based model and the magnetized and the unmagnetized models based on the V_f measurements. These results have been evaluated averaging the data for each measured radial position over the flat-top phase of a large database of homogenuous discharges. Fig.4.3 shows a reasonable agreement between the three applied methods.
A further check is provided by the reconstruction of the flow transient induced by pellet injection. In these special discharges two opposite Gundestrup pins have been set collecting I_s, while the remaining 6 pins were collecting V_f data, so that both measurements were simultaneously available. Since the contribution to the total plasma flow coming out from each couple of pins could be different, the two reconstructions of the M_{par} time evolution have been compared only as time fluctuations, not in absolute value. The transients observed with the two methods (fig.4.4) are similar.
To compare the estimation of the perpendicular edge flow M_{perp}, finally we considered the analysis carried out using another insertable system mouted on RFX-mod, the so called U-probe [77]. This probe can evaluate the plasma

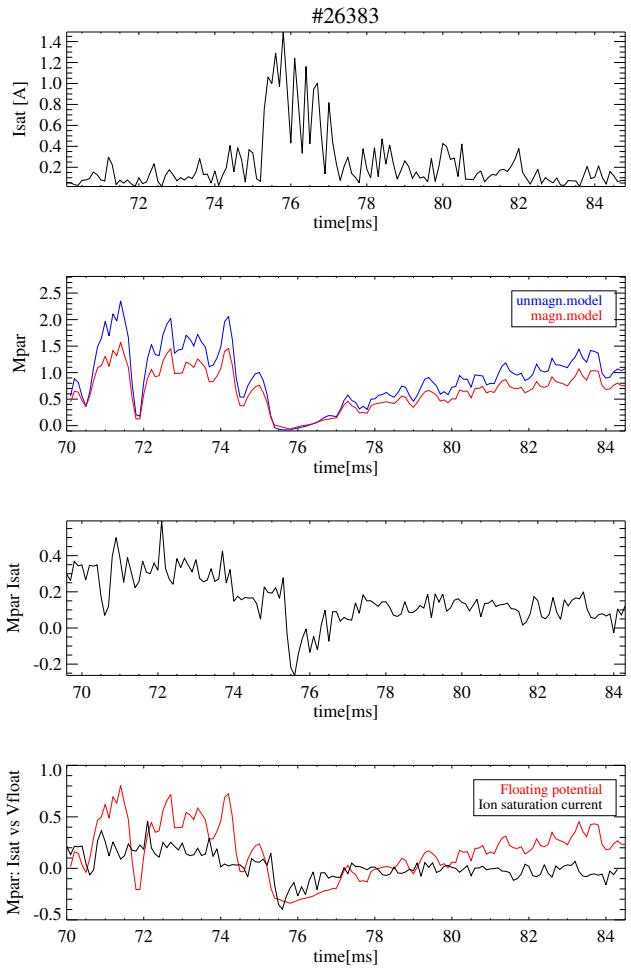

Figure 4.4: #26383. From the top: time evolution of I_s (proportional to the local electron density); M_{par} as evaluated from the V_f measurements; M_{par} deduced by the I_s measurements; plot of the same quantities subtracted from their mean value. The pellet injection is recognizable between 75 and 77 ms.

potential V_p and its radial derivative can be directly linked to the $v_{E\times B}$ flow, through the formula:

$$v_{E\times B} = -\frac{1}{B}\frac{dV_p(r)}{dr}.$$

In fig.4.5 the $v_{E\times B}$ radial profile [104, 105], evaluated by averaging the data on a large discharge database, is overplotted to the M_{perp} radial profile as obtained from the Gundestrup data in a similar discharge database analyzed in the light of the aforementioned models (magnetized and unmagnetized). Even if the absolute values are slightly different, the profile shapes appear

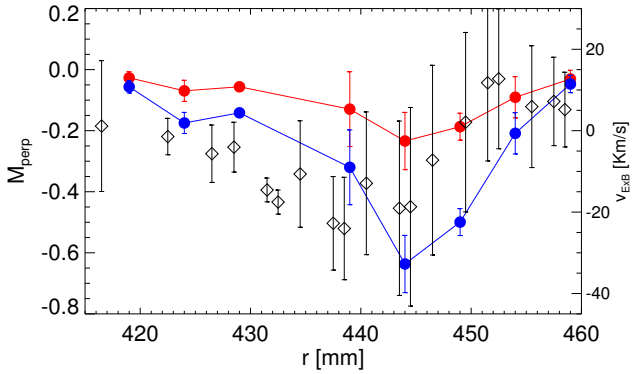

Figure 4.5: Radial profile of the perpendicular Mach number for the two different V_f based models, magnetized (red) and unmagnetized (blue) and radial profile of the $v_{E\times B}$ flow (black diamonds). Each symbol is obtained averaging the data over the flat top phase of the different considered discharges.

comparable, supporting the reliability of the V_f measurements for estimating the edge flow.

4.3.2 Gundestrup probe on ISTTOK

ISSTOK [114] is a large aspect ratio tokamak with a circular cross-section, a poloidal graphite limiter and an iron core transformer, in operation since 1991 at the IST laboratory in Lisbon (Portugal). The main parameters are described in table 4.2 and a sketch of the experiment is shown in fig.4.6

Table 4.2: Main ISTTOK parameters.

Major radius	46 cm
Minor radius	8.5 cm
Maximum toroidal magnetic field	2.8 T
Typical plasma current	~ 7 kA
Discharge duration	45 ms
Typical plasma density	$\sim 5 \times 10^{18} m^{-3}$

This machine is equipped with several insertable diagnostic systems in order to investigate the edge transport properties: a radial array of electrostatic probes (rake probe), a turbulent transport and Mach probe, a Gundestrup probe [101] and an electrode probe for biasing plasma experiments [115]. All probe systems are radially movable on a shot-to-shot basis.

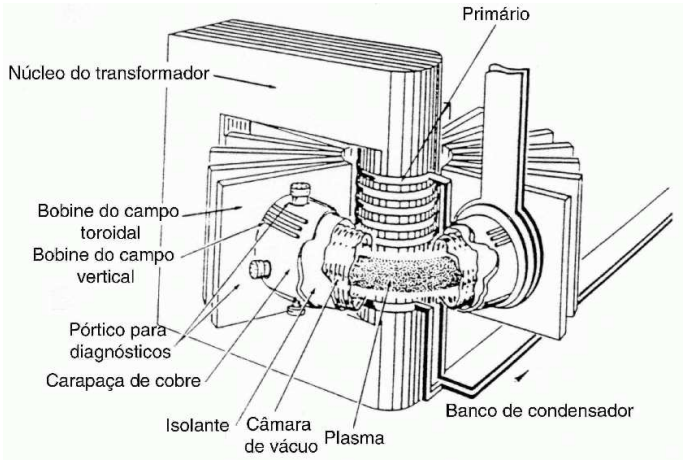

Figure 4.6: Schematic representation of the ISTTOK experiment

Similarly to the RFX-mod system, the Gundestrup probe mounted on IST-TOK consists of eight conducting segments (lenght 2.2 mm, width 4 mm) located in an insulating cylindrical case. This probe has also an extra central pin that can be swept to measure the electron temperature. Each pin can collect indipendently ion saturation current (I_s) or floating potential (V_f) signals.
Information on the plasma flow can, thus, be obtained from the ratios R between the opposite collected I_s signals [116] in the wake of the traditional theoretical models, through the Van Goubergen formula:

$$ln(R) = K\left[M_{par} - \frac{M_{perp}}{tan(\theta)}\right] \quad , \tag{4.14}$$

where K, M_{par} and M_{perp} have the same physical meaning of eq.4.3.
At the same time, the small size and the low power load delivered during the discharges, together with the whole available diagnostic set, made ISTTOK a very interesting machine in order to test and to validate the new Gundestrup model (see previous sections) based on the V_f measurements. The only significant difference, in fact, with the RFX-mod probe, relies in the different orientation θ of the pins with respect to the edge magnetic field (almost toroidal). Here, they are always 45° equispaced each other, but one of the couple relies in the plane perpendicular to the edge toroidal magnetic field and is not used to deduce the flow pattern, because of the reasons already discussed in section 4.2.3.
A whole dedicated experimental campaign in collaboration with the IST team provided more than 60 useful discharges. These experiments allowed a sis-

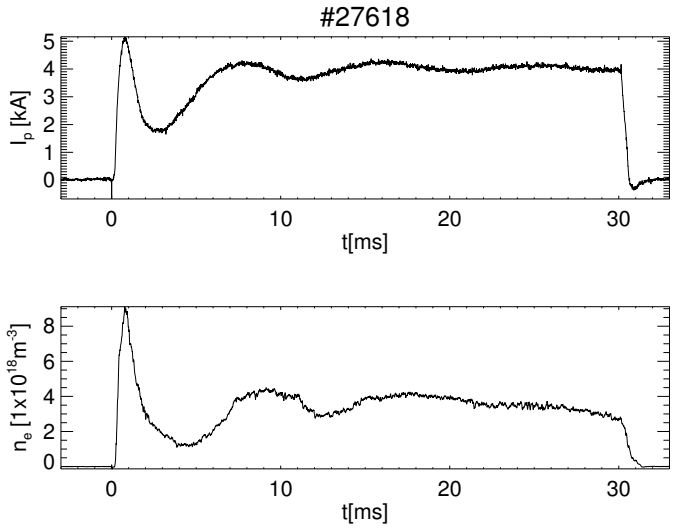

Figure 4.7: #27618: Typical time evolution of plasma current (top) and electron density (bottom) during the ISTTOK experimental campaign with the Gundestrup insertion

tematic comparison between the 2 Gundestrup configurations (I_s and V_f), highlighting the reliability of this new method and some critical points to be further deepened.
In these experiments I_p was usually kept around $4-5$ kA, $B_T \approx 0.5$ T and the line averaged electron density $n_e \approx 3 \div 4 \times 10^{18} m^{-3}$ (see fig.4.7). The electron temperature T_e has been measured directly by the Gundestrup and lies in the range [15÷45] eVs (see fig. 4.10).
Since in these experimental conditions the ion Larmor radius r_i is one order of magnitude smaller than the probe radius ($r_p = 1$ mm), all the collected data (both V_f and I_s) was analyzed by applying solely the magnetized model (according to the considerations discussed in section 4.2.3).
Similarly to the previous results on RFX-mod, a first cross-check involved the reconstruction of the edge flow radial profiles, averaged on a shot to shot basis during the flat top phase of the discharges. To produce a data set as homogeneous as possible, the experiments were performed by switching the Gundestrup configuration (I_s to V_f) at each discharge and by probing each radial position (up to 3 cm beyond the limiter position). Fig.4.8 shows the preliminary result for M_{par} and M_{perp} as evaluated by the two data sets. Although there were non-negligible differences (especially in the radial positions across the limiter, located at $r = 85$ mm), the two profiles, shown in fig.4.8, appear at least comparable.

Since for the model based on the V_f data (eq.4.11), the knowledge of the

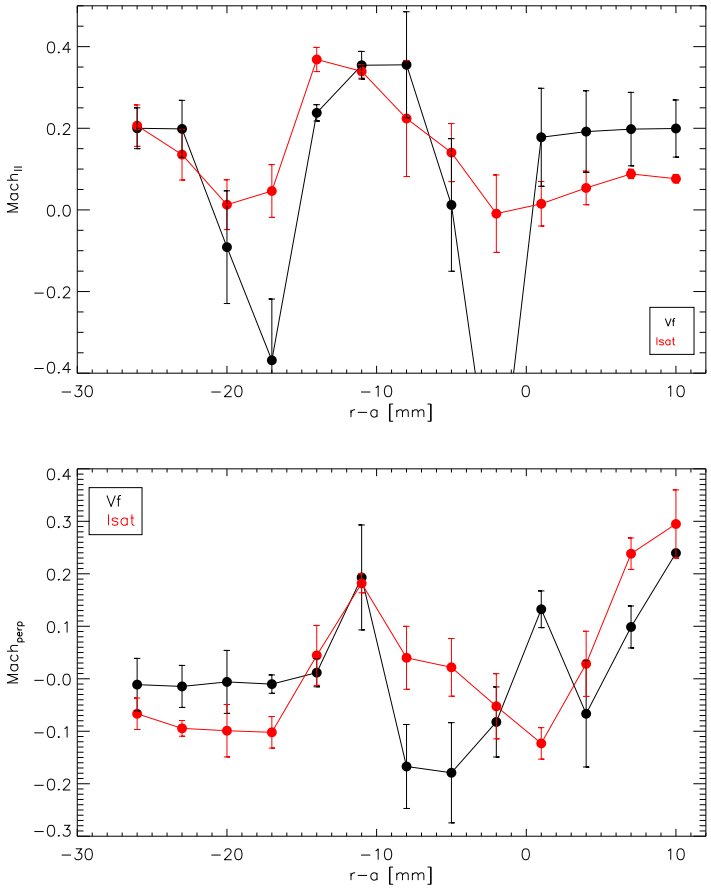

Figure 4.8: Averaged radial profiles of M_{par} (top) and M_{perp} (bottom) as evaluated using the magnetized model by the I_s (red) and the V_f (black) measurements. The poloidal limiter is located at $r = 85$ mm.

electron temperature T_e is crucial, a set of similar discharges has been devoted to sweeping the Gundestrup pins, in order to obtain the time evolution of the I-V characteristic curve. Unfortunately, the available power supplier turned out to be insufficient for all of the eight pins and because of that, after some preliminarly attempts, only two pins (those ones parallel to the toroidal magnetic field) have been swept. In fig.4.9 we reported an example for the pins 3 and 7.

Even if with a lower time resolution (1 ms), the analysis of these data allowed the complete reconstruction of the T_e radial profile, simultaneously to the I_s and V_f ones (fig.4.10). The fact that, especially toward the Scrape

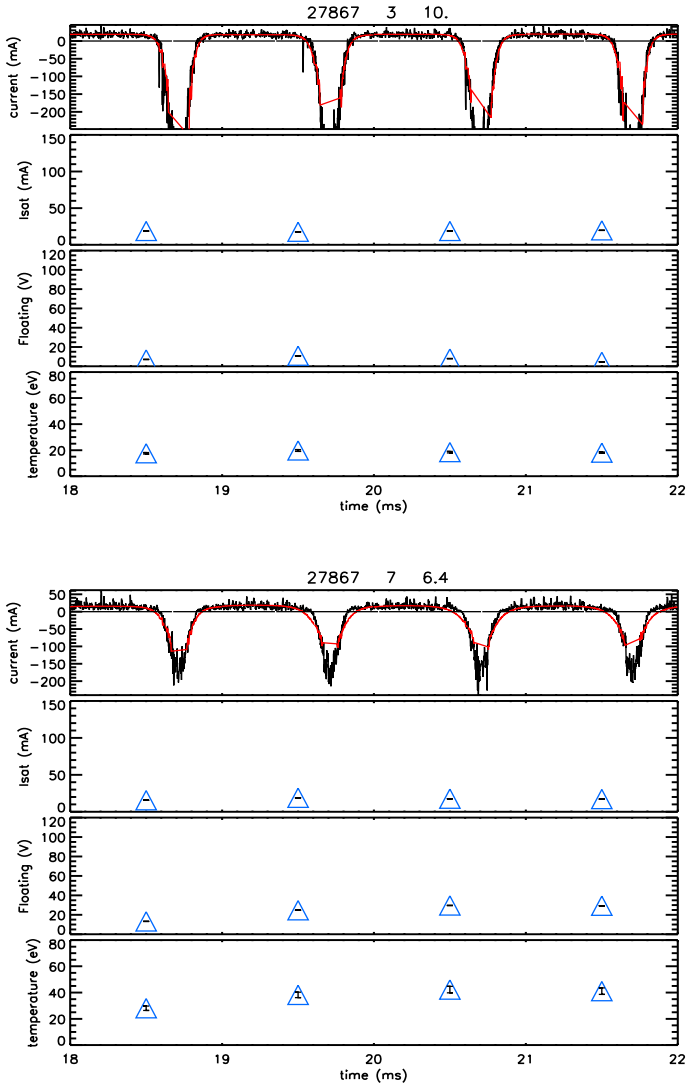

Figure 4.9: #27867: example of two opposite Gundestrup pins used in sweeping mode. From the top: current through the pins, I_s, V_f and T_e as fitted from the I-V characteristic curve.

Off Layer, the temperature measured by the two opposite pins can be significantly different, partially explains the inability of the V_f based model for some special radial positions to reproduce the results obtained using the I_s measurement. From a theoretical point of view, it seems very difficult to deduce a compact formula to link the V_f measurements to the edge flow components, when the temperature T_e measured by the opposite pins of the probe is different, and, in fact, all the calculations made in the section 4.2.2 started with the assumption that T_e were equal on both sides. Moreover, it would be interesting to investigate what is the mechanism leading to this phenomenology, since it seems more related to the local changes induced by the insertion in plasma of the probe than to a spontaneous plasma temperature gradient (usually one order of magnitude smaller for a lenght equal to the Gundestrup diameter). Definitely this opens further points to be focused, hopefully, in future works.

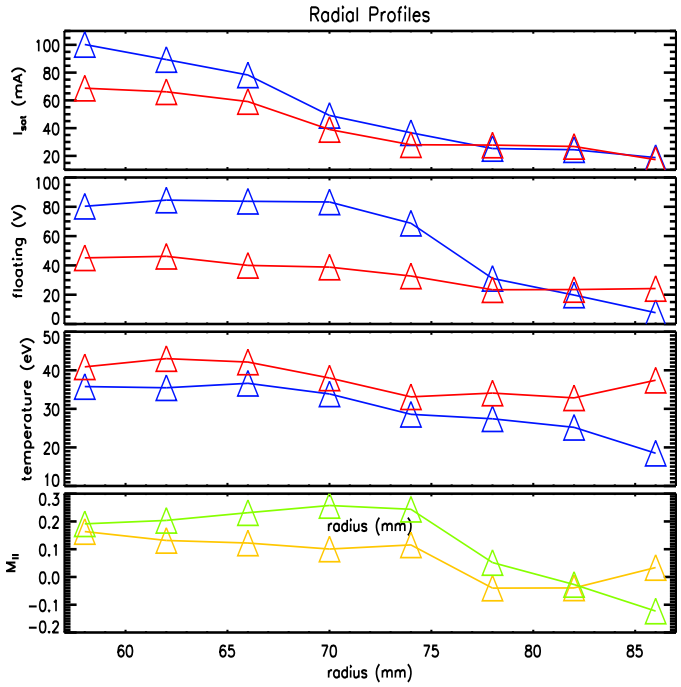

Figure 4.10: From the top: averaged radial profiles of I_s, V_f and T_e respectively for the upstream (red) and dowstream (blue) pin. In the bottom the M_{par} radial profile as evaluated using the magnetized model by the I_s (yellow) and the V_f (green) data. The limiter is located at $r = 85$ mm.

However, I_s, V_f and T_e simultaneously measured, have been used to deduce in a more accurate way the parallel flow M_{par}, according to the traditional Hutchinson model (eq.4.1) for I_s, and to the Jachmich model for V_f, modified by taking into account the exact value of T_e on both sides, so that:

$$\frac{\Delta V_f}{(T_{e,upstream} + T_{e,downstream})} = K M_{par} \tag{4.15}$$

The comparison between the reconstruction based on the two configurations is shown in last plot of fig.4.10. The good agreement found demonstrates the reliability of the V_f measurements to evaluate the edge flow, at least as long as the electron temperature on the two Gundestrup sides does not differ too much (experimental condition that appears occurring only in the SOL of ISSTOK).
As a further cross-check, we finally considered a set of discharges in which the plasma biasing electrode was applied during the flat top phase for a few ms in order to induce transient changes in the edge radial electric field. Some previous work on ISTTOK [115, 117] showed how the application of the biased electrode drives a radial current in the plasma, interacting with the magnetic field and finally leading to a plasma rotation increase.
The underlying idea was to verify how the two methods, I_s and V_f based, react to the fast transients induced by the electrode. In this case, a complete scan switching from I_s to V_f configuration has been performed, but in two different experimental days. figs.4.11 and 4.12 show a typical example of the flow transients induced by the electrode applications. As expected, while the electrode is switched on, the M_{perp}, driven by a modified $E \times B$ force, is affected by a significant increasing. Even more important is that, also in this case, the variations registered by the two configurations appear compatible.

In conclusion, these two sections reported a set of experimental evidence, supporting the reliability of a V_f measurements based model for the edge flow components evaluation. Definitely, the cross-checks carried out on two different machines and in several operative conditions, gave robust experimental basis to this new tool. On the other hand, a significant work for a more complete understanding of the conditions under which the V_f measurements can not reproduce the traditional method results has still to be done. However, all of the results presented in chapter 6, concerning the RFX-mod edge properties will be always accompanied by comparative data coming from well established diagnostic systems.

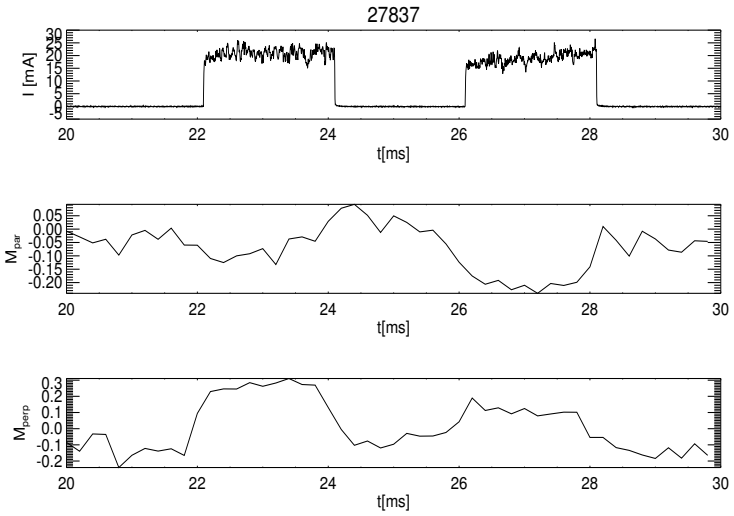

Figure 4.11: Time behaviour of the edge flow components (middle and bottom) during the application of the biasing electrode (top). In this discharge the Gundestrup was collecting I_s measurements.

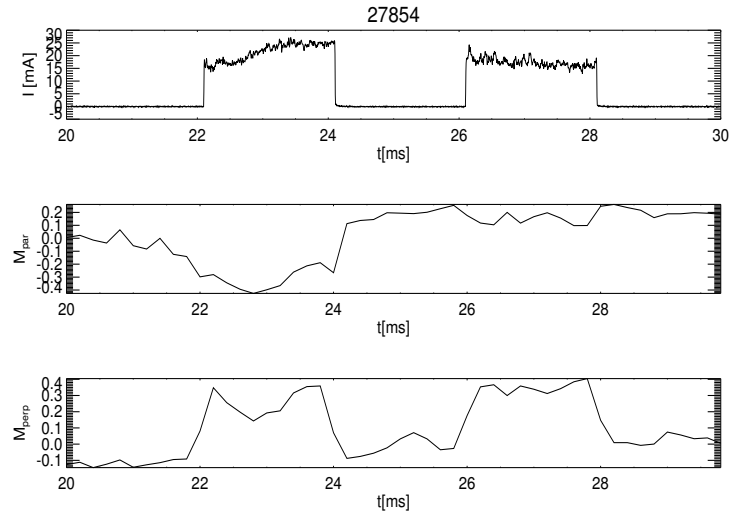

Figure 4.12: Time behaviour of the edge flow components (middle and bottom) during the application of the biasing electrode (top). In this discharge the Gundestrup was collecting V_f measurements.

Chapter 5

Edge density monitoring

5.1 Introduction

In chapter 3 we discussed the theoretical reasons and the experimental evidence that drove the upgrade to the present configuration of the RFX-mod reflectometer. A more detailed description of the original design and of the successive hardware modifications can be found respectively in [97] and [99]. This chapter is, instead, devoted to reviewing the experimental results obtained up to now on the RFX-mod device by using the ultra-fast microwave reflectometer. This will involve also the explanation of the experimental method used to infer the radial position of the cut-off layer and the validation of such a measurement through the comparison with well established diagnostics operating at the edge of RFX-mod (sect. 5.3).
Before discussing the plasma applications however, it is very useful (and chronologically correct as well) to deal with the calibration of the microwave sources that we use on the reflectometer circuit. A new technique (sect. 5.1) to deduce the time-frequency sweep law for each source has been developed since the traditional instruments for automatic calibration with such high time resolution capability are extremely expensive.

5.2 Calibration of the microwave sources

As already mentioned, in the swept frequency reflectometers the key information to infer from the experimental data is the so called *time delay* τ_g. For a wave traveling through vacuum, this quantity is, in fact, related to the

distance x_c of the reflecting layer as follows:

$$\tau_g = \frac{1}{2\pi}\frac{d\Phi(t)}{dt} = \frac{1}{2\pi}\frac{d\Phi(f)}{df}, \tag{5.1}$$

being

$$\Phi(f) = 2\frac{2\pi}{c}f(t)x_c. \tag{5.2}$$

In a real measurement, the problem arises of knowing exactly the evolution of the frequency during a sweep (namely the time-frequency characteristic curve), in order to minimize the error in eq.5.1 passing from the quantity $d\Phi(t)/dt$ (the output of the system) to $d\Phi(f)/df$ (physically related to x_c). According to the theoretical model presented in Chapter 3 and in [94], in the present configuration of the diagnostic system, to achieve the fast sweeping rate required the IMPATT source is driven by a voltage to current converter in 1 μs, modulated by an arbitrary waveform generator. The output of the system should produce a triangular wave with a sweeping rate $\alpha = 4GHz/\mu s$, as shown in fig.5.1 (continous line). Unfortunately, despite a linear driver input, the IMPATT oscillators are characterized by an intrinsic non-linearity, that has to be taken into account for a correct interpretation of the received signal. This problem is, actually, rather common in the sweep reflectometers, especially where an ultrafast modulation is applied. For this reason, in other machines different linearisations of the microwave sources are usually performed, by means of special frequency meters (see for instance [118]). These methods allow to 'compensate' the non linearity of the sources, by feeding them with a non linear current, but they have the drawback of introducing

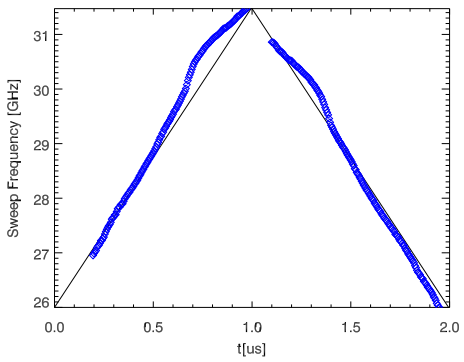

Figure 5.1: Theoretical (continous line) vs experimental (blue diamonds) time-frequency curve of the microwave source now operating on the RFX-mod reflectometer.

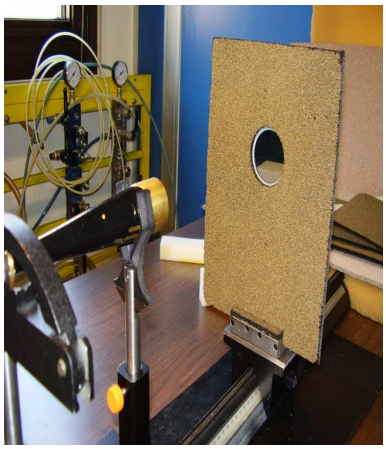

Figure 5.2: Picture of part of the calibration experimental setup (antenna and metallic mirror).

further noise into the system and/or to be very expensive.
A different calibration technique has been, instead, developed at RFX, aiming to 'measure' on the bench the output of the source (fig.5.1, blue diamonds) in the same conditions (modulation rate, optical path, waveguide size) present in the application on the plasma. This curve can be then used to rectify the received signal via software during the data processing phase.
Several benchtests has been performed by using the whole Ka-band system and a metallic mirror moveable at different positions d (picture in fig.5.2) Since the output of the mixer can be written as:

$$cos(\Phi(t,d)) = cos(2\frac{2\pi}{c}f(t)d), \tag{5.3}$$

by repeated reflectometric measurements with an ultrafast modulation rate (4 GHz/μs) it has been possible to reconstruct for each source the time-distance map of the received signal. In fig.5.3 we reported the characteristic interference pattern related respectively to the 27÷31 GHz, 32÷36 GHz and 35÷39 GHz IMPATT oscillators, covering the whole Ka-band frequency range (26÷40 GHz). The non-linearity of the system output is rather evident in all of the tested sources, especially when compared with the simulated interence pattern (fig.5.4), mimicking the reflectometric measurements (for an ideal source) at different positions d of the reflecting layer. From these plots, by considering the evolution of $cos(\Phi(t_i,d)$ at each fixed time instant t_i, as a function only of the distance d, it is possibile to deduce the associated frequency $f(t_i)$ (see eq.5.3). In this way, by fitting all the collected data with the help of the preliminary indications coming out from the simulation

work, we were able to reconstruct the complete time-frequency curve for each IMPATT oscillator (fig.5.5 shows the result for the lowest frequency source). The same method is applied simultaneously for the ascending and descending frequency modulation in order to obtain the result shown in fig.5.1.

Once reconstructed the exact characteristic frequency scale, the received signal can be rectified (e.g. interpolated on a linear scale) in order to avoid the typical folding effect (see fig.5.6) related to a non linear source. In fig.5.6, in fact, the importance of canceling this effect (the signal oscillations get squashed each other) is evident for a correct evaluation of the time delay. Finally, after the calibration of the source and the rectification of the signal, the data can be properly analyzed in the light of the model presented in Chapter 3. The same benchtests allowed, thus, to appreciate the accuracy of the experimental method, by comparing the real distance of the reflecting

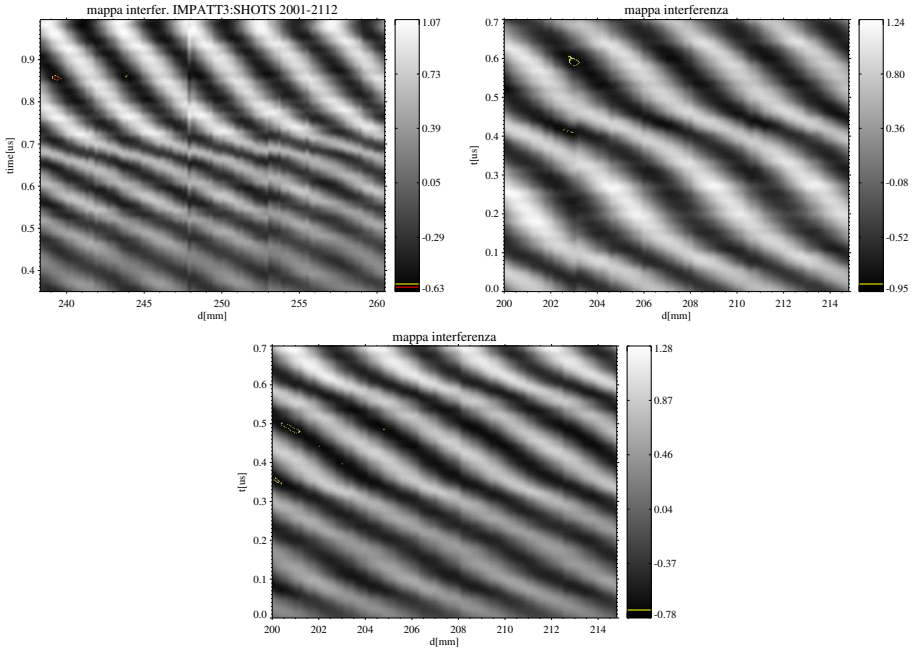

Figure 5.3: Interference pattern related to three different IMPATT microwave sources; these plots have been obtained by performing at each distance d between mirror and antenna, a 10 ms measurement with a triangular modulation. Then we reconstructed the whole map (ramp up and ramp down separately) by drawing the received signal (proportional to the cosine of the phase delay) for each shot. Here are shown for simplicty only the ascending frequency modulation for the 27÷31 GHz (top left), 32÷36 GHz (top right) and 35÷39 GHz (bottom) IMPATT oscillators.

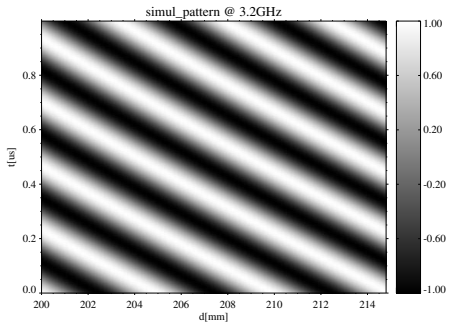

Figure 5.4: Simulated time-distance map, for an ideal source producing a microwave swept in 1 μs between 35 GHz and 39 GHz.

metallic mirror with the distance evaluated by fitting the reflectomer data. Even if the validation of such a measurement on the plasma application will be treated in the next section in a more detailed way, fig.5.7 gives already an hint about the reliability of the diagnostic.

Unfortunately, during this accurate calibration phase, two IMPATT oscillators (the 32÷36 GHz and the 35÷39 GHz) suffered severe faults. They have been found to be due to a malfunction of the protection system that allowed a current overload to be conveyed to the IMPATT oscillators. While it was impossible to repair the two sources (they are no longer used for more than 10 years), the system malfunction has been subsequentely fixed up assuring safe operations with the third one. The lowest frequency source has been correctly calibrated and it has been operational since 2009.

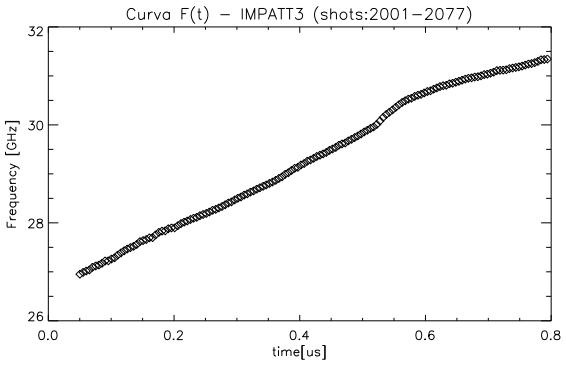

Figure 5.5: Time-frequency characteristic curve for the 27÷31 GHz IMPATT oscillator.

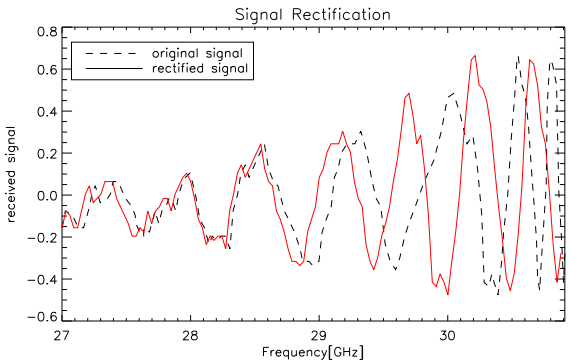

Figure 5.6: Example of signal reflected by the metallic mirror during a benchtest. The dotted line shows the typical folding effect at high frequencies where the microwave source is more markedly non linear. In the rectified signal, interpolated on a linear scale, this effect vanishes.

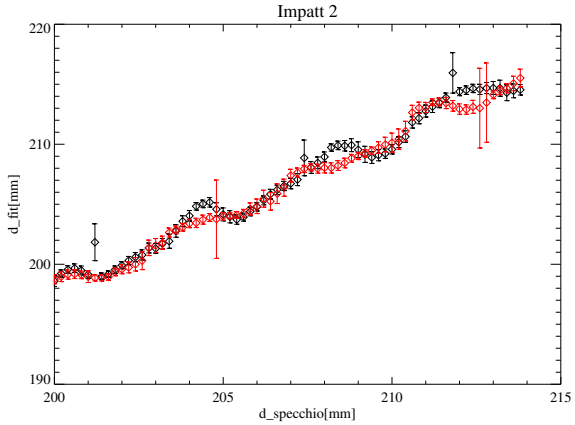

Figure 5.7: Real distance of the mirror (x-axis) vs reflectometric estimation (y-axis). Each point (black and red diamonds refer respectively to the ascending and descending ramp) is obtained by averaging the result over a 10 ms measurement. The agreement is quite good.

5.3 Experimental method and validation

The reflectometer circuit is located in a iron case outside of the RFX-mod vacuum vessel. This experimental setup aims to shield it from the large pertubations delivered by the RFX-mod magnetic circuit, especially when operating at high plasma current regimes. The microwave produced is conveyed through a flexible waveguide to the antenna. This latter is located at the back of a pipe (around 200 mm long) connected to the vacuum vessel

(at the toroidal angle $\phi = 352.3°$). The wave is, then, back reflected by the plasma towards the antenna and finally gets to the detector.

In the first year of operation, the system worked routinely in all of the different operative conditions of RFX-mod, collecting for each discharge (duration 0.5 s) a 200 ms signal approximative corresponding to the flat-top phase. However the acquisition time window has been occasionally moved to meet different kind of experiments. The so called *beat* signal is a 1d array of 4×10^6 elements. Moreover, to take into account the spurious reflections from the metallic parts of vessel and pipe, usually, a vacuum signal (before each discharge) is acquired and subtracted from the original one. The resulting pre-processed array (fig.5.8) can be, thus, divided according to the triangular frequency modulation (a sweep every μs) and analyzed separately for the ascending and descending ramp to deduce the group delay.

As already mentioned, only the $27\div31$ GHz IMPATT source is now available, corresponding to a critical density layer n_c of about $1\div1.2\times10^{19}m^{-3}$. In the approximation of edge linear density profile the measurement of the group delay τ_g can be directly linked to the cut-off layer position x_c through the model described in section 3.4. This allows to have an estimation of x_c every μs. However, to cancel the effect of the Doppler shift (due to the radial motion of the cut-off layer), an average over the ascending and descending modulations is required, producing an effective time resolution of $2\mu s$.
In all of the following plots the reflectometric data are presented in terms of distance d_c from the first wall (negative values). Positive values, where present, refer instead to the transient states in which the plasma slides into the pipe.
The accuracy of this measurement has been tested through different comparisons, involving the main diagnostic systems operating at the edge of RFX-mod (and synthetically described in Chapter 2).

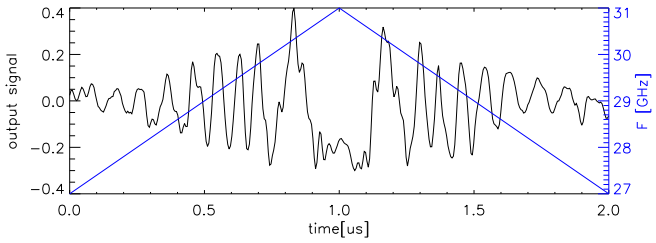

Figure 5.8: Example of beat signal (black) already subtracted from the vacuum contribution. The corresponding frequency modulation (blue) is also shown.

First of all, we considered the outermost chord of the interferometer measuring the time evolution of the line averaged density 150 mm far from the first wall and in a different toroidal position with respect to the reflectometer. Fig.5.9 shows a quite clear example of discharge in which that chord was measuring a density of about $1\times10^{19}m^{-3}$ (the same density of the plasma layer probed by the reflectometer) before a pellet injection. In this case, therefore, the variation in the edge density should be simultaneously measured in both the signals, as actually appears in the plot.

Similarly, in a different discharge (fig.5.10), the reflectometric signal is well correlated with the edge density fluctuations measured by the Thermal Helium Beam (THB) diagnostic [75]. In this case, actually, large low frequency oscillations are recognizable since a OFCD (Oscillated Field Current Drive) experiment was being performed. The distance d_c of the cut-off layer decreases according to the increasing density registered in the first 50 mm from the first wall by the THB.

Finally, aiming always to validate the estimation of the cut-off position made by the reflectometer, we analyzed the reconstruction of the edge density radial profile (up to 120 mm from the first wall) evaluated by the Edge Thomson

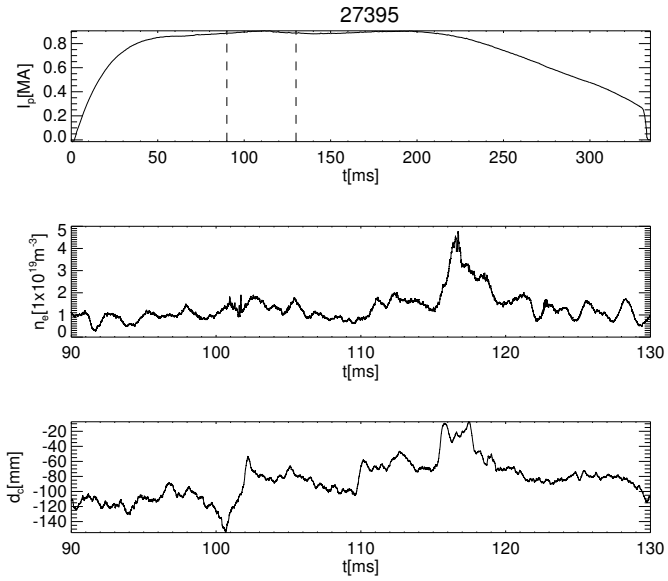

Figure 5.9: #27395. *Top*: Plasma current of the whole discharge (dashed lines mark the area zoomed in the plots below); *middle*: time evolution of the line averaged density as evaluated by the edge chord of the interferometer (the pellet injection is recognizable around 115 ms); *bottom*: cut-off layer distance from the first wall by the reflectometer.

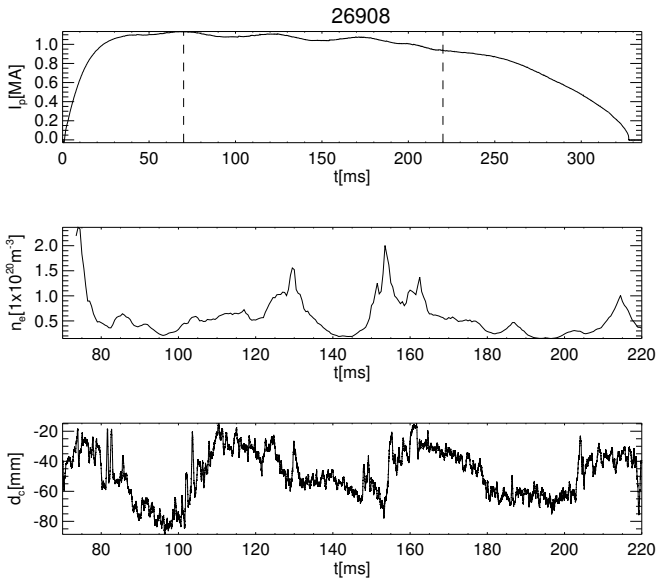

Figure 5.10: #26908. *Top*: Plasma current of the whole discharge (dashed lines mark the area zoomed in the plots below); *middle*: time evolution of the local density as evaluated by the THB (at 50 mm from the first wall); *bottom*: cut-off layer distance from the first wall from the reflectometer

Scattering (ETS) [73]. This system produces, unfortunately, a single snapshot for each discharge (see fig.5.11), anyway the agreement is quite good with the reflectometric signal averaged in the same time instants for two different kind of discharges.

These comparisons with the results coming out from Interferometer, THB and ETS represented a first preliminary validation of the reliability of the ultrafast reflectometer to diagnose the RFX-mod edge density dynamics. Moreover, they confirmed 'a posteriori' the soundness of the hypothesis of edge linear density profile, used to deduce the distance d_c of the cut-off layer from the group delay measurement. In particular the ETS data (fig.5.11) showed how in two of the most typical operative conditions for RFX-mod, namely low density QSH state and high density MH state (see chapter 2), the edge profile is almost linear, despite a high turbulence level characterizing all the RFP regimes.

The last consideration, before discussing in a more detailed way the experimental results, arises just from the density fluctuations. Actually, this reflectometer scheme aims to counteract their deleterious effect on the measurement (see chapter 3). However, this first year of operation showed also that the measured group delay τ_g still suffers from a moderate level of noise

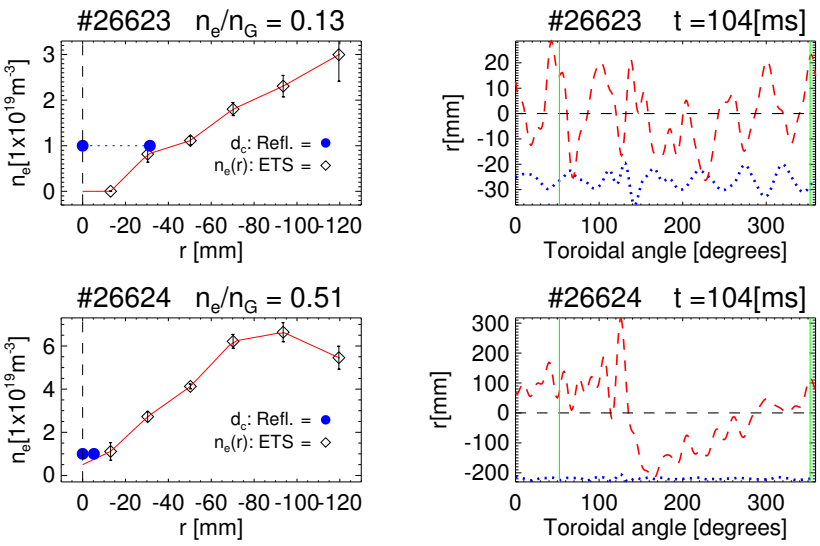

Figure 5.11: Left column: edge density profiles (as evaluated from the ETS) and d_c values for the same time instants referred to 2 different discharges. Right column: reconstruction of the whole toroidal magnetic topology referred to the same time instants and discharges. The toroidal positions of the ETS ($\phi = 52.3$) and the reflectometer ($\phi = 352.3$) are also shown.

due to the spatial density fluctuations. Even if this does not compromise the correct recovery of the cut-off position, but simply requires a reasonable data smoothing, it pointed towards a further increase of the modulation rate, in order to make possible the study of the high frequency edge turbulence and the estimation of the Doppler shift. A first preliminary attempt (4 GHz/500 ns) has been made at the end of the 2010 experimental campaign without any significant improvement. Nevertheless in order to seriously face this problem, a more general upgrade of several hardware components would be strongly needed.

5.4 Edge density and local magnetic topology

The high time resolution ($\Delta t = 2\mu s$) of the ultrafast reflectometer enabled us to compare its results with a large set of diagnostic systems operating on the RFX-mod experiment. The results presented in the previous section aimed to validate the experimental method, but they did not allow a direct comparison in terms of density fluctuations since the comparitive measurements were performed in different toroidal positions and with a lower time

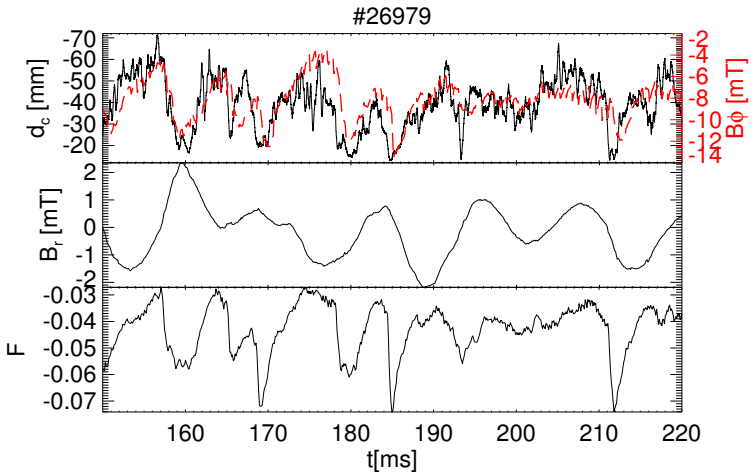

Figure 5.12: #26979. Top: Time evolution of d_c signal (continuous black line) and local B_Φ (red dashed line). Middle: Time evolution of the local B_r. Bottom: typical behaviour of the F signal.

resolution.
For this reason, we moved towards a more local analysis by considering the time evolution of the different magnetic field components at the edge. Fig.5.12 reveals a clean correlation between $d_c(t)$ and the local toroidal magnetic field $B_\phi(t)$ and a lower anti-correlation with the radial one $B_r(t)$, both evaluated with an external array of magnetic probes.
The recurrence of this correlation suggests a relation between the edge density dynamics and the local magnetic topology, being the magnetic field fluctuations linked to the presence of the $m = 1$ and $m = 0$ MHD modes. A detailed description of the RFX-mod edge magnetic topology can be found in chapter 2. However, in the same figure, it is possible to notice in the F signal how the periodic sawtooth activity produces large structures that rapidly travel to the first wall (d_c decreases). These magnetic relaxations (often called "crashes") tipically develop in different toroidal positions occuring along with a complete reorganization of the precast magnetic order [62]. The analysis performed by means of the reflectometer together with an internal toroidal distributed array of magnetic sensors [119] confirmed that significant plasma structure are associated to the crash evolution. A more detailed description of this study can be found in [120].
Since we monitor a layer with constant density, its dynamics, depending on the central electron density n_e, can be linked to different magnetic flux surfaces (located at different radial positions). In particular, as already mentioned in chapter 2, in RFX-mod radially moving from the edge towards the

core, the launched wave can meet first the m=0 poloidally simmetric perturbation and, then, the m=1 helical one.

Fig.5.13 ($n_e = 3.5 - 4 \times 10^{19} m^{-3}$) proposes a more explicit comparison with

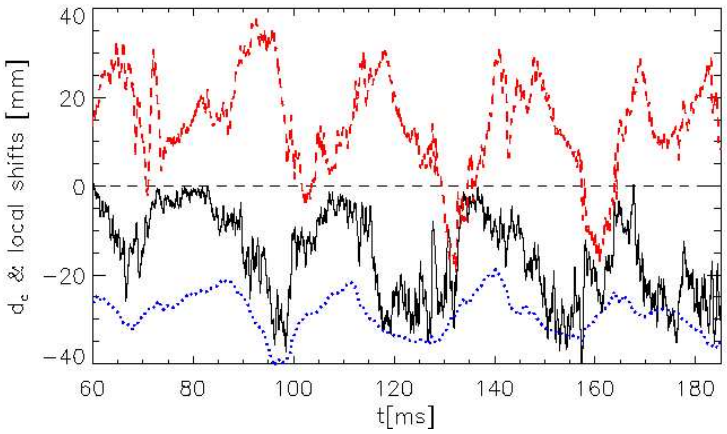

Figure 5.13: #28743. The evolution of the local magnetic topology figurated by the $\delta_{m=1}$ (blue dotted line) and the $\delta_{m=0}$ (red dashed line) deformation is overplotted to the time evolution of d_c (black continuous line). Only when $\delta_{m=0} < 0$ (around 130 and 160 ms) it seems to well describe the d_c dynamics, otherwise correlated to the $\delta_{m=1}$ oscillation. The first wall limit is also shown at $y = 0$.

the local magnetic topology reconstructed using the local displacements $\delta_{m=1}$ and $\delta_{m=0}$ (referred to the average shift of the plasma column [63]) for the m=1 and the m=0 modes. The time evolution of d_c (continuous line in fig.5.13) appears to be well correlated (at low frequency) with the regular oscillation related to the more internal QSH deformation (dotted line), even if the amplitude of this oscillation (around 10 mm) is too small to justify the larger fluctuations (around 30 mm) observed in the d_c signal. On the other hand, when the m=0 deformation (dashed line) is more consistent in terms of amplitude (around 30-40 mm), it is able to describe the evolution of the cut-off layer only as long as $\delta_{m=0} < 0$ (i.e. the field lines related to the m=0 islands close into the chamber).

This last concept is more evident in fig.5.14, where the effect of the m=0 islands dynamics is longer than the previous case. As long as $\delta_{m=0} > 0$ the reflectometer measurement gives a d_c mean value of about 40-50 mm (according to the averaged behaviour usually registered for that global density, see next section and fig.5.18). When $\delta_{m=0}$ transiently becomes negative (between 120 and 140 ms and successively at 150 ms), namely the m=0 island

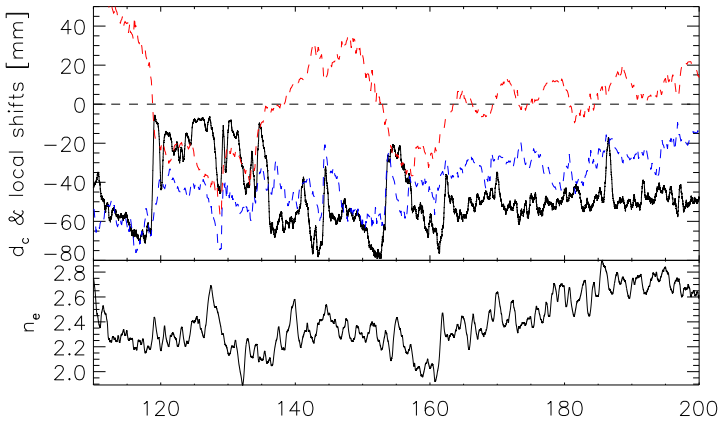

Figure 5.14: #28205. Top: time evolution of the local magnetic topology figurated by the $\delta_{m=1}$ (blue dotted line) and the $\delta_{m=0}$ (red dashed line) deformation, overplotted to the d_c signal. Bottom: line averaged density of the central chord of the interferometer.

in front of the reflectometer antenna closes entirely into the chamber, the smaller d_c value reveals a increased localized plasma wall interaction. It is worth noting that the global n_e dynamics does not appear correlated with the d_c evolution, supporting the idea that these phaenomena are local.

A further indication in this sense comes from the bolometer data [61, 76] and, in particular, from the total radiated power measured by the bolometric tomography. At the edge a larger radiated power can be interpreted as a local temperature decrease and, thus, as an increased local plasma wall interaction. In fig.5.15 we considered two discharges representative of two different local magnetic topologies. In the first one the plasma wall interaction is localized according to the clear $\delta_{m=1}$ modulation, similarly to what already discussed in fig.5.13. This picture appears consistent with the typycal QSH edge magnetic topology, already discussed in chapter 2 and represented by the reconstructions made by the ORBIT and FLiT codes in figs. 2.9 and 2.10, with the characteric phase relation $\Phi = \pi/4$ between the 2 main deformation in the equatorial plane.
In the second one (fig.5.16), the $\delta_{m=0}$ is almost always negative and the bolometer registers a completely different radiative pattern, featuring a more continuous local plasma wall interaction and above all symmetrically distributed on both sides of the chamber (thus following a $m = 0$ geometry).
Finally, a last indication of the role that the $m = 0$ deformation could play in the local plasma-wall interaction comes from the analysis of a special ex-

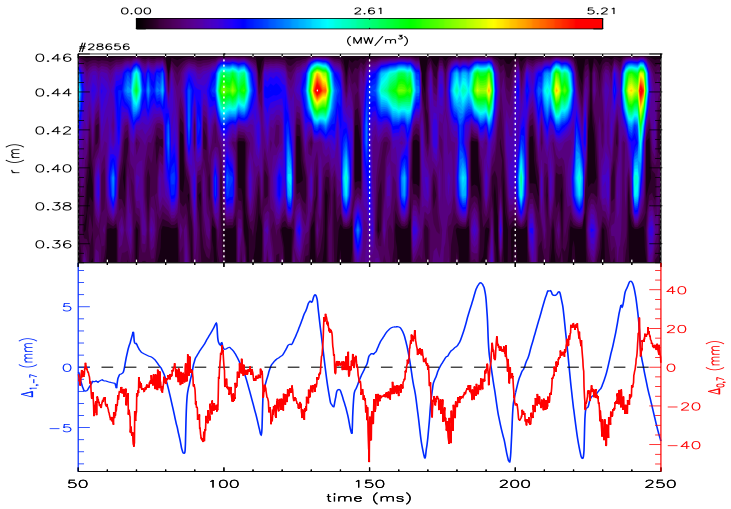

Figure 5.15: Top:#28656.Time evolution of the local radiative pattern as evaluated by the bolometer in the edge region. Bottom: time evolution of the local $\delta_{m=1}$ (blue) and $\delta_{m=0}$ (red)

.

periment in which a slow ramp has been induced in the F value (fig.5.17). During this transient, passing from shallow to a deeper and deeper configuration ($n_e = 4 \times 10^{19} m^{-3}$), the distance, d_c, of the cut-off layer decreases, while on the local magnetic topology side, the $m = 0$ islands, whose field lines were initially intercepting the first wall, progressively close into the chamber.
As it is discussed in the next section, the control of the edge density appears crucial to improve the RFX-mod performance especially in high density regimes. However, these data reveal how any attempt to characterize the edge dynamics needs to take into account the evolution of the different component of the edge magnetic topology. In particular, a control of the $m = 0$ islands, in both of their amplitude and distance from the wall, would really produce an effective improvement of the edge conditions for the high plasma current operations.

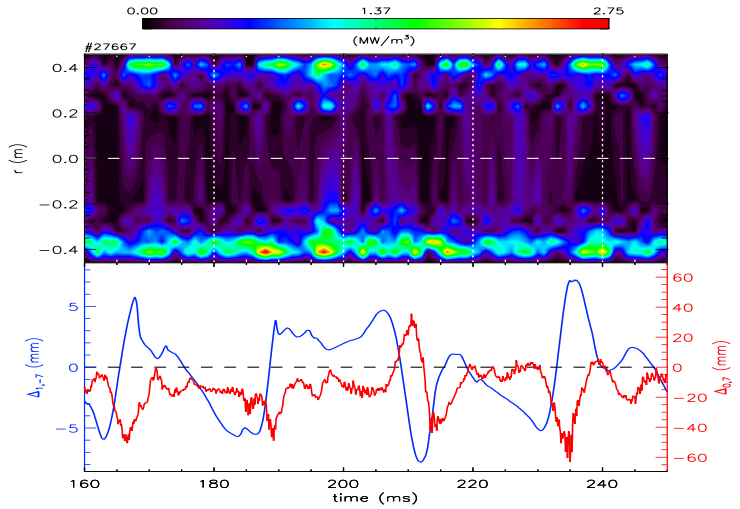

Figure 5.16: Top:#27667.Time evolution of the local radiative pattern as evaluated by the bolometer for the whole equatorial plane. Bottom: time evolution of the local $\delta_{m=1}$ (blue) and $\delta_{m=0}$ (red)

.

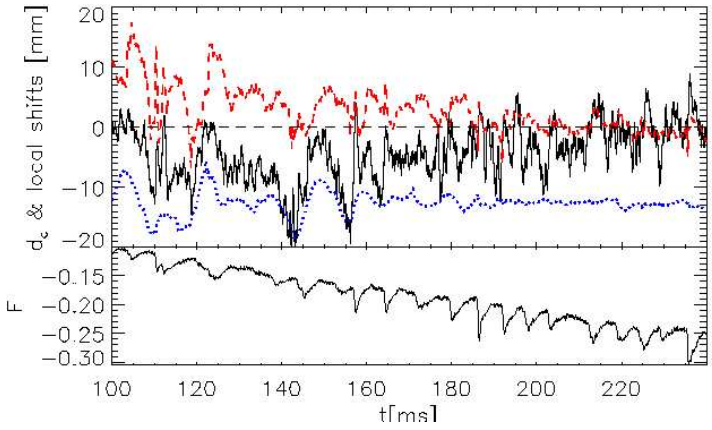

Figure 5.17: #27747: d_c progressively decreases (top), while a ramp in the F signal is induced (bottom). At the same time, the reconstruction of the local magnetic topology ($\delta_{m=0}$ red dashed line and $\delta_{m=1}$ blue dotted line) highlights how the $m = 0$ islands move inwards till closing into the chamber ($\delta_{m=0} < 0$). The first wall limit is also shown at $y = 0$.

5.5 Average behaviours

The analysis of the complex edge density dynamics removes all doubts on the significant role played by the local plasma parameters. However, important information can be deduced also by looking at the average behaviour of the radial distance of the cut-off layer with respect to the global discharge parameters.

In this section we present the results obtained by averaging the reflectometric data on a shot to shot basis only during the QSH states, in order to avoid the large fluctuations produced by the sawtooth oscillations, which have a transient nature and are not completely linked to the global parameters (electron density and plasma current, for instance).

In fig.5.18 a clear trend of d_c is recognizable as a function of the global electron density n_e obtained from the central chord of the interferometer. In other words, the edge density seems to increase by increasing the central density. This is not surprising for RFX-mod since the low density discharges are characterized by a magnetic order level higher than the high density ones [61]. The fact that the distance d_c measured by the reflectometer goes rapidly to 0 above certain n_e values probably reflects a lower optimization of the high density operations.

A very similar behaviour, shown in fig. 5.19, is found when plotting d_c as a function of the ratio n_e/n_G. Also in this case, a threshold value is recognizable for $n_e/n_G \geq 0.3$ and it is consistent with some previous results [75, 61, 64] obtained on the RFX-mod device. In the same figure a pre-

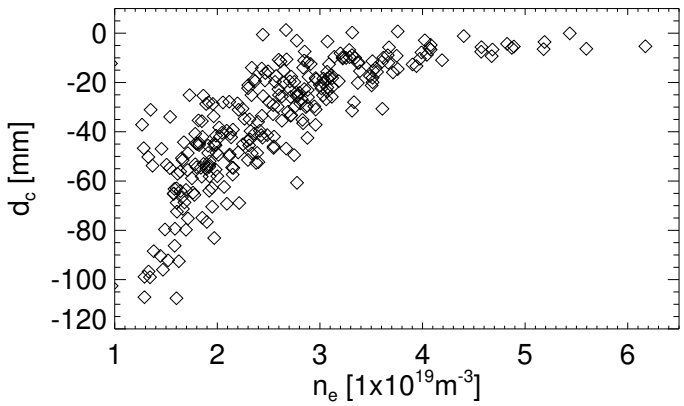

Figure 5.18: Scaling plot of $< d_c >$ vs n_e measured by the interferometer. At high values of n_e corresponds a minor plasma-wall distance (d_c close to 0).

liminary comparison with the Edge Thomson Scattering [73] is presented, in a discharge database with comparable n_e/n_G values. From the interpolation of these data we deduced the distance from the wall of the density layer (1-1.1$\times 10^{19} m^{-3}$) corresponding to the cut-off layer probed with the reflectometer. The agreement is quite good, even if the Thomson scattering database lacks low n_e/n_G measurements, and confirms a kind of empirical density limit for RFX-mod.

On the other hand this result seems also to assign a role, maybe minor, to the plasma current I_p through the parameter n_G. Fig.5.20, in fact, shows that the distance of the cut-off layer linearly increases by increasing I_p. In this case to pull apart the significant contribution due to the global density, we considered only discharges with similar n_e values (in the range 2.7-3.2$\times 10^{19} m^{-3}$) and, as further condition, with the same F values ([-0.05,-0.02]). Since the high plasma current operations are characterized by a large power load delivered to the wall and during the QSH states different diagnostics reveal a strong periodic (according to the helical structure) plasma-wall interaction, this result could probably appear contradictorly. Nevertheless, it describes an average behaviour, mixing together situations of both maximum and minimum local interaction (see previous section and fig.5.15 for instance).
Futhermore, in fig.5.21, considering a set of discharges with comparable global density n_e (2.7-3.2$\times 10^{19} m^{-3}$) and plasma current I_p (1-1.2 MA), we found that also the global magnetic configuration (i.e., the F value) can slightly modify the local plasma-wall interaction. In particular, since the radial position of the m=0 islands is globally defined by the F value, this

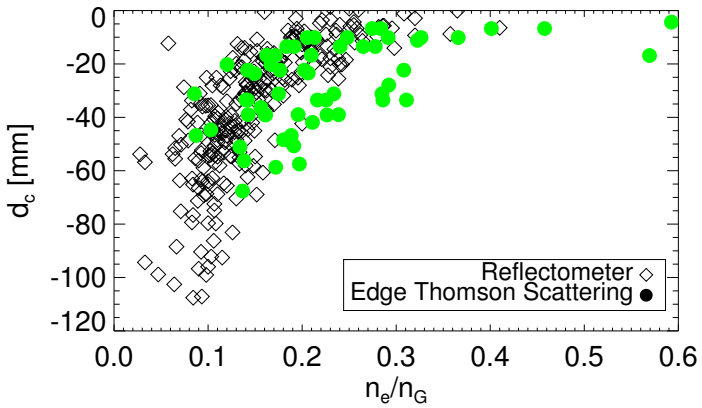

Figure 5.19: Scaling plot of $< d_c >$ vs n_e/n_G (black diamonds) and of the same quantity deduced from the edge Thomson Scattering data (green balls).

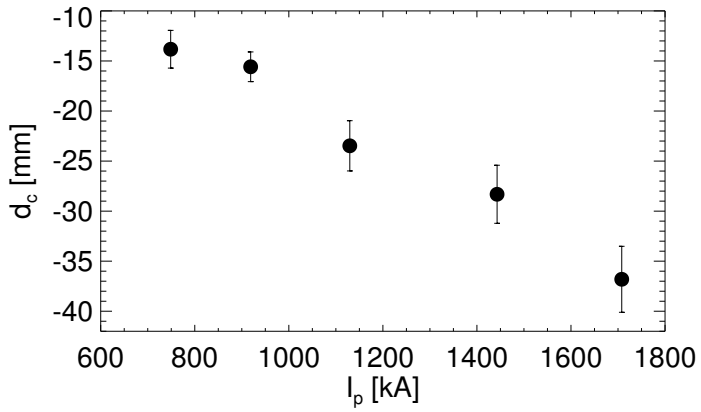

Figure 5.20: Scaling plot of $< d_c >$ vs I_p.

plot depicts in a different way the aforementioned interplay between the m=1 and m=0 deformation, passing from a 'shallow' to a deeper configuration (see previous section and fig.5.17). Also, it is consistent with a previous analysis (fig.5 in [56]) highlighting the dependence on the reversal parameter F of the distance from the first wall of the last closed flux surface.
Looking at the customary RFX-mod operations, these last four plots photograph a very realistic picture, in which the improved regimes, such as QSH states, appear much more frequently at high plasma currents I_p, shallow F configurations and density values below a certain threshold. One of the reasons of these limits could be probably a too high edge density [64, 75]. The

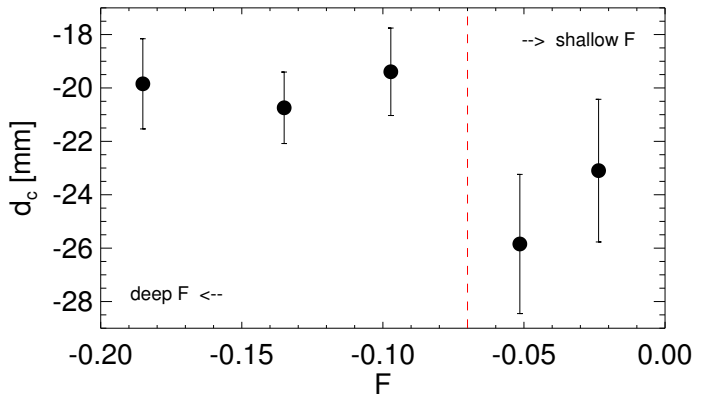

Figure 5.21: Scaling plot of $< d_c >$ vs the reversal parameter F.

RFX-mod first wall is entirely covered by graphite tiles, that up to now did not allow a proper control of the global density [66]. Recently, in order to overcome this limit, a gradual lithization of the first wall through pellets injection, has been undertaken and the first results have been already presented [67].
To study the effect of the lithium deposition on the edge density, analogously to what made previously, we compared the clear trend of the cut-off layer distance d_c with respect to the global density n_e, for 2 different sets of discharges, before and after the wall conditioning (fig.5.22). The presence of the lithium at the edge seems to produce an inward shift of the cut-off density layer of about 1-2 cm. This beneficial effect is not yet comparable with the large spread in the d_c behaviour induced by the central density variations (fig.5.18 and fig.5.22). If a more extensive use of the lithium will produce more significant results in the edge density control, it could make the RFX-mod able to overcome the actual operational limitations.
Otherwise, a possible alternative solution could be to perform a glow cleaning discharge (GDC) before each shot [68]. This would allow to minimize the hydrogen recycling by the graphite wall (emptied by the GDC) and, thus, to improve the density control.

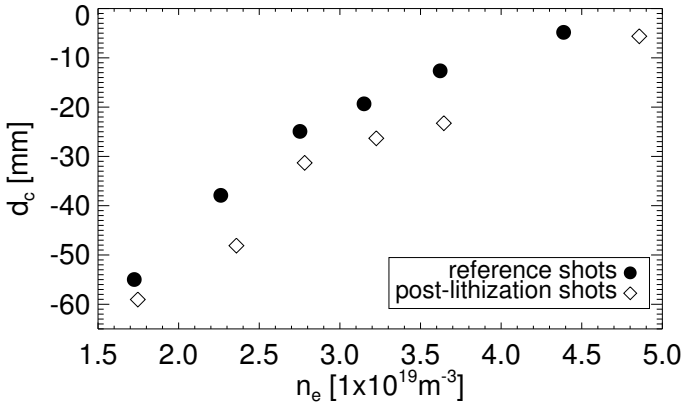

Figure 5.22: Scaling plot of $< d_c >$ vs n_e for 2 different discharges set, referring to before (balls) and after (diamonds) wall conditioning with Lithium.

Chapter 6

Edge flow measurements

6.1 Introduction

In fusion oriented plasmas, for any machine configuration, an understanding of the edge transport mechanisms as complete as possible is crucial. In particular, in the Reversed Field Pinches the edge transport is recognized to be strongly affected by its peculiar magnetic pattern [105, 57] . Aiming to cope with part of the large topic represented by the transport features in the RFPs, in this chapter we present the most important results obtained on the RFX-mod experiment using the Gundestrup probe.
All of these results are based on the innovative experimental method, already presented and validated in chapter 4, to deduce the edge flow components starting from the V_f measurements, but at the same time, many comparative analysis are proposed.
The significant power loads delivered during the customary high plasma current discharges ($\geq$ 10 MW/m^2) would make the insertion of the any solid objects inside the RFX-mod chamber very dangerous. For this reason, usually, to investigate the edge transport properties through the electrostatic probes, dedicated low plasma current experimental campaignes (see fig. 4.2) are scheduled in the RFX-mod operation planning. In these discharges the probe insertion r_p is, however, limited to the most external 10% of the minor radius (a = 459 mm). This allowed the study of the edge flow properties both in terms of the statistical reconstruction on a shot to shot basis (see sect. 6.2.1) and the analysis of special transients induced by pellet injection and changes in the magnetic equilibrium (see sect. 6.2.2).
Later, since the discovery of the improved RFP regimes (see chapter 2), at the moment achievable solely at high plasma current, it has grown the interest in studying also the flow features of the Quasi Single Helicity (QSH)

states. While some spectroscopic measurements [69] polarized their attention on the plasma core, the Gundestrup probe, although confined at the extreme edge ($r_p/a = 1$) in high plasma current operations, revealed strong flow modulations. These quite interesting results are presented in the second part of the chapter.

6.2 Low plasma current operations

Thanks to an improved magnetic boundary control with a reduced plasma wall interaction [42] and to a feedforward controlled reversal parameter [121] a set of reproducible discharges has been obtained with a plasma current I_p always kept below 400 kA to allow the probes insertion and a shallow F ($F > -0.07$) equilibrium. The Greenwald parameter n_e/n_G experienced, instead, large variations in the range $0.2 \div 0.7$, due to a poor control of the plasma density n_e caused by the interaction of the plasma with the graphite first wall [66].
Due to the low plasma current, the magnetic configuration in the considered discharges is normally in the so called Multiple Helicity (MH) states (see chapter 2), characterized by a wide spectrum of tearing modes limiting the machine performance. This has important consequences on the magnetic topology and, similarly, on the flow pattern. In particular, in the MH states, the RFX-mod edge is dominated by the presence of a chain of poloidally symmetric m=0 islands that, as shown in the next sections, can seriously affect the edge flow dynamics.

6.2.1 Reconstruction of the edge flow radial profiles

A statistical study of the edge flow properties has been undertaken by considering the data coming from a large set of edge diagnostic systems such as the Gundestrup probe, the U-probe [77] and the Gas Puffing Imaging (GPI) [75]. These different measurements confirmed the presence of a strong toroidal flow (up to ten times larger than in Tokamaks) at the edge of RFX-mod, building up from the interaction between the radial electric field E_r and the main poloidal edge magnetic field $B \cong B_\theta$, thus as a result of the $\mathbf{E} \times \mathbf{B}$ drift.
In this section we present the reconstruction of the edge radial profiles of both the flow components expressed in terms of Mach number, M_{par} and M_{perp}, respectively parallel and perpendicular to the poloidal magnetic field. These profiles have been obtained by averaging the data over the plasma current

flat-top phase on a shot to shot basis. In particular the Gundestrup probe has been set to collect V_f measurements and it has been moved at different radial positions at each discharge coherently with the U-probe (30° toroidally far from the Gundestrup probe), providing the electron temperature T_e at the same radial position.
The average radial profile of the perpendicular flow component M_{perp} is shown in fig.6.1 for the two models (a magnetized and an unmagnetized) described in the chapter 4 by the eqq. 4.11 and 4.13.
The profiles shapes are very similar between the two interpretation models,

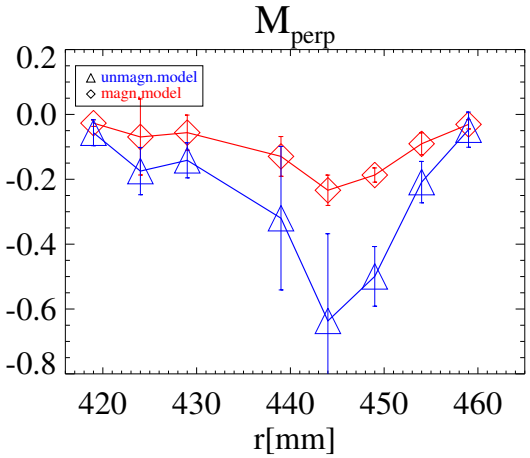

Figure 6.1: Radial profile of the perpendicular Mach number for the two different V_f based models: magnetized (red) and unmagnetized (blue). Each symbol is obtained averaging the data over the flat top phase of the different considered discharges.

even if at the positions of the maximum shear (roughly within 2 cm from the wall), they differ in absolute value. In both the innermost and outermost radial positions instead, this result suggests an inversion of the toroidal flow as also highlighted by spectroscopic measurements [64] on RFX-mod.
This picture could be easily explained as the result of the E_r behaviour at the edge of RFX-mod [122]. In this sense a direct comparison comes from the electrostatic pins of the U-probe, able to measure the $v_{E\times B}$ velocity, by accounting for the radial derivative of the plasma potential $V_p(r)$ (see chapter 4). Fig.6.2 shows how the shape of the toroidal velocity is coherent with the Gundestrup result also concerning the double inversion occurring at the extreme edge and in the innermost probed positions.
Information on edge toroidal flow can also be obtained by the magnetic array mounted on the U-probe (see chapter 2), able to reveal the local coherent

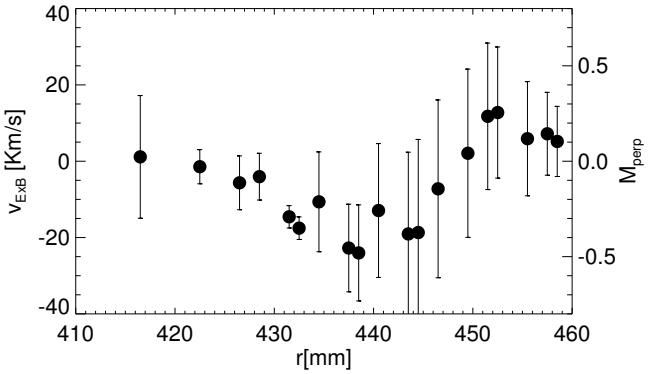

Figure 6.2: Radial profile of the $E \times B$ velocity evaluated by the U-probe. The right scale indicates the same values rescaled by considering the ion sound velocity c_s. Each symbol is obtained averaging the data over the flat top phase of the different considered discharges.

MHD activity properties. In particular, by means of two pins measuring the poloidal magnetic field $\dot{B}_\theta$ in different toroidal positions (the two arms of the U-probe, $\Delta\phi \simeq 5.6 \times 10^{-3}\ 2\pi$), and applying the two-points technique [123], it has been possible to measure the toroidal periodicity value associated to the observed MHD modes [124]. Fig.6.3 shows the frequency spectrum of each toroidal Fourier component (the so called $S(n, f)$) as evaluated in different low current discharges at different radial positions. In the figure, due to the limited spatial resolution of the toroidal coils array, the computed $S(n, f)$ spectra are affected by aliasing. Actually, part of the high frequency negative n values corresponds to the positive one.
A detailed analysis demonstrated that these fluctuations (having a $m = 0$ poloidal periodicity) follow a linear dispersion relation $\omega = (n/R)\ V_{ph}$, being V_{ph} the phase velocity in the toroidal direction [124]. V_{ph} can be, thus, estimated (of the order of 20-30 Km/s) from the slope of the MHD activity distribution curve in the $S(n, f)$ plot. In fig.6.3 two propagation directions (namely two slopes) are observed, confirming also in this case, a propagation reversal while probing the innermost plasma layers, consistently with the measured $\mathbf{E} \times \mathbf{B}$ flow.

On the other hand, since as already mentioned the magnetic field at the edge is mainly poloidal, a significant plasma flow is found also in that direction. The average radial profile of this parallel flow, M_{par}, obtained with the Gundestrup probe according to the eqq. 4.11 and 4.13 and for the same set of discharges used to infer the M_{perp} profile, is shown in fig. 6.4. Also in this case, the results from the two methods appear very similar, highlighting the

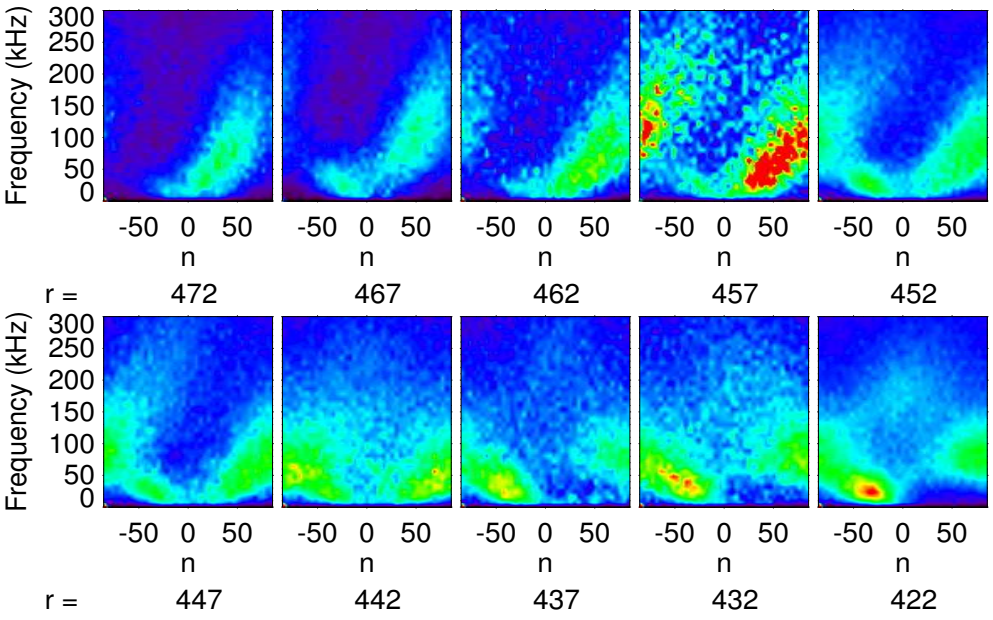

Figure 6.3: Frequency spectra of each toroidal Fourier component, $S(n, f)$, as evaluated in different low current discharges at different radial positions, r, by the Uprobe.

fact that a clear regime (between magnetized and unmagnetized plasma) can not be identified, at least in these operative conditions.

Unfortunately, there are not many diagnostic system able to evaluate the flow along the field line in the edge of the RFX-mod experiment. For this reason, it is not easy to explain the radial behaviour of the M_{par}, featuring a peak very close (a few cm) to the first wall.

An interesting consideration comes from the analysis of the edge magnetic topology. This region is, in fact, characterized by the presence of the aforementioned m=0 islands, surrounding poloidally the whole chamber. These MHD modes are destabilized because of the inversion of the toroidal magnetic field B_ϕ and the consequent creation of a q=0 surface. Some previous measurements on RFX-mod [57] revealed a flat temperature profile inside these islands, whose radial position is roughly defined by the F value. A more detailed analysis has been, thus, undertaken aiming highlighting a possible correlation between flow and magnetic topology and is presented in the next section.

It can be also noticed that, also in this case, an inversion of the parallel flow could, perhaps, occur in the more internal region, at the moment not inves-

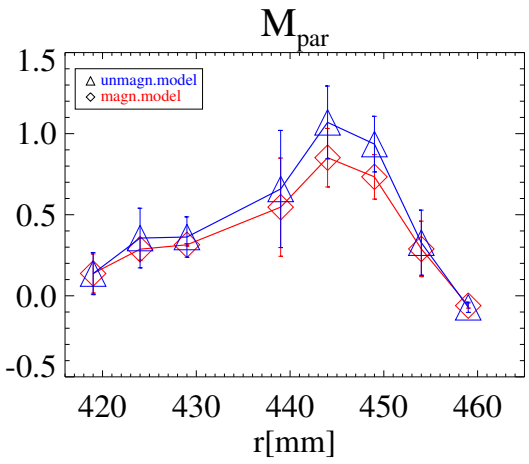

Figure 6.4: Radial profile of the parallel Mach number for the two different V_f based models: magnetized (red) and unmagnetized (blue). Each symbol is obtained averaging the data over the flat top phase of the different considered discharges.

tigated with the Gundestrup probe.

6.2.2 Time behaviour of the edge flow components

The high time resolution of the Gundestrup probe allowed the study of the transient phenomena taking place at the edge of RFX-mod or that have, however, an indirect effect on the edge flow components.
A first analysis in this sense was carried out in the wake of the previous results on the average radial profiles, suggesting a possible interaction between edge magnetic islands and local plasma flow. A specific experiment has been conceived exploiting the versatility of the magnetic boundary control system of the RFX-mod experiment. A step transient has been induced in the F parameter during the discharge flat-top phase so that different equilibria can be compared within the same discharge.

Specifically a phase with a shallow reversal ($F > -0.05$) and a phase with deeper reversal ($F < -0.15$) have been induced, the transition occurring within a time interval of about 5 ms. The Poincaré plots shown in fig. 6.5, obtained with the aforementioned field line tracing code (FLiT) [59], describe the different magnetic topologies at the edge related respectively to the shallow and the deeper equilibrium.
During this experiment the Gundestrup probe was located at $r = 440mm$,

approximatively corresponding to the region of maximum parallel flow shear as shown in fig. 6.4. The F values were chosen in order to make sure that the $m = 0$ islands overlapped the probe measurement point. The reconstruction of the edge flow components, $M_{par}(t)$ and $M_{perp}(t)$, made by the Gundestrup probe, referred to the same time window, are shown in fig. 6.7 together with

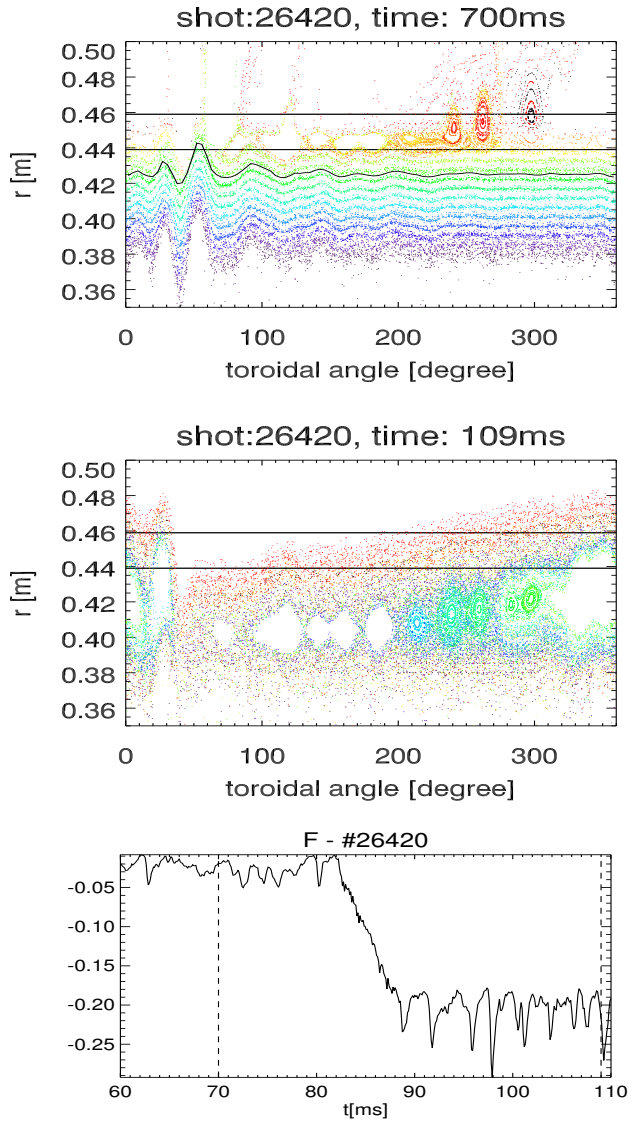

Figure 6.5: #26420: Poincaré plots in the (r,ϕ) plane of the edge region of RFX-mod, before (top) and after (middle) the F-step (whose the signal is also shown at the bottom). The toroidal region of the probe positions has been evaluated with a better resolution.

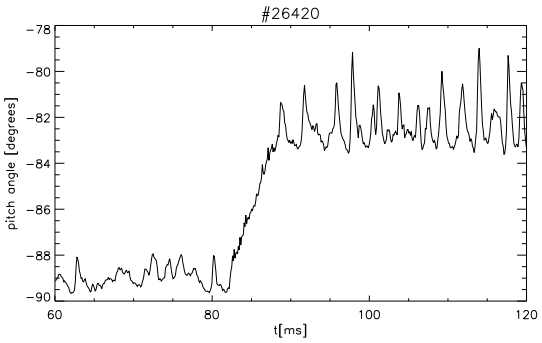

Figure 6.6: #26420: Orientation of the main edge magnetic field with respect to the equatorial direction during the F-step.

a more detailed zoom on the local magnetic toplogy.
The analysis of this experiment leads to some interesting considerations. First of all, the overlapping of the $m = 0$ islands on the Gundestrup measurement point (at t $\approx$ 84 ms) produces significant changes in the edge flow, appearing in the clear peak present on the M_{par} signal in the same time instant. When the island have completely overcrossed the probe position, the parallel flow becomes again considerably smaller.
For completeness we report also the orientation θ_B of the main edge magnetic field (fig. 6.6) with respect to the equatorial direction during the F-step in order to demonstrate that the parallel flow increasing (more than the 50% in the absolute value) can not be justified by a simple geometrical change due to the different equilibrium (θ_B varies of less than the 10%).
This is a very important result, since it can be directly related to the average radial profiles presented in the previous section. To study that behaviour a set of reproducible discharges (similar plasma current and equilibrium) were performed and the probe was located at different radial positions. In that case the position of the m=0 islands should not have changed. Thus, the high parallel flow shear observed near the wall could be interpreted as being due to the presence of a parallel flow within the $m = 0$ islands.
The M_{perp} time evolution during this experiment is not as much clear and the possible interaction with the magnetic topology is still under debate.
Another important fact, that can be deduced looking at the fig. 6.7, concerns the effect on the edge density dynamics. In the same experiment, the U-probe (30° toroidally far from the Gundestrup) was located at the same radial position. This probe can evaluate the local electron temperature and density with a radial resolution $\Delta = 7mm$ (see chapter 2), and thus, the local pressure gradient can be estimated. While the islands approach the measure-

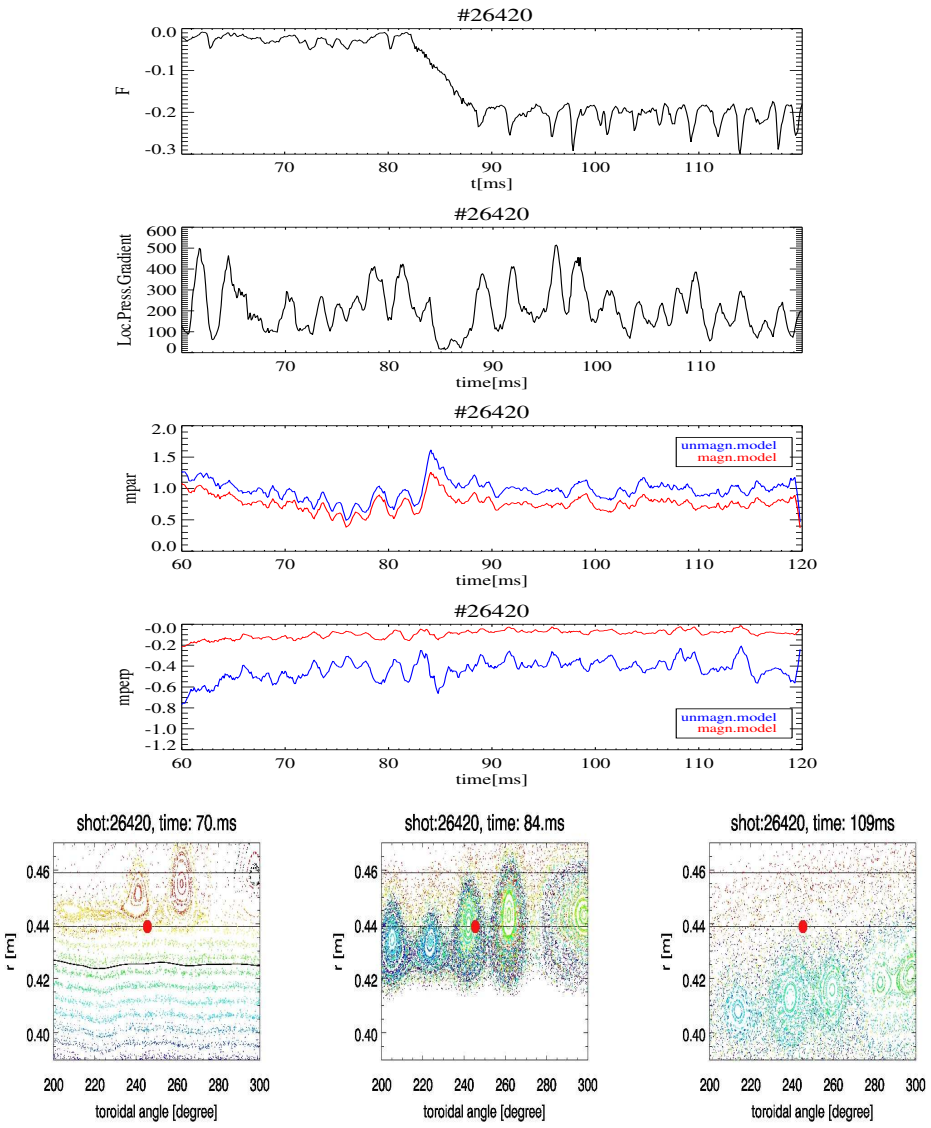

Figure 6.7: #26420: from the top, the time evolution of F parameter, the local pressure gradient by the U-probe, the parallel flow M_{par} and the perpendicular one M_{perp} by the Gundestrup for the magnetized (red) and the unmagnetized (blue) model. In the bottom row, a zoom of the local magnetic topology referred to before (left), in between (middle) and after (right) the F-step. The Gundestrup measurement points are also shown (red dots).

ment point the local pressure gradient goes rapidly to zero, supporting the thesis of flat density profile inside the magnetic islands and confirming some previous results [57] obtained with the Edge Thomson Scattering on RFX-

mod.

The relation between flow, density and magnetic topology, hence, appears very deep and the results presented in the next section will strenghten even more this concept, generalizing it also to the high plasma current regimes characterized by a completely different edge magnetic configuration.

The edge region of RFX-mod and its flow properties appear very complex and sensitive not only to the magnetic topology. Actually, as already proved by the microwave reflectometer in the previous chapter, it behaves like a

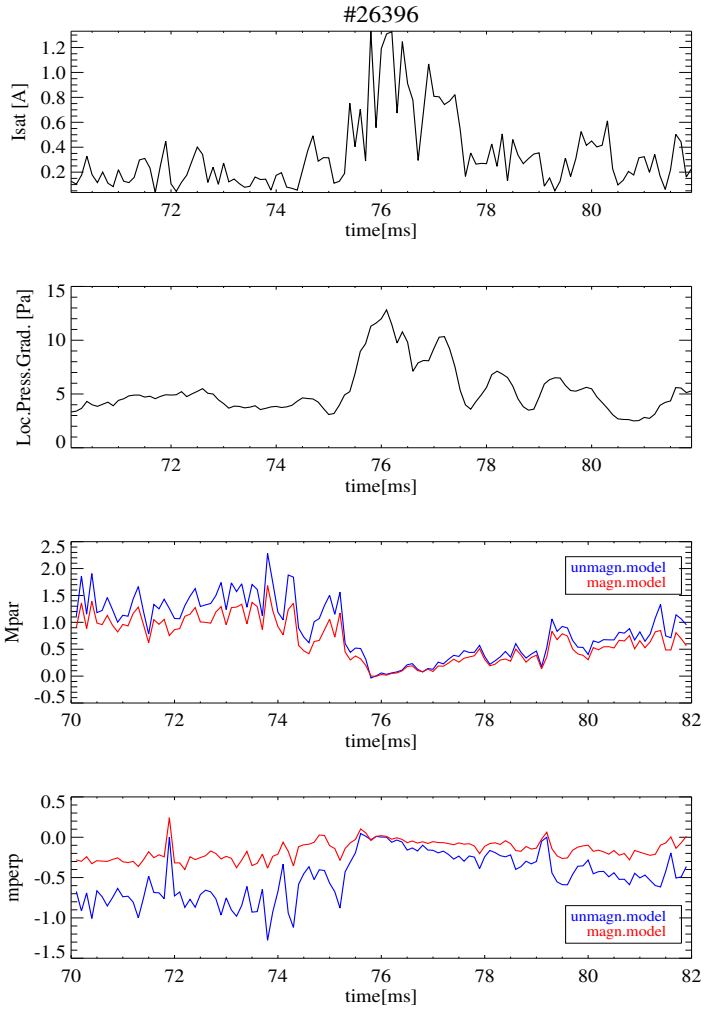

Figure 6.8: #26396: from the top, the time evolution of I_s signal proportional to the local density, the local pressure gradient by the U-probe, the parallel flow M_{par} and the perpendicular one M_{perp} by the Gundestrup for the magnetized (red) and the unmagnetized (blue) model.

sponge or a sounding board, absorbing all of the perturbations coming from the inner plasma layers or from the external, and reacting in different ways. Some preliminary tests involved, for example, the pellet injection. These experiments (see fig. 6.8) were carried out in order to study how the modifications in the global density, temperature and pressure induced by the pellet, interact with the edge transport properties.
It is not surprising that the pellet injection is able to modify the edge pressure gradient. Indeed, this was exactly one of the aims of this experiment, since this condition should mimic what happens in Tokamaks during the L-H transition, that some theoretical models [125] link to a possible edge transport changes. Perhaps, what could be less obvious, is that also the edge flow behaviour is strongly affected by the pellet ablation. In fig. 6.8 a strong reduction (simultaneously to the pellet ablation) in absolute value as well as in the fluctuation level is evident in both the edge flow components, $M_{par}(\mathrm{t})$ and $M_{perp}(\mathrm{t})$, obtained by the Gundestrup.
Actually, a similar behaviour, observed also in the I_s Gundestrup configuration (see chapter 4, fig. 4.4), is not confirmed by other experimental evidence on RFX-mod. In this case a critical point could be pinpointed in the exact reconstruction of the local electron temperature T_e. This is usually provided by the U-probe (thus, not really *local*), but probably, during the pellet ablation T_e experiences very rapid fluctuations that should be evaluated in the proximity of the Gundestrup measurement point. Similarly, we can not shut out possible asymmetries always in the T_e distribution along the Gundestrup probe, in the wake of what already seen on ISTTOK device (see chapter 4) and able to make a little stumbling the V_f based model.
For all of these reasons this result, even if extremely reproducible, probably merits further deepenings.

6.3 Tridimensional flow during the QSH states

The low plasma current regimes, although very interesting because they allow the probe insertion and, thus, a direct study of several fusion-relevant phenomena, suffer the limitation represented by the strong MHD activity spread over a large frequency and modal range. Moreover, since the discovery of the improved RFP regimes characterizing the high plasma current operations and featuring a global helical magnetic structure (see chapter 2), it became clear that also the edge conditions during the QSH states are quite different with respect to the probed MH states.

Unfortunately at these plasma currents ($I_p > 1.5MA$) the probe activity

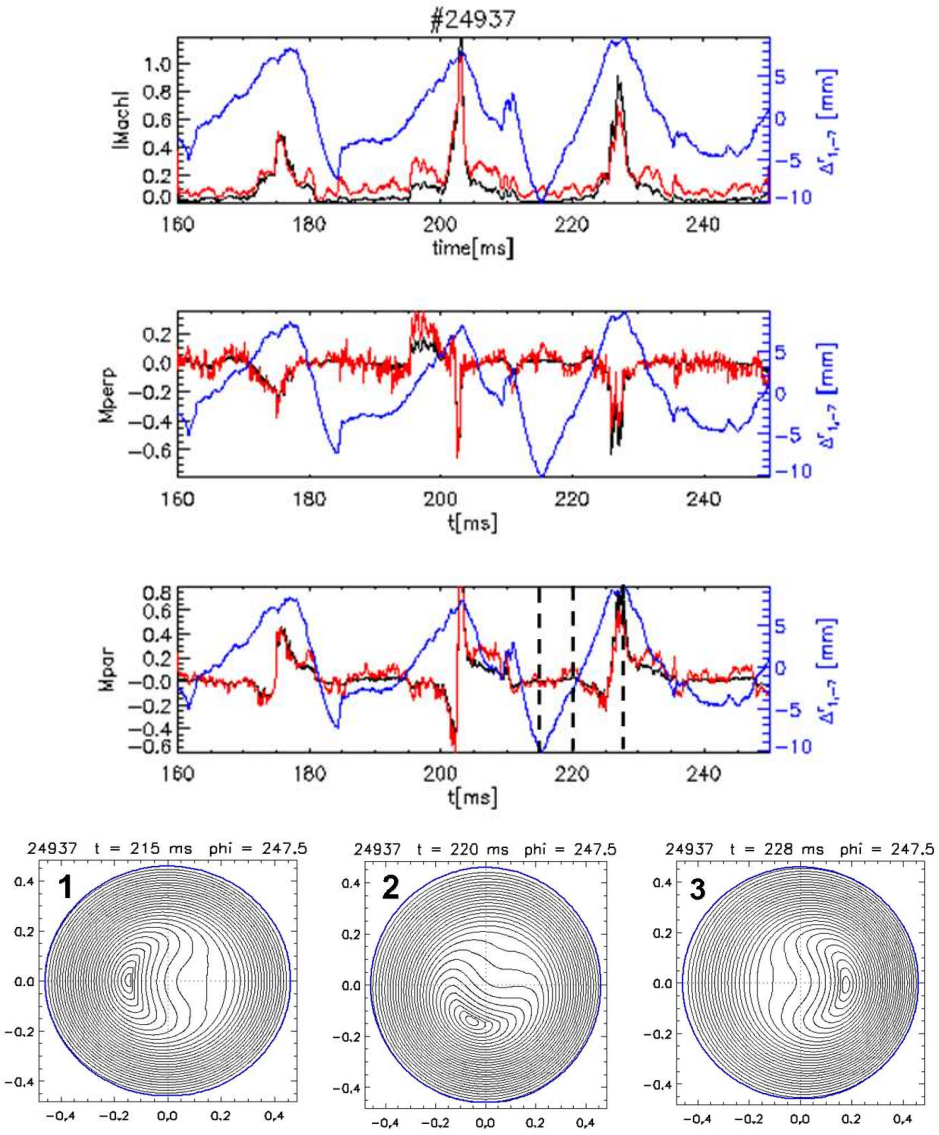

Figure 6.9: #24937: from the top, the time evolution of $|M|$, M_{perp} and M_{par} by the Gundestrup by considering a constant T_e or that one computed by the triple probe (black). The blue line represents the local shift $\Delta_{1,-7}$ induced by the QSH oscillation. In the bottom row, the reconstruction of the helical magnetic structure referred to three time instants marked with the dashed lines on the previous plot.

is significantly limited and the edge transport properties are usually investigated by means of spectroscopic techniques (the low Z ions diffusion) or by the Gas Puffing Imaging diagnostic. However, since the great interest

around the new perspective of the improved RFP regimes, by exploiting the protection offered by the graphite tiles composing the RFX-mod first wall, the Gundestrup probe has been located at the outermost plasma exposed radial position ($r_p/a = 1$) acting as a monitor for the edge flow components. Fig. 6.9 shows the typical behaviour of M_{par}, M_{perp} and $|M|$ (the total Mach modulus) obtained while a clear QSH state was affecting the local edge topology near the measurement point. The black and red curves refer respectively to the same quantities obtained by assuming a constant temperature or a fluctuating one accordingly to the T_e measurement made by the triple fixed probe [79, 80] in a different toroidal position.
It has to be pointed out that the above described helical magnetic structure is characterized by a helical Last Closed Flux Surface (LCFS) [56] appearing in the very edge region as a $m = 1$, $n = -7$ perturbation of the main magnetic configuration. The relative radial displacement of such perturbation, the $\Delta_{1,-7}$ shift, can be reconstructed starting from the edge magnetic measurement [63].
For completeness it is worth noting that the helical structure rotates toroidally, so that the time behavior of the shift measured in a given edge toroidal position exhibits a periodic oscillation. In the example shown in fig.6.9, the local shift, measured during a time interval of 90 ms at the local position of the Gundestrup probe, is overplotted to the edge flow evolution.
In order to better clarify the meaning of such oscillation the helical magnetic equilibrium reconstruction, based on the solution of Newcomb's equation

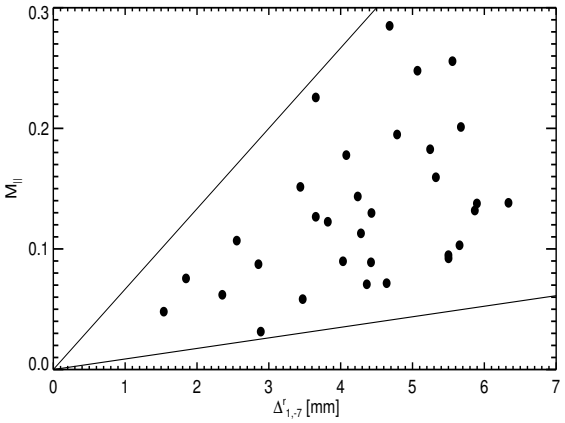

Figure 6.10: The M_{par} behaviour (in absolute value) with respect to the local shift $\Delta_{1,-7}$. Each point is evaluated by averaging the flow data over a very narrow time window around the $\Delta_{1,-7}$ maxima for several shots.

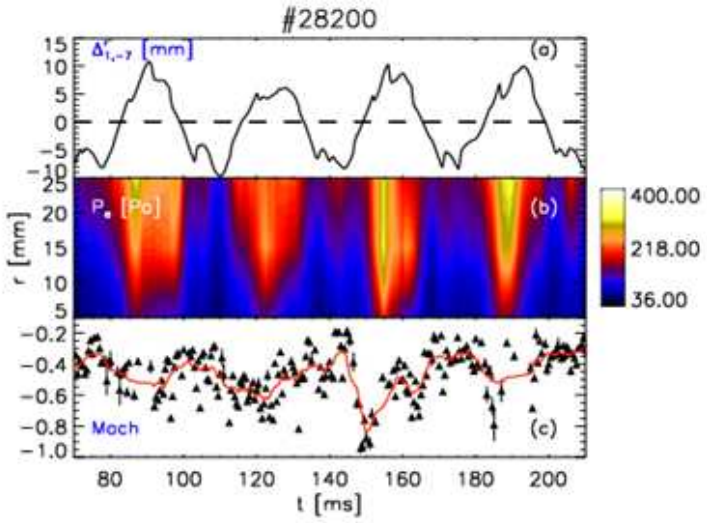

Figure 6.11: GPI perpendicular flow and pressure gradient time behavior:(a) Displacement of the magnetic surface due to the mode m=1, n=-7; (b): Time evolution of the electron pressure profile; (c): Time evolution of the perpendicular (toroidal) Mach number (triangles) and its smooth (red lines).

[126] for the dominant mode, has been provided at different time instants in the corresponding poloidal section and is shown in the same aforementioned figure (bottom). The time sequence shows clearly that the oscillation corresponds to a different poloidal position of the helical island with respect to the measurement point. In particular the minimum (instant 1) and the maximum (instant 3) of the shift correspond to the island O-point at the opposite and at the corresponding position respectively of the probe location measurements, in other words the positive shift means that the magnetic perturbation radially approaches the probe.
In all quantities a periodic variation is observed according to the shift periodicity, in particular around the shift maxima an abrupt variation with a change of the parallel flow sign is observed, whereas a strong increase of perpendicular flow (absolute value) is observed correspondingly. Both elements contribute to the total $|M|$, so that a strong increase in the flow value is observed when the shift is approaching the measurement point.

This trend could be interpreted as the presence of a sheared velocity surrounding the helical structure and is differently displayed in fig. 6.10, where a more statistical analysis over several discharges confirms a strong increase in the parallel flow M_{par} (in absolute value) according to the local shift $\Delta_{1,-7}$. A perpendicular flow modulation, according to the edge magnetic oscillation

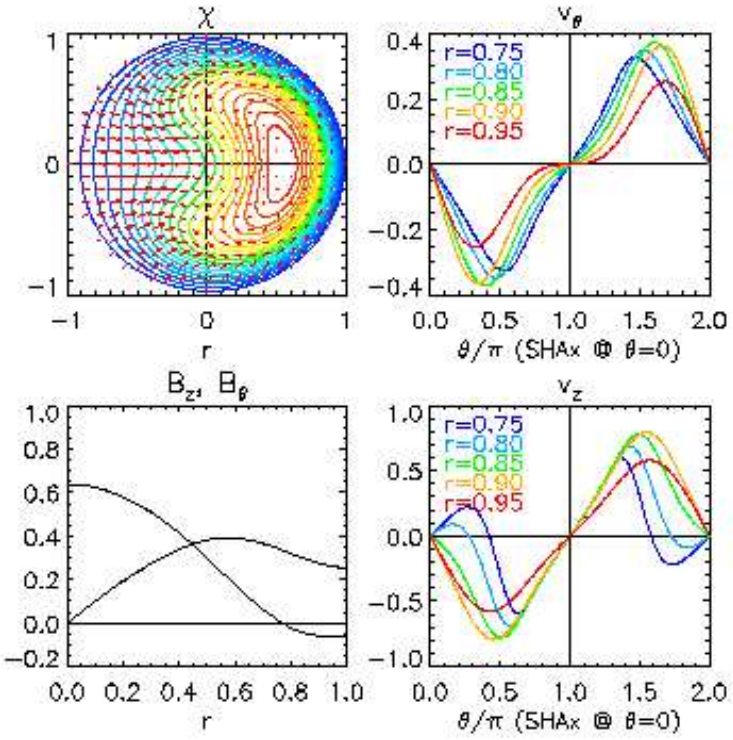

Figure 6.12: MHD simulation of the velocity field during a QSH state. On the left are shown the helical island with the corresponding tridimensional flow (top) and the magnetic field profiles (bottom). On the right the evolution of the flow components, v_θ and v_z, as function of the poloidal component θ. The different colors refer to different radial positions (the red one is the most external at $r/a = 0.95$).

during the QSH states, is also revealed by the GPI diagnostics [126, 74, 75]. Fig. 6.11 shows how significant increases in the toroidal flow (with values comparable to those obtained by the Gundestrup probe) are associated to the positive values of the local $\Delta_{1,-7}$(t). Moreover, in the same figure the time evolution of the local pressure profile is shown, confirming the result coming from the Reflectometer data in fig. 5.13 (positive values of local $\Delta_{1,-7}$ imply high edge local density). Also in this case the strong relation between magnetic perturbations, density dinamics and flow fluctuations is confirmed.

Concerning the parallel flow dynamics, some analogous measurements by means of the spectroscopic technique [69] cofirmed the suitability of the link between flow and magnetic topology also in the plasma core. In fact, these measurements revealed a velocity field surrounding the main magnetic helical islands and producing a global tridimensional helical flow. The rotation of

the magnetic structure during the QSH states would justify the modulation seen at the edge by the Gundestrup probe.
Furthermore, this velocity field was supposed by the MHD simulations [127] to have an important role in the formation of the helical states in RFX-mod. A very simplified example is shown in fig. 6.12. The velocity field, surrounding the whole magnetic island, creates at the edge a modulation in both of the flow components (called in the figure v_θ and v_z in the place respectively of M_{par} and M_{perp}). The evolution of v_θ and v_z is plotted as a function of the poloidal coordinate θ; however, in a rotating geometry (in which $\theta = \theta(t)$), a fixed measurement point (as the Gundestrup position) experiences the whole island crossing. For this reason these simulated plots could be directly related with the results shown in fig.6.9. While the measured parallel flow component evolution appears similar to the simulated one (but in the opposite direction), the perpendicular velocity is too difficult to be compared and also other effects can likely affect the flow properties, due to localized plasma wall interaction pattern, that characterizes such kind of discharges.
In all cases, therefore, low plasma current operations and improved QSH regimes, the comparison between probe measurements and magnetic reconstructions appears a very useful tool and a clever interpretation key for the complex phenomena taking place at the edge of RFX-mod, that, often (this thesis work demonstrated this concept for density dynamics and flow properties) can not be simply explained using the data coming from a single diagnostic.

Chapter 7

Conclusions

7.1 Two more diagnostic tools

The whole doctorate work, described to a large extent in this thesis, has been devoted to developing two different diagnostic systems, the ultrafast microwave reflectometer and the Gundestrup probe, that allowed us to look at the edge of RFX-mod with new tools and to analyze the strong relation linking density and flow dynamics to the magnetic topology.
Actually, beyond the results coming from the data analysis (and discussed in the next section), another important achievement of this research activity has been represented by the partecipation to the setting up and to the calibration of the hardware components, in the case of the microwave reflectometer, and by the introduction of an innovative diagnostic method and the study of the theoretical models on which this diagnostic method is based, in the case of the Gundestrup probe.
All this work met the requirements of a fusion oriented experiment, as RFX-mod, that rapidly grew in these last years and approached Tokamaks and Stellarators if not in terms of performance, at least in the common demand to achieve a better knowledge and eventually control of the mechanisms regulating the edge physics.
The development and validation of a Gundestrup model to evaluate the edge flow components through the floating potential measurements, arose exactly from this need, opening the possibility of measuring up to a deeper radial insertion, being the traditional method limited by technological problems (see chapter 4). In this sense, the first flow measurements (using an insertable probe) at high plasma currents and the direct validation of this innovative method on a different machine, the ISTTOK tokamak, have been very gratifying and enlarged significantly the possible Gundestrup research area.

However, putting in operation of the first band of the microwave reflectometer, aroused an even wider interest for many reasons. First of all for the long and difficult problems that this diagnostics encountered in the past years in its application on RFX-mod and more in general on the RFPs. It is worth mentioning that, this represented, so far, the first reflectometric measurements on a Reversed Field Pinch.
On the other hand, the complex edge density dynamics driven by its peculiar magnetic configuration, makes the RFP a very interesting machine for the study of the fast phenomena taking place at the edge and affecting the global performance. Hence, in the wake of Tokamaks and Stellarators, the unavoidable need for a diagnostic system simple, flexible, with a high time resolution and able to reveal the local properties of the edge plasma. The reflectometer results described in chapter 5 enhanced the reliability of this tool and encouraged us in accomplishing the work still lacking (see last section).

7.2 Discussion of the experimental results

The experimental results have been the object of the chapters 5 and 6. As the whole doctorate work, they could appear suffering from a sort of dichotomy. From a side the edge density monitor performed by the ultrafast microwave reflectometer. This new (with respect to the RFPs experience) system has been calibrated and validated through the comparison with a large set of diagnostics mounted on RFX-mod. Thanks to the high time resolution and to the ability to operate in several experimental conditions, the reflectometer was able to carry out significant results in terms of average behaviour of the edge density dynamics, confirming the presence of an empirical density limit for n_e/n_G values (being n_G the Greenwald parameter) larger than 0.3. Crossing this threshold has usually the effect to increase the plasma wall interaction, as the figures 5.18 and 5.19 clearly show, to cause a loss of the density control [66] and, finally, to strongly limit the global performance [64, 61].
Unfortunately, the higher n_e/n_G value regimes are also the most interesting in order to demonstrate the fusion worthiness of a possible RFP reactor.
The reflectometer was also able to demonstrate the beneficial effects of the preliminary lithization [67], undertaken to reduce the significant wall recycling. This procedure seems to offer a possible way out (see fig. 5.22) from the strong limitations in improving the high density RFX-mod performace, imposed by the interaction between plasma and graphite first wall.
The reflectometer experimental results, when carefully viewed, could indicate also another possible solution to the problem of the detrimental plasma wall

interaction. The figures 5.13, 5.14, 5.15, 5.17, highlighted the deep relation between edge density dynamics and local magnetic topology. In particular, they shed a light on the role of the $m = 0$ magnetic islands (see chapter 2), especially at the high plasma current regimes, in which the interplay with the inner QSH modulation makes very difficult a clear discrimination between cause and effect in the result interpretation. The high time resolution and the ability to probe the real local plasma dynamics, enabled instead the reflectometer to indentify the local edge magnetic configurations leading to an increase of the local plasma wall interaction (see in particular figs. 5.15 and 5.17). These phenomena have been related to a not yet totally understood dynamics of the $m = 0$ MHD modes, that, however, appear linked to the empirical RFX-mod density limit [61]. Thus, a further question to be answered in the future is: could a better control of the edge magnetic topology (namely, the $m = 0$ islands) make RFX-mod able to overcome the actual operative limitations?

From the other side, the development of an innovative method to evaluate the edge flow components using the Gundestrup probe allowed a more detailed study of the flow properties in the low plasma current regimes. In particular, in chapter 6 a complete reconstruction of the radial profiles of both perpendicular and parallel (with respect to the magnetic field) plasma flow has been presented. These profiles have been also related respectively to the radial electric field E_r (see figs. 6.1 and 6.2) and with the presence at the edge of (once again) the $m = 0$ islands. Together with the preliminary studies about the pellet injection (fig. 6.8), the time behaviour analysis during the transient changes induced in the magnetic boundary confirmed that these islands affect the parallel plasma flow.

Thus, starting from a totally different point of view and exceeding the dreaded dichotomy, the Gundestrup probe and the reflectometer data analysis converged on a similar topic: the strong relation between density, flow and magnetic topology in the edge of RFX-mod. Moreover, the flow measurements at high plasma current (see section 6.3) consolidated and generalized this concept to almost all the RFP operative scenarios.

Next to these interesting conclusions, it is worth noting that all of the presented results, coming from both reflectometer or Gundestrup probe, greatly benefited from the constant comparison with the different diagnostics operating on RFX-mod and, of course, with the people working on them. The RFP edge appears a too complex region to be investigated by a single diagnostic tool, only a diagnostic set as complete and varied as possible could get a more deep knowledge of the underlying physics and hopefully help to fill the gap that is now separating the RFP performance from those of Tokamaks and Stellarators.

7.3 Future work

Concerning the ultrafast microwave reflectometer, this first operative phase has already achieved its main goal, namely demonstrating the feasibility of such a diagnostic system on the Reversed Field Pinch. To accomplish this task the single Ka-band has been operational since the mid of 2009. As shown in this thesis, actually, the present diagnostic configuration achieved more notable results than a simple hint on its potential capabilities. However, these encouraging outcomes stress the importance of upgrading the RFX-mod microwave reflectometer to a more complete form.
At the moment two different improvements have been considered: the installation of the other two bands and the rising of the frequency modulation rate. This latter has been already preliminarly undertaken at the end of the RFX-mod 2010 experimental campaign since it is simpler and does not require any hardware modifications. Some tests with a doubled modulation rate ($\alpha = 8\ GHz/\mu s$ with respect to the old $4\ GHz/\mu s$) gave some indications about an improvement on the effect of the density fluctuations on the reflected signal. On the other hand, they suggested a further increase (up to $20\ GHz/\mu s$), in order to make possible a real study of the edge density dynamics. In fact, some previous measurements [128] on RFX-mod through magnetic probes revealed a strong coherent egde turbulence driven by a wide spectrum of high frequency MHD modes. This magnetic activity should have a significant effect on the edge density and only the achievement of the maximum modulation rate of the reflectometer could confirm these measurements.
The installation of the other two bands (at higher frequency) is, instead, scheduled for the next months. The microwave sources are already available, since were part of the original scheme of the RFX reflectometer (see chapter 3). The lacking part is represented by the electronic drivers that should feed the source with the ultrafast modulated signal. The project design has been already conceived and the development will start as soon as possible. It is probably superfluous underlining the large amount of information that this diagnostic upgrade could produce and how much the possibility to have an edge density profile every μs could help the difficult understanding of the complex edge region of RFX-mod. Perhaps, in this sense, a hint could be deduced by looking at the fig.5.11, showing the good agreement between the Ka-band of the reflectometer and the edge density profiles obtained by the Edge Thomson Scattering. As described in chapter 2, this latter diagnostic (not operating since 2008) is the only one that provides a (single) density profile at the edge on RFX-mod, while the high plasma current regimes seem strongly affected by the edge conditions. Adding a tool such as the upgraded

reflectometer appears of vital importance.
For the Gundestrup probe the outlook is quite different. RFX-mod has planned to explore in the next years high plasma current regimes, trying, hopefully, to improve the optimization of the more advanced scenarios. It is clear that the traditional insertable probes are going to have a marginal role in the future diagnostic plan.
Within this framework, this diagnostic system will shortly (hopefully during next year) be replaced by a fast reciprocating manipulator equipped with several electrostatic probe arrays [129]. This will enable more detailed studies on the relation between flow and magnetic topology and will allow a partial probe insertion also in the high plasma current regimes, at the moment only brushed by the Gundestrup.

Bibliography

[1] Press conference at *An Alliance for Climate Protection* meeting (12 October 2007), `http://www.climateprotect.org/press/`.

[2] R. J. Goldstone and P. H. Rutherford. *Introduction to Plasma Physics.* Institute of Physics Publishing, London, 1995.

[3] F.F.Chen. *Introduction to Plasma Physics and Controlled Fusion.* Plenum Press, New York, 1984.

[4] J. D. Lawson. *Proc. Phys. Soc. B*, 70:6, 1957.

[5] W. H. Bennet. *Physical Review*, 45:890, 1934.

[6] A. A. Ware. *Philos. Trans. R. Soc. London*, 243(Ser. A):957, 1934.

[7] S. W. Cousins and A. A. Ware. *Proc. Phys. Soc. London*, B 64:159, 1951.

[8] J.P. Freidberg. *Ideal Magnetohydrodynamics.* Plenum Press, New York, 1987.

[9] L.D.Landau and E.M. Lipschiftz. *Fluid Mechanism.* Pergamon Press, Oxford, 1959.

[10] S.I.Braginski. *Transport processes in plasmas in* Reviews of Plasma Physics. Consultant Bureau, 1965.

[11] E. J. Caramana and D. A. Baker. *Nuclear Fusion*, 24:423, 1984.

[12] S. Ortolani. *Magnetohydrodynamics of Plasma Relaxation.* 1993.

[13] A.Intravaia et al. *Physical Review Letters*, 83:5499, 1999.

[14] J. Wesson. *Tokamaks.* Clarendon Press, Oxford, 1987.

[15] Y. Yagi, S. Sekine, H. Sakakita, H. Koguchi, K. Hayase, Y. Hirano, I. Hirota, S. Kiyama, Y. Maejima, Y. Sato, T. Shimada, , and K. Sugisaki. Design concept and confinement prediction of tpe-rx reversed field pinch device. *Fusion Engineering and Design*, 45:409, 1999.

[16] L.A.Artsimovitch. *Nuclear Fusion*, 12:215, 1972.

[17] H.A.B.Bodin. *Nuclear Fusion*, 20:1255, 1980.

[18] H.A.B.Bodin. *Nuclear Fusion*, 30:1717–1737, 1990.

[19] J. B.Taylor. *Physical Review Letters*, 33:1139, 1974.

[20] E.P. Butt et al. Culham, 1965. 2nd IAEA Fusion Energy Conference, vol.2, p.751 .

[21] D.C. Robinson et al. *Plasma Physics and Controlled Fusion Research*, 1:263, 1968.

[22] B. B. Kadomtsev. *Nuclear Fusion Supplement*, Part 3:969, 1962.

[23] H. Ji and S. C. Prager. *Magnetohydrodynamics*, 18:191–210, 2002.

[24] W.Shen and J.C.Sprott. *Physics of Fluids B*, 3:1225, 1991.

[25] S.Ortolani. Varenna(Italy, 1983. Proceedings of the International School of Plasma Physics, Course on Mirror-based and Field reversed approach to Magnetic Fusion, p. 513.

[26] H. Ji et al. *Physical Review Letter*, 73:668–671, 1994.

[27] Harold P. Furth, John Killeen, and Marshall N. Rosenbluth. Finite-Resistivity Instabilities of a Sheet Pinch. *Physics of Fluids*, 6:459, 1963.

[28] Teruo Tamano, Wayne D. Bard, Cheng Chu, Yoshiomi Kondoh, Robert J. La Haye, Paul Ss Lee, Milton Saito, Michael Jj Schaffler, and Peter Ll Taylor. Observation of a new toroidally localized kink mode and its role in Reversed Field Pinch plasmas. *Physical Review Letters*, 59:1444, 1987.

[29] R. Bartiromo and RFX team. Recent progress in reversed field pinch research in the RFX experiment. *Nuclear Fusion*, 39:1697, 1999.

[30] P. Sonato et al. Machine modification for active MHD control in RFX. *Fusion Engineering and Design*, 66-68:161–168, 2004.

[31] G. Rostagni. *Fusion Engineering and Design*, 25:301, 1995.

[32] `http://www.igi.pd.cnr.it/`.

[33] `www.cnr.it/`.

[34] `http://www.enea.it/`.

[35] `http://www.unipd.it/`.

[36] `www.acciaierievenete.com/`.

[37] `http://www.infn.it/`.

[38] P. Martin et al. Overview of RFX-mod fusion science program. 2010. *Proc. of the 24th IAEA conference, OV/5-3Ra.*

[39] P. Martin et al. Overview of RFX-mod results. *Nuclear Fusion*, 49:104019, 2009.

[40] A. Lucchetta et al. `http://www-naweb.iaea.org/napc/physics/FEC/FEC2006/html/index.htm`, 2006. *Proc. 21st Int. Conf. on Fusion Energy.*

[41] S. Martini et al. Active MHD control at high currents in RFX-mod. *Nuclear Fusion*, 47:783–791, 2007.

[42] P. Zanca et al. *Nuclear Fusion*, 47:1425, 2007.

[43] L. Marrelli et al. Active control of resistive kink-tearing modes in RFX-mod. 2008. *Proc. of the IAEA conference.*

[44] P. Zaccaria, S. Dal Bello, and D. Marcuzzi. Tests and analyses for the mechanical and thermal qualification of the new RFX first wall tiles. *Fusion Engineering and Design*, 66-68:289 – 293, 2003. 22nd Symposium on Fusion Technology.

[45] R. Paccagnella and F. D'Angelo. *Physics of Plasmas*, 3:2353, 1996.

[46] J. M. Finn, R. Nebel, and C. Bathke. *Physics of Fluids B*, 4:1262, 1992.

[47] S. Cappello and R. Paccagnella. *Physics of Fluids B*, 4, 1992.

[48] P. Martin et al. *Nuclear Fusion*, 43:1855, 2003.

[49] D. F. Escande et al. *Physical Review Letter*, 85:1662, 2000.

[50] P. Martinl. *Plasma Physics and Controlled Fusion*, 41:A247, 1999.

[51] R. Lorenzini et al. Single-helical axis states in reversed field pinch plasmas. *Physical Review Letter*, 101:025005, 2008.

[52] R. Lorenzini et al. Self-organized helical equilibria as a new paradigm for ohmically heated fusion plasmas. *Nature Physics*, 5:570, 2009.

[53] D. F. Escande et al. *Physical Review Letter*, 85:3169, 2000.

[54] M. Gobbin, D. Bonfiglio, D. F. Escande, A. Fassina, L. Marrelli, A. Alfier, E. Martines, B. Momo, and D. Terranova. Vanishing magnetic shear and electron transport barriers in the rfx-mod reversed field pinch. *Phys. Rev. Lett.*, 106(2):025001, Jan 2011.

[55] M. E. Puiatti et al. Internal and edge electron transport barriers in the RFX-mod Reversed Field Pinch . 2010. *Proc. of the 24th IAEA conference, EXC/P4-10.*

[56] E. Martines, R. Lorenzini, B. Momo, S. Munaretto, P. Innocente, and M. Spolaore. The plasma boundary in single helical axis rfp plasmas. *Nuclear Fusion*, 50(3):035014, 2010.

[57] N. Vianello et al. Transport mechanisms in the outer region of rfx-mod. *Nuclear Fusion*, 49:045008, 2009.

[58] P. Zanca et al. *Physics of Plasmas*, 8:516, 2001.

[59] P. Innocente et al. *Nuclear Fusion*, 47:1092, 2007.

[60] R. B. White and S. M. Chance. *Physics of Fluids*, 27:2455, 1984.

[61] Gianluca Spizzo, Paolo Scarin, Matteo Agostini, Alberto Alfier, Fulvio Auriemma, Daniele Bonfiglio, Susanna Cappello, Alessandro Fassina, Paolo Franz, Lidia Piron, Paolo Piovesan, Maria Ester Puiatti, Marco Valisa, and Nicola Vianello. Investigation on the relation between edge radial electric field asymmetries in rfx-mod and density limit. *Plasma Physics and Controlled Fusion*, 52(9):095011, 2010.

[62] M Zuin, N Vianello, M Spolaore, V Antoni, T Bolzonella, R Cavazzana, E Martines, G Serianni, and D Terranova. Current sheets during spontaneous reconnection in a current-carrying fusion plasma. *Plasma Physics and Controlled Fusion*, 51(3):035012, 2009.

[63] P. Zanca and D. Terranova. *Plasma Physics and Controlled Fusion*, 46:1115, 2004.

[64] M.E. Puiatti, P. Scarin, G. Spizzo, M. Valisa, M. Agostini, A. Alfier, A. Canton, L. Carraro, E. Gazza, R. Lorenzini, R. Paccagnella, I. Predebon, D. Terranova, D. Bonfiglio, S. Cappello, R. Cavazzana, S. Dal Bello, P. Innocente, L. Marrelli, R. Piovan, P. Piovesan, F. Sattin, and P. Zanca. High density physics in reversed field pinches: comparison with tokamaks and stellarators. *Nuclear Fusion*, 49(4):045012, 2009.

[65] P. Scarin et al. Magnetic structures and pressure profiles in the plasma boundary of RFX-mod: high current and density limit in helical regimes . 2010. *Proc. of the 24th IAEA conference, EXD/P3-29.*

[66] S. Barison et al. Analysis of the interaction between plasmas and the graphite first wall in rfx-mod. *accepted for publication on J.Nucl.Mater*, 2011.

[67] S. Dal Bello et al. First effect of lithization on rfx-mod experiment. 2010. *Proceedings of the 37th EPS conference on Plasma Physics.*

[68] A. Canton et al. Density control in rfx-mod reversed field pinch device. volume 32D, pages D–1.002. ECA, 2008. *Proceedings of the 35th EPS conference on Plasma Physics.*

[69] F. Bonomo et al. Role of the flow in the formation of the helical states in RFX-mod. page O2.101, Dublin (Ireland), 2010. *37th EPS Conference on Plasma Physics.*

[70] P. Innocente and S. Martini. A two color multichord infrared interferometer for RFX . 1992. *Proceedings of the 9th topical conference on high temperature plasma diagnostics, vol. 63, pages 4996-4998.*

[71] P. Innocente et al. Upgrade of the RFX CO2 interferometer using in-vessel optics for extended edge resolution. 1997. *In Proceedings of the eleventh topical conference on high temperature plasma diagnostics, vol. 68, pages 694-697.*

[72] A. Alfier and R. Pasqualotto. New Thomson scattering diagnostic on RFX-mod. *Review of Scientific Instruments*, 78:013505, 2007.

[73] A. Alfier and R. Pasqualotto. Edge thomson scattering on rfx-mod. *Review of Scientific Instruments*, 77(10):10E501, 2006.

[74] R. Cavazzana, P. Scarin, G. Serianni, M. Agostini, F. Degli Agostini, V. Cervaro, L. Lotto, Y. Yagi, H. Sakakita, H. Koguchi, and Y. Hirano. Optical and electrical diagnostics for the investigation of edge turbulence in fusion plasmas. *Review of Scientific Instruments*, 75(10):4152 –4154, October 2004.

[75] M. Agostini et al. Edge turbulence characterization in rfx-mod with optical diagnostics. *Plasma Physics and Controlled Fusion*, 51:1050003, 2009.

[76] P. Martin, A. Murari, A. Buffa, L. Marrelli, W. Baker, G. Gadani, O. Hemming, G. Manduchi, A. Parini, C. Taliercio, A. Hoffmann, G. Stasek, and R. Wirth. Soft x-ray and bolometric tomography in rfx. *Review of Scientific Instruments*, 68(2):1256–1260, 1997.

[77] M. Spolaore et al. *J. Nucler Mat.*, 390-391:448, 2009.

[78] M. Spolaore et al. Magnetic and electrostatic structures measured in the edge of the rfx-mod experiment. *Journal of Nuclear Materials*, 390-391:448, 2009.

[79] H. Y. W. Tsui, R. D. Bengtson, G. X. Li, H. Lin, Ch. P. Ritz, and A. J. Wootton. A new scheme for Langmuir probe measurement of transport and electron temperature fluctuations. *Rev. Sci. Instrum.*, 63:4608, 1992.

[80] Vincenzi Pietro. Studio statistico dell'andamento di densitá e temperatura al bordo del plasma in RFX-mod . Master's thesis, Universitá degli Studi di Padova, Italy, 2003.

[81] I. H. Hutchinson. *Principles of plasma diagnostics*. 1987.

[82] V. Ginzburg, J. Sykes, and R. Tayler. *Propagation of electromagnetic waves in plasmas*, volume 7 of *International Series of Monographs on Electromagnetic Waves*. Pergamon Press, 1996.

[83] E. Mazzucato. Numerical study of microwave reflectometry in plasmas with two-dimensional turbulent fluctuations. *Review of Scientific Instruments*, 69(4):1691–1698, 1998.

[84] E. Mazzucato. Microwave reflectometry for magnetically confined plasmas. *Review of Scientific Instruments*, 69(6):2201–2217, 1998.

[85] P. Varela, M.E. Manso, A. Silva, the CFN Team, and the ASDEX Upgrade Team. Review of data processing techniques for density profile evaluation from broadband fm-cw reflectometry on asdex upgrade. *Nuclear Fusion*, 46(9):S693, 2006.

[86] M. Hirsch, E. Holzhauer, J. Baldzuhn, B. Kurzan, and B. Scott. Doppler reflectometry for the investigation of propagating density perturbations. *Plasma Physics and Controlled Fusion*, 43(12):1641, 2001.

[87] G. D. Conway et al. Doppler reflectometry on asdex upgrade: foundations and latest results. pages 30–36, 2007. *8th International Reflectometry Workshop - IRW8.*

[88] G. J. Kramer, R. Nazikian, and E. Valeo. Correlation reflectometry for turbulence and magnetic field measurements in fusion plasmas (invited). *Review of Scientific Instruments*, 74(3):1421–1425, 2003.

[89] Ph. Moreau, F. Clairet, J. M. Chareau, M. Paume, and C. Laviron. Ultrafast frequency sweep heterodyne reflectometer on the tore supra tokamak. *Review of Scientific Instruments*, 71(1):74–81, 2000.

[90] A. Silva, M. E. Manso, L. Cupido, M. Albrecht, F. Serra, P. Varela, J. Santos, S. Vergamota, F. Eusébio, J. Fernandes, T. Grossmann, A. Kallenbach, B. Kurzan, C. Loureiro, L. Meneses, I. Nunes, F. Silva, and W. Suttrop ASDEX Upgrade Team. Ultrafast broadband frequency modulation of a continuous wave reflectometry system to measure density profiles on asdex upgrade. *Review of Scientific Instruments*, 67(12):4138–4145, 1996.

[91] T. Tokuzawa, A. Mase, N. Oyama, A. Itakura, and T. Tamano. Ultrafast broadband frequency-modulation reflectometer for density profile measurements in gamma 10. *Review of Scientific Instruments*, 68(1):443–445, 1997.

[92] K. W. Kim, E. J. Doyle, T. L. Rhodes, W. A. Peebles, C. L. Rettig, and Jr. N. C. Luhmann. Development of a fast solid-state high-resolution density profile reflectometer system on the diii-d tokamak. *Review of Scientific Instruments*, 68(1):466–469, 1997.

[93] R. Cavazzana, F. Chino, M. Moresco, A. Sardella, and E. Spada. First reflectometric measurements on a rfp plasma with high density fluctuations. volume 21a, pages 361–364, 1997. *24th EPS conference on Plasma Physics.*

[94] Roberto Cavazzana and Maurizio Moresco. Robust measurement of group delay in the presence of density fluctuations by means of ultrafast swept reflectometry. *Review of Scientific Instruments*, 79(10):10F105, 2008.

[95] P. Scarin, M. Agostini, R. Cavazzana, F. Sattin, G. Serianni, and N. Vianello. Edge turbulence in rfx-mod virtual-shell discharges. *Journal of Nuclear Materials*, 363-365:669 – 673, 2007. Plasma-Surface Interactions-17.

[96] V. Antoni, H. Bergsker, G. Serianni, M. Spolaore, N. Vianello, R. Cavazzana, G. Regnoli, E. Spada, E. Martines, M. Bagatin, and J.R. Drake. Anomalous particle transport and flow shear in the edge region of rfp's. *Journal of Nuclear Materials*, 313-316:972 – 975, 2003. Plasma-Surface Interactions in Controlled Fusion Devices 15.

[97] M. Moresco, R. O'Dubhghaill, and E. Spada. Application of microwave reflectometry for plasma density diagnostics in a reversed-field pinch machine. *International Journal of Infrared and Millimeter Waves*, 12(5):609–624, 1992.

[98] M. Moresco, R. Cavazzana, A. Sardella, and E. Spada. First results in reflectometric plasma density measurements on rfx. *Review of Scientific Instruments*, 66(1):406 –408, jan. 1995.

[99] R. Cavazzana, M. Moresco, N. Pomaro, A. Sardella, and E. Spada. Upgrade of the rfx microwave frequency modulated reflectometer to ultrafast sweeping rate. *Review of Scientific Instruments*, 70(1):1056–1059, 1999.

[100] Cyrus S. MacLatchy, Claude Boucher, Deborah A. Poirier, and James Gunn. Gundestrup: A Langmuir/Mach probe array for measuring flows in the scrape-off layer of TdeV. *Review of Scientific Instruments*, 63(8):3923–3929, 1992.

[101] H. Figuereido et al. volume 29C, pages P–2.036, 2005. *32nd EPS Conference on Plasma Physics.*

[102] J. P. Gunn, C. Boucher, P. Devynck, I. Duran, K. Dyabilin, J. Horaček, M. Hron, J. Stöckel, G. Van Oost, H. Van Goubergen, and F. Záček. Edge flow measurements with Gundestrup probes. volume 8, pages 1995–2001. AIP, 2001. *The 42nd annual meeting of the division of plasma physics of the American Physical Society and the 10th international congress on plasma physics.*

[103] M. Hudis and L.M. Lidsky. Directional Langmuir Probe. *Physics of Plasmas*, 41(12):5011, 1970.

[104] M. Spolaore, G. De Masi, N. Vianello, R. Cavazzana, R. Lorenzini, E. Martines, B. Momo, P. Scarin, G. Serianni, S. Spagnolo, and M. Zuin. Parallel and perpendicular flow measurements in the edge region of RFX-mod. volume 33E. ECA, 2009. *36th EPS Conference on Contr. Fusion and Plasma Phys.*

[105] G. De Masi, M. Spolaore, R. Cavazzana, P. Innocente, R. Lorenzini, E. Martines, B. Momo, S. Munaretto, G. Serianni, S. Spagnolo, D. Terranova, N. Vianello, and M. Zuin. Flow measurements in the edge region of the RFX-mod experiment. *Contributions to Plasma Physics*, 50:824–829, 2010.

[106] B. J. Peterson, J. N. Talmadge, D. T. Anderson, F. S. B. Anderson, and J. L. Shohet. Measurement of ion flows using an "unmagnetized" Mach probe in the interchangeable module stellarator. *Review of Scientific Instruments*, 65(8):2599–2606, 1994.

[107] I. H. Hutchinson. A fluid theory of ion collection by probes in strong magnetic fields with plasma flow. *Physics of Fluids*, 30(12):3777–3781, 1987.

[108] V. Antoni, D. Desideri, E. Martines, G. Serianni, and L. Tramontin. Plasma flow in the outer region of the RFX reversed field pinch experiment. *Nuclear Fusion*, 36(11):1561, 1996.

[109] H Van Goubergen, R R Weynants, S Jachmich, M Van Schoor, G Van Oost, and E Desoppere. A 1d fluid model for the measurement of perpendicular flow in strongly magnetized plasmas. *Plasma Physics and Controlled Fusion*, 41(6):L17, 1999.

[110] I. H. Hutchinson. The invalidity of a Mach probe model. *Physics of Plasmas*, 9(5):1832–1833, 2002.

[111] S. Jachmich, H. Van Goubergen, and R. R. Weynants. Influence of plasma flow on the floating potential and an ensuing novel technique for measuring parallel flows. volume 42, pages 832–835. ECA, 2000. *27th EPS Conference on Contr. Fusion and Plasma Phys.*

[112] H.S. Massey D. Bohm, E.H.S. Burhop and R.W. Williams. *The Characteristics of electrical discharges in magnetic fields.* National Nuclear Energy series. McGraw-Hill, 1949.

[113] P.C. Stangeby and G. M. McCracken. *Nuclear Fusion*, 30:1225, 1990.

[114] C.A.F. Varandas et al. *Fusion Technology*, 29:105, 1996.

[115] C. Silva et al. *Plasma Physics and Controlled Fusion*, 46:163, 2004.

[116] H. Figueiredo et al. Plasma flow and transport on the isttok boundary plasma. *Journal of Nuclear Materials, in press*, 2010.

[117] C. Silva et al. *Plasma Physics and Controlled Fusion*, 48:727, 2006.

[118] C. Laviron, Ph. Moreau, F. Clairet, J. M. Chareau, and M. Paume. Automatic linearisation of swept microwave sources for density profile reflectometry. page 119, 1997. *Proceedings of the 3rd Workshop on Microwave Reflectometry for Fusion Plasma Diagnostics.*

[119] T. Bolzonella, N. Pomaro, G. Serianni, and D. Marcuzzi. New wide bandwidth in-vessel magnetic measurement system for rfx. *Review of Scientific Instruments*, 74(3):1554–1557, 2003.

[120] R Vignaga, R Cavazzana, and E Martines. Studio della posizione radiale del bordo del plasma nell'esperimento RFX-mod. Master's thesis, Universitá degli Studi di Padova, Italy, 2010.

[121] M. Cavinato et al. *Fusion Engineering Design*, 82:220, 2008.

[122] V. Antoni, D. Desideri, E. Martines, G. Serianni, and L. Tramontin. Plasma potential well and velocity shear layer at the edge of reversed field pinch plasmas. *Phys. Rev. Lett.*, 79(24):4814–4817, Dec 1997.

[123] J. M. Beall, Y. C. Kim, and E. J. Powers. *J. Appl. Phys*, 53:3933, 1982.

[124] M. Zuin et al. *Nuclear Fusion*, 50:052001, 2010.

[125] O. D. Gurcan et al. *Physic of Plasmas*, 14:042306, 2007.

[126] M. Spolaore et al. Parallel and perpendicular flows in the RFX-mod edge region. *to appear on J.Nucl.Mat.*, 2011.

[127] S.Cappello, D. Bonfiglio, and D. F. Escande. *Phys. Plasmas*, 13:056102, 2006.

[128] S. Spagnolo et al. Alfven eigenmodes in the RFX-mod reversed field plasma. page p4.187, Dublin (Ireland), 2010. *37th EPS Conference on Plasma Physics.*

[129] P. Agostinetti, A. Barzon, M. Pavei, M. Spolaore, F. Rossetto, and L. Trevisan. Specifiche tecniche del Manipolatore Veloce per RFX. Technical report, Consorzio RFX, 2009.

Acknowledgements

...E infine i ringraziamenti...mi scuso fin da subito se dimenticheró qualcuno, ma alle 10.30 di sera a RFX senza aver cenato...non é che si possa essere proprio lucidi!
Dunque, prima di tutto mi preme ringraziare le persone che hanno contribuito maggiormente a questo lavoro di tesi. In primis ovviamente Emilio...dove l'ovviamente non é dovuto per il suo ruolo di capogruppo (e nemmeno perché entrambi veniamo da sotto il Po), ma per la sua immensa umanitá che non ha mai smesso di dimostrarmi nemmeno per un secondo in questi 3 anni. Saper di poter contare su una persona cosí, specialmente in ambito lavorativo, rende tutto davvero molto piú facile.
Poi, come dimenticare Monica e Roberto. Ho iniziato le conclusioni della tesi dicendo che il lavoro svolto in questi 3 anni é in buona parte contenuto in queste pagine. Ebbene c'é un'altra importantissima parte, fatta di oscilloscopi, schede di acquisizione, tester, guide d'onda, messe a terra e cavi BNC che per forza di cosa non possono essere descritte in un lavoro di tesi, ma che, per uno che si é laureato in Astrofisica, avrebbero potuto rappresentare un ostacolo difficilissimo. E allora grazie a entrambi per avermi reso (un pó) meno sperimentalmente incapace e aver risposto con un sorriso a ogni mia cavolata. E grazie anche alla sempre cordiale presenza del Prof. Moresco, alle chiaccherate sul whiskey irlandese e alla preziosa assistenza nella distruzione degli IMPATT... E anche un grazie piú generale al gruppo piú figo (e diciamolo!) di RFX, il meraviglioso gruppo FB!!!
Grazie ai sempre troppo in anticipo commensali (nell'accezione tutta mia di "persone con cui vado a mangiare a mensa") e a tutti gli amici di RFX (specie a quelli che in questi febbrili giorni pre-consegna tesi mi hanno aiutato in svariati modi). A elencarvi tutti, dimenticherei sicuro qualcuno...perció accontentatevi!
Grazie alla mia famiglia, lontana ahimé piú di 1000 km, ma sempre vicina col cuore, con la mente o con skype e sempre disposta a girare il mondo per seguire i miei spostamenti...Grazie, grazie, grazie!!!
Grazie a Giorgia, uno splendente raggio di Sole tra la nebbia padana...orgogliosa

di me (tendenzialmente di d.) perché l'introduzione di questa tesi sembra il manifesto della "decrescita". A lei vorrei dedicare le parole piú belle, perché si é fatta carico di un compito difficilissimo...quello di sopportarmi e accettarmi per quello che sono, nei momenti belli e in quelli piú difficili. Spero solo che ci riesca per molto altro tempo ancora!
Un ultimo grazie, doveroso anche questo, a tutta la comitiva della mitica via Rudena, a chi c'era e ora ha cambiato piano, cittá oppure continente, a chi c'é, a chi ci viene solo ogni tanto per scroccare una cena o ritrovare vecchi amici e a chi ci sará...